LINEARIZED HARMONIC METHODS FOR UNSTEADY AIRFOIL SIMULATIONS

A THESIS SUBMITTED TO
THE GRADUATE SCHOOL OF NATURAL AND APPLIED SCIENCES
OF
MIDDLE EAST TECHNICAL UNIVERSITY

BY

MERT ŞENKARDEŞLER

IN PARTIAL FULFILLMENT OF THE REQUIREMENTS
FOR
THE DEGREE OF MASTER OF SCIENCE
IN
MECHANICAL ENGINEERING

AUGUST 2023

Approval of the thesis:

LINEARIZED HARMONIC METHODS FOR UNSTEADY AIRFOIL SIMULATIONS

submitted by **MERT ŞENKARDEŞLER** in partial fulfillment of the requirements for the degree of **Master of Science in Mechanical Engineering Department, Middle East Technical University** by,

Prof. Dr. Halil Kalıpçılar
Dean, Graduate School of **Natural and Applied Sciences** _____

Prof. Dr. Mehmet Ali Sahir Arıkan
Head of Department, **Mechanical Engineering** _____

Assist. Prof. Dr. Özgür Uğraş Baran
Supervisor, **Mechanical Engineering, METU** _____

Prof. Dr. Ender Ciğeroğlu
Co-supervisor, **Mechanical Engineering, METU** _____

Examining Committee Members:

Prof. Dr. M. Metin Yavuz
Mechanical Engineering, METU _____

Assist. Prof. Dr. Özgür Uğraş Baran
Mechanical Engineering, METU _____

Prof. Dr. Ender Ciğeroğlu
Mechanical Engineering, METU _____

Assist. Prof. Dr. Sıtkı Uslu
Mechanical Engineering, TOBB _____

Assist. Prof. Dr. Onur Baş
Mechanical Engineering, TED University _____

Date:08.17.2023

I hereby declare that all information in this document has been obtained and presented in accordance with academic rules and ethical conduct. I also declare that, as required by these rules and conduct, I have fully cited and referenced all material and results that are not original to this work.

Name, Surname: Mert Şenkardeşler

Signature :

ABSTRACT

LINEARIZED HARMONIC METHODS FOR UNSTEADY AIRFOIL SIMULATIONS

Şenkardeşler, Mert
M.S., Department of Mechanical Engineering
Supervisor: Assist. Prof. Dr. Özgür Uğraş Baran
Co-Supervisor: Prof. Dr. Ender Ciğeroğlu

August 2023, 100 pages

Airfoils, subjected to continuous transient motions, encounter cyclical disturbances such as pitching and plunging motions and mechanical vibrations. Conventional methods for examining these disturbances rely on computationally demanding temporal domain solvers. These approaches often require multiple runs for fluid-structure coupling, further amplifying their inefficiency.

This research addresses these issues by reframing the compressible flow equations into the complex domain, synchronizing them with standard complex variable formulations of the vibration problems in the structural domain. The study retools the harmonic method—previously used in turbomachinery analyses—to investigate cyclical disturbances over airfoils. The proposed complex-variable-based method offers a highly efficient solution, capturing frequency, phase, and amplitude information, thus facilitating fluid-structure interactions.

By utilizing this advanced approach, solution speeds are accelerated by two to three orders of magnitude compared to traditional methods. This reduction in computa-

tional time paves the way for more in-depth airfoil performance analysis under varied conditions. The proposed method had been tested on unsteady problems with NACA012 and NACA64A010 airfoils where in the case of former, the results matched with the experimental findings. Further testing is done on the NACA012 airfoil on canonical flutter test case. Testing confirms the accuracy of the method, demonstrating its potential for practical applications in airfoil design and analysis.

Keywords: CFD, Compressible Flow, Harmonic Method, Vibration, Airfoil

ÖZ

HAREKETLİ KANAT ANALİZLERİ İÇİN DOĞRUSAL HARMONİK METODLAR

Şenkardeşler, Mert
Yüksek Lisans, Makina Mühendisliği Bölümü
Tez Yöneticisi: Dr. Öğr. Üyesi. Özgür Uğraş Baran
Ortak Tez Yöneticisi: Prof. Dr. Ender Ciğeroğlu

Ağustos 2023 , 100 sayfa

Süreklilik gösteren geçici hareketlere maruz kalan kanatlar, salınımlı ve dalgalanma hareketleri ve mekanik titreşimler gibi döngüsel hareket davranışı gösterirler. Bu hareketleri incelemek için geleneksel yöntemler, hesaplama yoğunluğu yüksek olan zamansal çözücüler kullanmaktadırlar. Bu yaklaşımlar genellikle sıvı-yapı bağlantısını sağlamak için birden fazla çözücü iterasyonu gerektirmekte ve bu da gereken işlem gücü miktarını daha da artırmaktadır.

Bu araştırma, bu sorunları ele almak için sıkıştırılabilir akış denklemlerini kompleks uzaya çevirip orada çözerek ve bunları yapısal titreşim metodlarının standart kompleks değişken formülasyonlarıyla senkronize ederek çözüm bulmaktadır. Çalışma, kanat profilinin üzerindeki döngüsel hareketleri incelemek için turbomakineler analizinde daha önce kullanılan harmonik yöntemi, eldeki problem için yeniden uyarlamaktadır. Önerilen kompleks uzay tabanlı yöntem, frekans, faz ve genlik bilgilerini yakalayan ve böylece sıvı-yapı etkileşimlerini kolaylaştıran yüksek derecede verimli bir çözüm sunmaktadır.

Bu yaklaşımı kullanarak, çözüm hızları, geleneksel yöntemlere göre radikal olarak hızlandırılabilmektedir. Bu verimlilik ve hesap maliyetindeki gelişme, daha ayrıntılı kanat profil performans analizlerinin önünü açmaktadır. Titiz testler, çözümün doğruluğunu onaylayıcı niteliktedir ve kanat profil tasarımı ve analizi uygulamalarında kullanım için gelecek vaat etmektedir.

Anahtar Kelimeler: HAD, Harmonik, titresim, kanat, Çırpıntı

ACKNOWLEDGMENTS

Huge thanks to my advisor, Professor Ozgur Ugras Baran. You've been there for me in good times and bad, always ready with advice and encouragement. When I felt stuck, you shone a light on the path forward. You've given so much of your time and energy to help me succeed. Without you, this paper wouldn't exist. Your wisdom has made me a better scholar, and your kindness has made me a stronger person. Thanks for everything.

Following this, I cannot overlook the immeasurable support and guidance provided by Serkan Gözübüyük, whose influence went far beyond the realms of the professional, venturing into personal terrains to aid my growth in ways uncommon and extraordinary. Your help has been a cornerstone of my journey, making a significant impact on my path. A heartfelt thank you for being there in every way possible.

TABLE OF CONTENTS

LIST OF TABLES

TABLES

LIST OF FIGURES

FIGURES

CHAPTER 1

INTRODUCTION

The aeronautic and aerospace industries heavily rely on Computational Fluid Dynamics (CFD) for essential design and analysis tasks. The advances in computational power making CFD solvers increasingly compelling, there is an ongoing need for sophisticated computational resources to handle complex, unsteady phenomena.

This work specifically concentrates on unsteady phenomena that exhibit periodic behavior in time. By leveraging this periodicity, time-dependent flow equations can be transformed into time-independent equations within the frequency domain.

The relevance of this approach extends to various industrial applications, including those involving aerodynamic components like airfoils and aircraft wings. A significant example is flutter, a destructive vibration arising from the interplay of aerodynamic, structural, and inertial forces. Flutter is crucial in aircraft wing design and analysis as it can lead to significant structural damage.

Flutter is a type of fluid-structure interaction (FSI) where the solid domain (the airfoil) and the fluid domain are intimately interconnected. Such interaction requires an iterative solution for both domains, as changes in one directly impact the other. In the flutter context, the airfoil's unsteady motion necessitates a computationally intensive unsteady solution, further complicated by the need for multiple solutions corresponding to each updated structure. Thus, accurately simulating flutter through FSI involves substantial computational demand.

The common way of solving flutter problems is to obtain a unsteady CFD solution, in time domain, using time accurate time marching CFD methods [4]. Time-accurate methods in computational fluid dynamics (CFD) employ a semi-discrete form of

equations, where space is discretized while time remains continuous. This approach, known as the method of lines, captures the entirety of fluid flow linearity and non-linearity, obtaining accurate, but rather expensive solutions. However, in our case where the aircraft wing's motion is periodic, it can be proposed that there must be a way to use this to reduce computational expense. A similar approach had been proposed, and developed by Arash (2017) [1], albeit in a different unsteady flow problem involving turbomachinaries.

By shifting the problem into the frequency domain, computational cost becomes time-independent, resulting in more efficient numerical solutions. In his work, Arash proposed [1], converting the problem from the time domain, into frequency domain, solving it there, and converting back to time domain at the end, would exponentially decrease the computational expense of the solution. It had also been mentioned by Mitchell in his PHD thesis [5] that, in unsteady time marching simulations where the desired phenemona is periodic in behavior, 95% of the total simulation time is spent on initial transient case before the unsteady solution converges to its final oscillatory phase, as it is shown in figure 1.1. This initial transient case is irrelevant to our desired end solution.

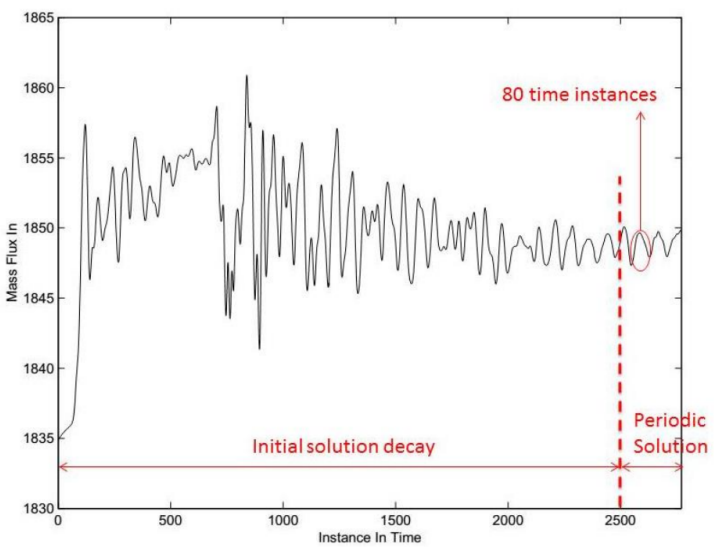

Figure 1.1: Time marching simulation on periodic problem [1]

It can be suggested that if long initial transient is such a big problem, why not in-

crease the time step of the time marching solver, so that less iterations are spent there. However the issue here is that it is desired to capture the final periodic behavior of the unsteady system, and in order to capture it the time step must be sufficiently small to detect the periodic unsteadiness of the final system.

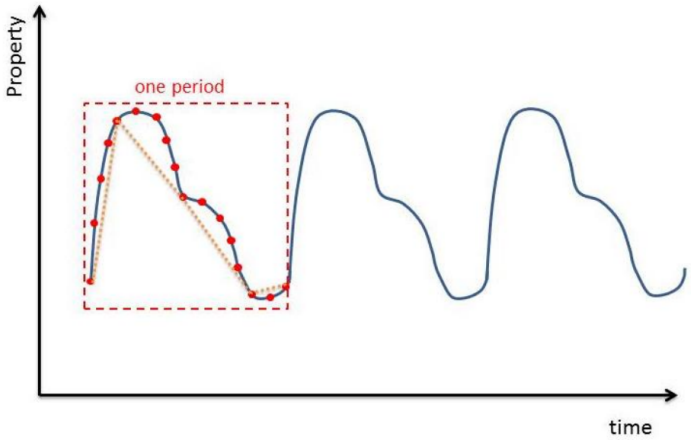

Figure 1.2: Time steps to get harmonic solution [1]

As shown in figure 1.2, the timesteps should be sufficiently small to accurately detech the periodic unsteadyness of the solution, where too large of a timestep would lead to difficulties in capturing the overal behaviour. This limitation on time step size leads to the previous findings leading to time marching methods wasting 95 percent of their time solving the irrelevant parts of the unsteady solution.

Therefore a better method of approaching these problems, where the unsteadiness is peripodic in time, is to transform the problem from time domain into frequency domain, and convert the obtained frequency domain solution back into time domain at the end. The proposed method for this transformation is to linearize the unsteadiness of the flow, around the mean state of the flow. Solve the steady state and harmonic perturbation component seperately, combining them at the end. This approach would directly solve for the desired harmonic unsteady response of the system, not wasting any compute on the transient part.

Oscilating airfoil problems share similarities with the turbomachinary problems, in that they are also undergoing harmonic unsteady perturbations, allowing the use of

the mentioned frequency domain solution approach. Given a harmonic oscillation of a airfoil, or any other component in an external flow problem, it is possible to decompose the problem into mean and perturbation parts, and solve for both separately directly obtaining the desired unsteady harmonic response of the system. The method also has the advantage that harmonic perturbation solver essentially is a steady state solver, acting on a larger set of perturbed conserved variables, where the formulation allows for implicit time marching schemes resulting in substantially faster convergence times.

Overall the motivation behind this paper is to derive and implement a linearized harmonic solver, showcasing the potential of frequency-domain solutions and modern computational techniques to analyze computationally expensive unsteady flow phenomena such as flutter.

1.1 Historical Development and Basic Concept of the Linearized Harmonic Method

The method utilized in this paper, the linearized harmonic method, is developed in 70s by Ni, R. H. and Sisto, F. [6]. The method was originally used on potential flow solvers. Hall later founded the use of linearized harmonic method on turbomachinary solutions. [7] The method first implemented on 2d harmonic problems, focusing on channel and turbomachinery flows.

The Linearized Harmonic (LH) method is premised on the decomposition of unsteady variables into a steady mean part and a harmonic perturbation. This can be represented as:

$$X = X_{mean} + X_{perturbation}$$

The crux of this approach lies in substituting the mean solution with a steady one, leading to a system where steady-state and first-order disturbance systems are decoupled and can be independently solved. The steady-state system, reliant solely on steady variables, is solved independently, while the disturbance system, dependent

on both steady and disturbance variables, is solved once the steady solution is determined.

In this method, although the mean solution influences the disturbance solution, the converse is not true, allowing for separate handling of multiple disturbances and subsequent superposition of solutions. The disturbance solution is solved in the frequency domain, encapsulating all potential flow states in the time domain through its amplitude, phase, and frequency components. Thus, the LH method systematically handles and solves unsteady variables by decoupling, independent solving, and subsequent assembly of steady and perturbed variables.

1.2 Applications and Limitations of the Linearized Harmonic Method

The Linearized Harmonic (LH) method has been significantly applied to flow problems involving turbomachinery cascades [8] [9]. In such scenarios, harmonic disturbance arises due to rotor-stator interaction, creating periodic pressure fluctuations or waves. The frequency of these fluctuations corresponds to a harmonic of the rotor's rotational frequency and may cause various interference effects, including shock wave interactions and boundary layer transitions. These disturbances propagate upstream and downstream, influencing the entire flow field and potentially inducing blade flutter, a significant issue for turbomachinery design.

However, the LH method has drawbacks. Notably, it equates the steady flow with the mean flow, thus neglecting any effects the perturbations might have on the mean state of the flow. This assumption produces noticeable errors, particularly in the presence of large flow perturbations.

To address this, Ning and He proposed a Nonlinear Harmonic method [10]. This technique employs a time-averaged flow field as the basis for the harmonic perturbations, accommodating the nonlinear effects of unsteadiness on the time-averaged flow. Although more computationally intensive than the LH method (by a factor of 1.6 [10]), it remains significantly faster than conventional time-marching methods [11] [12], while keep being accurate in cases where linearized harmonic methods would have trouble [13]. The non-linear harmonic (NLH) method serves as a solution to the lim-

itations seen in the Linearized Harmonic Approach.

1.3 Advancement Towards the Harmonic Balance Technique and Aeroelastic Applications

In his landmark paper, Hall expanded upon the idea of the Linearized Harmonic method, introducing the Harmonic Balance technique [14]. This method, designed for modeling unsteady, nonlinear flows in turbomachinery, employs Fourier series to represent flow conservation variables that are periodic in time. This concept hinges on many turbomachinery flows being periodic. By representing unsteady flow variables as a Fourier series in time, Hall derived a harmonic balance form of the governing Euler or Navier-Stokes flow equations.

The Harmonic Balance technique differs significantly from previous time-domain and frequency-domain approaches. The time-domain technique uses Computational Fluid Dynamics (CFD) to discretize flow equations and march the solution across time levels. Despite being able to model both linear and nonlinear disturbances, this method requires small time steps for accuracy and stability, leading to extensive computational times. The frequency-domain or time-linearized technique calculates the time-averaged (steady) flow first and then linearizes the governing flow equations around this mean flow. However, this method fails to model dynamic nonlinearities.

Hall's method merges the strengths of these two techniques, capturing both linear and nonlinear disturbances like the time-domain method, and achieving computational efficiency similar to the frequency-domain approach.

While harmonic methods have primarily been used for turbomachinery problems, they are also suitable for analyzing unsteady flows of airfoil structures, as demonstrated by Thomas and Dowell [15]. Earlier studies involved flutter analysis on 2d airfoils, later expanded in use to 3d simulations [16] This approach succesfully models the unsteady aerodynamic forces caused by airfoil oscillation, allowing aeroelastic (fluid-structure interaction) analysis when combined with an appropriate structural model. HB provides more accurate results even when compared to Non-Linear harmonic method, but its computational cost is much higher, making it impractical for

anything but validation runs.

One such is can be found where the harmonic balance technique is applied to model the F-16 fighter aircraft's limit cycle oscillation behavior [17]. A nonlinear frequency-domain harmonic method was used to assess the aircraft's flutter onset Mach number and subsequent dynamic response.

More recent research, such as a study by Howison [18], employs the Harmonic Balance technique to model unsteady airflow behavior around wind turbines. This work, the first to use the Harmonic Balance method in a wind turbine aeroelastic model, contributes a novel approach to the analysis of unsteady wind turbine aerodynamics.

In the general case for aeroelasticity problems concerning airfoils, the most recent works involve one shot method using Harmonic balance method by Ekici [19] A Fixed Point Iteration scheme along with harmonic flow solver [20]. In the proposed fixed point iteration scheme, for a given initial guess, the method computes the aerodynamic forces using the harmonic balance flow solver. These forces are then used to solve the aeroelastic equations with the Newton-Raphson method, yielding updated aeroelastic states. These updated states are then used as the input for the next iteration of the harmonic balance solver. This loop continues until convergence is reached, meaning that the aeroelastic states no longer change significantly between iterations. The methodology has been demonstrated on a benchmark transonic airfoil aeroelastic configuration, focusing on aeroelastic issues like flutter.

1.4 Current Work

The primary goal of this research is to create an efficient, Fluid-Structure Interaction (FSI) enabled Linearized Harmonic (LH) Euler solver, ultimately to use it on external compressible flows with oscillating wings in fixed-wing aircraft, thereby addressing the need for a practical, cost-effective method to predict flutter speed.

In the current state of art, unsteady harmonic external flow simulations either implement time-accurate time marching methods in the time domain, or utilize harmonic balance technique. Former is too computationally expensive, rendering it useless on anything other than research endeavors. Although the latter is much more efficient than time-marching methods, it still is orders of magnitudes more expensive than linearized harmonic methods. It had been developed to solve issues in the domain of turbomachinary, where the method shows its strength, and its trade-offs are justified. The current proposed work, utilizes the latest works on linearized harmonic methods, which is done by Arash (2022) [21].

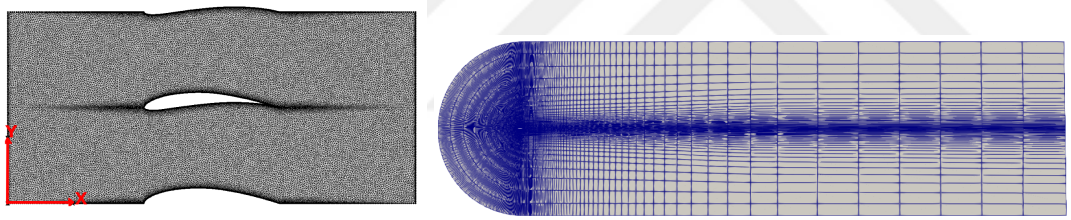

(a) Turbomachinery Problem Domain [21]

(b) Airfoil Problem Domain

Figure 1.3: Flow Problem Domain Comparison

External flow airfoil problems pose significant advantages for linearized harmonic methods, differing significantly from turbomachinary problems as shown in figure 1.3. The flow domain substantially bigger and the disturbances are introduced from the airfoil surface instead of inlet and outlet boundaries. This leads a flow solution where the perturbations have significant effect only in regions very close to the airfoil body, where most of the flow domain is comparable unaltered. This means that, effective harmonic problem domain, is orders of magnitudes smaller than what the mesh

would suggest. The fact that we are mostly interested in flow results near the airfoil boundary surfaces further amplifies this effect, overall making harmonic solution significantly cheaper than the steady state mean flow solution. The steady state can be calculated only once, and then be used on multiple harmonic solutions with minimal cost. This advantage is completely negated when harmonic balance technique is utilized, since its implementation doesn't decompose unsteady flow into its steady and perturbing parts. The use of linearized harmonic methods, on external flow problems such as flutter, is overlooked, necessitating a revisit.

This research includes comprehensive revisit of the CFD theory, derivation, and implementation, later utilizing similar ideas to implement Linearized Harmonic numerical scheme for compressible flow simulations. It will delve into the fundamentals of compressible Euler equations, their discretization through the finite volume method, and the use of conserved flow variables. Later introducing complex flow variables and their conservation relations, and how they are implemented in complex domain conservative compressible flow governing equations. The work includes open forms of the underlying governing equations and their revised forms for seamless numerical implementation. This work, builds on top of the work done by Arash [21] where the governing equations are implemented used Steger-Warming-based flux vector splitting method [22] differing from other work in the literature of harmonic CFD methods, where use of central schemes such as Lax-Friedrich [23] are the norm. Formulations and implementation the harmonically oscillating moving wall boundaries are also provided, where different components in governing equations are discussed in detail.

The proposed method and boundary conditions are tested and validated, where their results are compared with experimental and analytical data. The validation test cases involve, unsteady aerodynamics cases for NACA012 and NACA64A010 airfoils where experimental results are available in literature, NACA012 being the defacto airfoil for flutter testing, with freely available experimental results [24]. After validating the proposed implementation, it had been used on canonical 2D vibration airfoil flutter case, where the results are compared with analytical predictions of Theodersen theory. In the flutter simulation runs, efficiency and the accuracy of the proposed method is successfully showcased.

1.5 The Outline

Chapter 1 - Introduction: This chapter lays the groundwork for the entire thesis by providing background information, outlining the problem statement, proposing methods and models to tackle the issue at hand, and presenting the unique contributions and novelties of this study.

Chapter 2 - Background on Euler Equations: An in-depth review of the Euler equations is presented, including its tensor and vector notations, and the integral form of the governing equations. The chapter then transitions into discussing how these equations are discretized for the Finite Volume Method. Overall purpose is to properly look through all the procedures in implementing a CFD solver, which will prove to be useful when we will do the same with implementing harmonic method.

Chapter 3 - Linearized Harmonic Method for Euler Equations: Building on the background established in the previous chapter, this chapter introduces the theory of the Linearized Harmonic Method, including the formulation of major perturbed flow variables. The discretization of harmonic governing equations is discussed, as well as the theory for boundary conditions. The chapter concludes with an outline of the numeric implementation of the linearized harmonic method.

Chapter 4 - Flutter Analysis via Harmonic Method: This chapter leverages the concepts from earlier sections to present a comprehensive approach to flutter analysis using the harmonic method. An iterative solution strategy, in this case, Newton's method, is outlined, with a specific focus on its application for a 2-degree of freedom airfoil.

Chapter 5 - Results and Discussions: The penultimate chapter presents the results and discussions from the application of methods described in earlier chapters. Various scenarios, including the pseudo steady state lift predictions, unsteady aerodynamics for a pitching airfoil, 2D flutter speed predictions, are presented and discussed.

Chapter 6 - Conclusion and Future Work: The final chapter will summarize the findings and contributions of this research. It will also discuss the implications of the results and suggest future research directions.

CHAPTER 2

BACKGROUND ON EULER EQUATIONS FOR CFD

The core equations governing a compressible Computational Fluid Dynamics (CFD) solver encompass the conservation laws of mass, momentum, and energy.

The Continuity Equation, representing the conservation of mass within a fluid, posits that the rate of density change within a control volume equals the negative divergence of the mass flux across its boundaries:

$$\frac{\partial \rho}{\partial t} + \nabla \cdot (\rho \mathbf{u}) = 0 \tag{2.1}$$

The Navier-Stokes Equations account for the conservation of momentum in a fluid. They connect the momentum change rate within a control volume to the pressure gradient, viscous forces, and any external forces acting on the fluid:

$$\frac{\partial (\rho \mathbf{u})}{\partial t} + \nabla \cdot (\rho \mathbf{u}\mathbf{u}^T) = -\nabla p + \nabla \cdot \tau + \mathbf{f} \tag{2.2}$$

The total energy equation represents the conservation of energy within a fluid. It describes the rate of change of total energy within a control volume as a result of heat conduction, work done by pressure and viscous forces, and external forces:

$$\frac{\partial (\rho E)}{\partial t} + \nabla \cdot (\rho E \mathbf{u} + p\mathbf{u}) = \nabla \cdot (\mathbf{q} + \tau \cdot \mathbf{u}) + \mathbf{f} \cdot \mathbf{u} \tag{2.3}$$

For inviscid flow, we consider a fluid with no viscosity, meaning that the viscous stress tensor τ and the heat flux vector $\mathbf{q}$ are set to zero. This simplification leads to the Euler equations:

Mass conservation (continuity equation):

$$\frac{\partial \rho}{\partial t} + \nabla \cdot (\rho \mathbf{u}) = 0 \tag{2.4}$$

Momentum conservation (Euler equations):

$$\frac{\partial (\rho \mathbf{u})}{\partial t} + \nabla \cdot (\rho \mathbf{u}\mathbf{u}^T) = -\nabla p + \mathbf{f} \tag{2.5}$$

Energy conservation (total energy equation):

$$\frac{\partial (\rho E)}{\partial t} + \nabla \cdot (\rho E \mathbf{u} + p\mathbf{u}) = \mathbf{f} \cdot \mathbf{u} \tag{2.6}$$

The Euler Equations portray the behavior of an inviscid, or frictionless, fluid. In this scenario, we disregard the impacts of viscosity and heat conduction, simplifying the problem and centering on the primary forces of pressure and external forces, such as gravity or body forces. These equations are extensively employed in computational fluid dynamics for modeling issues where viscosity effects are negligible or secondary compared to pressure and external forces.

2.1 Conservation-Law Form In Tensor Notation

While working with Cartesian coordinates (x, y, z), expressing the divergence of the flux tensor as the summation of three vectors, $\mathbf{F}$, $\mathbf{G}$, and $\mathbf{H}$, corresponding to the flux vectors in the x, y, and z directions respectively, proves convenient. This configuration enables an easier interpretation of the individual components and their interplay within the conservation law. The governing equation can thus be articulated as:

$$\frac{\partial \mathbf{U}}{\partial t} = -\nabla \cdot \mathbf{H} + \mathbf{S} \tag{2.7}$$

Here, the divergence of the flux tensor, $\nabla \cdot \mathbf{H}$, signifies the net flow of conserved variables entering or leaving the control volume. The term $\mathbf{S}$ represents a source term accounting for any additional processes that may alter the conserved variables, such as mass, momentum, or energy sources or sinks.

For compressible fluid simulations, the conserved variables vector and the flux tensor are defined as:

$$\mathbf{U} = \begin{bmatrix} \rho \\ \rho\mathbf{u} \\ \rho E \end{bmatrix} \tag{2.8}$$

$$\mathbf{H} = \begin{bmatrix} \rho\mathbf{u} \\ \rho\mathbf{u} \otimes \mathbf{u}^T + p\mathbf{I} \\ \rho E\mathbf{u} + p\mathbf{u} \end{bmatrix} \tag{2.9}$$

In this representation, $\mathbf{I}$ denotes the identity matrix. The conserved variables vector and the flux tensor are expressed in terms of the fluid's density ρ, velocity $\mathbf{u}$, pressure p, and total energy per unit mass E.

When working with Cartesian coordinates (x, y, z), the flux tensor can be explicitly written as:

$$\mathbf{H} = \begin{bmatrix} \rho u & \rho u^2 + p & \rho uv & \rho uw & u(E+p) \\ \rho v & \rho uv & \rho v^2 + p & \rho vw & v(E+p) \\ \rho w & \rho uw & \rho vw & \rho w^2 + p & w(E+p) \end{bmatrix} \tag{2.10}$$

This open-form expression of the flux tensor provides a clear view of the individual components and their interactions, which is valuable for understanding the underlying physics and developing numerical methods for solving the governing equations.

2.2 Conservation-Law form in Vector notation

When working with Cartesian coordinates (x, y, z), it is convenient to express the divergence of the flux tensor as the sum of three vectors, $\mathbf{F}$, $\mathbf{G}$, and $\mathbf{H}$, which correspond to the flux vectors in the x, y, and z directions, respectively. This form allows for easier interpretation of the individual components and their interactions within the conservation law. The governing equation can be written as:

$$\frac{\partial \mathbf{U}}{\partial t} = -\left(\frac{\partial \mathbf{F}}{\partial x} + \frac{\partial \mathbf{G}}{\partial y} + \frac{\partial \mathbf{H}}{\partial z}\right) + \mathbf{S} \tag{2.11}$$

Here, the flux vectors $\mathbf{F}$, $\mathbf{G}$, and $\mathbf{H}$ are defined as:

$$\mathbf{F} = \begin{bmatrix} \rho u \\ \rho u^2 + p \\ \rho uv \\ \rho uw \\ u(E+p) \end{bmatrix} \tag{2.12}$$

$$\mathbf{G} = \begin{bmatrix} \rho v \\ \rho uv \\ \rho v^2 + p \\ \rho vw \\ v(E+p) \end{bmatrix} \tag{2.13}$$

$$\mathbf{H} = \begin{bmatrix} \rho w \\ \rho uw \\ \rho vw \\ \rho w^2 + p \\ w(E+p) \end{bmatrix} \tag{2.14}$$

These flux vectors offer a clear representation of the conservation law, making it more straightforward to understand the underlying physics and develop numerical methods for solving the governing equations. Moreover, this vector notation explicitly shows the contribution of each spatial direction, providing insights into the conservation of mass, momentum, and energy in each dimension.

2.3 Integral Form of the Governing Equations

To apply the finite volume method, we need to convert the governing equations from their conservative form to integral form. This process involves integrating the governing equation over a control volume Ω, which is bounded by a control surface $\partial\Omega$. The integral form provides a more suitable representation for discretization, as it accounts for the conservation of quantities within the control volume.

First, we integrate both sides of the governing equation over the control volume Ω:

$$\frac{\partial}{\partial t}\int_{\Omega}\mathbf{U}d\Omega = -\int_{\Omega}\left(\frac{\partial\mathbf{F}}{\partial x}+\frac{\partial\mathbf{G}}{\partial y}+\frac{\partial\mathbf{H}}{\partial z}\right)d\Omega+\int_{\Omega}\mathbf{S}d\Omega \tag{2.15}$$

Next, we apply the divergence theorem to the second term on the right-hand side of the equation, which states that the volume integral of the divergence of a vector field is equal to the surface integral of the vector field itself. This results in:

$$\frac{\partial}{\partial t}\int_{\Omega}\mathbf{U}d\Omega = -\left(\oint_{\partial\Omega}\mathbf{F}\cdot\hat{\mathbf{n}}d\sigma+\oint_{\partial\Omega}\mathbf{G}\cdot\hat{\mathbf{n}}d\sigma+\oint_{\partial\Omega}\mathbf{H}\cdot\hat{\mathbf{n}}d\sigma\right)+\int_{\Omega}\mathbf{S}d\Omega \tag{2.16}$$

Here, $\hat{\mathbf{n}}$ is the outward unit normal vector to the control surface $\partial\Omega$, and $d\sigma$ is the differential surface area of the control surface.

The resulting equation is the integral form of the conservation law:

$$\frac{\partial}{\partial t}\int_{\Omega}\mathbf{U}d\Omega = -\oint_{\partial\Omega}(\mathbf{F}+\mathbf{G}+\mathbf{H})\cdot\hat{\mathbf{n}}d\sigma+\int_{\Omega}\mathbf{S}d\Omega \tag{2.17}$$

We can denote the term inside the surface integral as the net flux leaving through the surface $d\sigma$, which we define as $\vec{\mathbb{F}} = (\mathbf{F}+\mathbf{G}+\mathbf{H})$.

Now we have the integral form of the conservation law expressed in terms of volume and surface integrals over the control volume Ω and its bounding control surface $\partial\Omega$:

$$\frac{\partial}{\partial t}\int_{\Omega}\mathbf{U}d\Omega = -\oint_{\partial\Omega}\vec{\mathbb{F}}\cdot\hat{\mathbf{n}}d\sigma + \int_{\Omega}\widehat{\mathbf{S}}d\Omega \tag{2.18}$$

In this equation, the left-hand side corresponds to the time rate of change of the conserved variables $\mathbf{U}$ within the control volume Ω. The first term on the right-hand side is the net flux leaving through the control surface $\partial\Omega$, which is denoted as $\vec{\mathbb{F}}$. The dot product between $\vec{\mathbb{F}}$ and the outward unit normal vector $\hat{\mathbf{n}}$ determines the net amount of conserved quantities crossing the control surface. The integral over the control surface $\partial\Omega$ sums up the contributions of these fluxes. The second term on the right-hand side, $\int_{\Omega}\widehat{\mathbf{S}}d\Omega$, accounts for additional processes, such as sources or sinks, that can influence the conserved variables within the control volume.

2.4 Discretization of the Governing Equations for Finite Volume Method

To discretize the integral form of the conservation law for use in a finite volume solver, the following steps are taken, as they can be found in detail in Blazek's textbook [25]:

First, segment the computational domain into a series of distinct control volumes Ω_i. Taken together, these control volumes encompass the entirety of the domain.

Next, perform integration on the conservation equation over each individual control volume

$$\frac{\partial}{\partial t}\int_{\Omega_i}\mathbf{U}d\Omega = -\oint_{\partial\Omega_i}\vec{\mathbb{F}}\cdot\hat{\mathbf{n}}d\sigma + \int_{\Omega_i}\mathbf{S}d\Omega \tag{2.19}$$

Approximate the surface integral by summing the fluxes through each face of the control volume:

$$\frac{d\bar{\mathbf{U}}_i\Omega_i}{dt} = -\sum_{j=1}^{N_f}\vec{\mathbb{F}}_{ij}\cdot\hat{\mathbf{n}}_{ij}\Delta\sigma_{ij} + \bar{\mathbf{S}}_i\Delta\Omega_i \tag{2.20}$$

In this equation, $\bar{\mathbf{U}}_i$ and $\bar{\mathbf{S}}i$ are the average values of $\mathbf{U}$ and $\mathbf{S}$ over the control volume Ω_i, and $\Delta\Omega_i$ is the volume of the control volume. N_f is the number of faces in the control volume, $\vec{\mathbb{F}}ij$ is the net flux through the j-th face, $\hat{\mathbf{n}}ij$ is the outward unit normal vector to the j-th face, and $\Delta\sigma ij$ is the area of the j-th face.

We can write this equation as:

$$\frac{d\bar{\mathbf{U}}_i\Omega_i}{dt} = -\mathbb{R}(\bar{\mathbf{U}}_\mathbf{i}) \tag{2.21}$$

where $\mathbb{R}(\bar{\mathbf{U}}_\mathbf{i})$ the residual includes complete spatial discretization of fluxes along with the source term, and is a function of $\bar{\mathbf{U}}$

$$\mathbb{R}(\bar{\mathbf{U}}_\mathbf{i}) = \sum_{j=1}^{N_f}\vec{\mathbb{F}}_{ij}\cdot\hat{\mathbf{n}}_{ij}\Delta\sigma_{ij} - \bar{\mathbf{S}}_i\Omega_i \tag{2.22}$$

By discretizing the conservation law, we can create a system of algebraic equations that can be solved using numerical techniques. The finite volume method ensures that the conservation of physical quantities is maintained within each control volume during the solution process.

2.4.1 Explicit Temporal Discritization

To discretize the time derivative appearing in the discretized conservation law equation, an appropriate time integration scheme can be employed. Examples of these schemes include forward Euler, backward Euler, or more sophisticated methods like Runge-Kutta.

Focusing initially on the forward Euler method, we can express it as follows:

$$\frac{\bar{\mathbf{U}}i^{n+1} - \bar{\mathbf{U}}i^{n}}{\Delta t}\Omega_i = -\mathbb{R}(\bar{\mathbf{U}}_\mathbf{i})^n \tag{2.23}$$

where $\mathbb{R}(\bar{\mathbf{U}}_\mathbf{i})^n = \sum_{j=1}^{N_f} \vec{\mathbb{F}}_{ij}^n \cdot \hat{\mathbf{n}}_{ij}\Delta\sigma_{ij} - \bar{\mathbf{S}}_i^n\Omega_i$

In this equation, Δt is the time step size, and the superscripts n and $n+1$ denote the values at the current and next time levels, respectively. The residual $\mathbb{R}(\bar{\mathbf{U}}_\mathbf{i})^n$ is given by:

Next, we solve the discretized equation for $\bar{\mathbf{U}}_i^{n+1}$:

$$\bar{\mathbf{U}}i^{n+1} = \bar{\mathbf{U}}i^{n} + \frac{\Delta t}{\Omega_i}\left[-\sum_{j=1}^{N_f} \vec{\mathbb{F}}_{ij}^n \cdot \hat{\mathbf{n}}_{ij}\Delta\sigma_{ij} + \bar{\mathbf{S}}_i^n\Omega_i\right] \tag{2.24}$$

To compute the net flux, $\vec{\mathbb{F}}_{ij}^n$, across the faces of the control volume, we can adopt various numerical schemes. Examples of these schemes include central differencing, upwind schemes. In this work for the steady state solver, the Rieman Solver of Roe [26] is utilized where the detailed implementaion can be found in Toro's textbook [27].

The explicit temporal discretization method, as demonstrated, is simple to implement but may come with stability limitations. The shortcomings are that it can take very long to achieve steady state, or in some cases may even exhibit unstable behavior leading to nonsensical steady solutions.[28] For more robust and efficient solvers, implicit or semi-implicit time integration schemes must be utilized.

2.4.2 Implicit Temporal discritization

Implicit temporal discretization schemes, unlike explicit ones, evaluate the residual at the next time step, $t = n + 1$. While these schemes can offer increased stability compared to explicit ones, they typically require more computational resources, but also their higher stability allows for orders of magnitude larger time steps, overall leading to much faster convergence times. The following steps detail how to discretize the temporal derivative using an implicit scheme:

Starting with the spatially discretized conservation equation:

$$\frac{\Delta \bar{\mathbf{U}}_i}{\Delta t}\Omega_i = -\mathbb{R}(\bar{\mathbf{U}}_\mathbf{i})^{n+1} \tag{2.25}$$

Express the residual $\mathbb{R}(\bar{\mathbf{U}})^{n+1}$ in terms of flow variables at the current time step ${\mathbf{U}_\mathbf{i}}^n$. To do this, one can use the Taylor expansion of the residual $\mathbb{R}(\mathbf{U}^{n+1})$ around the current time step "n":

$$\mathbb{R}(\mathbf{U}^{n+1}) = \mathbb{R}(\mathbf{U}^n) + \left.\frac{\partial \mathbb{R}}{\partial \mathbf{U}}\right|_{\mathbf{U}^n} \Delta\mathbf{U} + O(\Delta\mathbf{U}^2)$$

$$\mathbb{R}(\mathbf{U}^{n+1}) \approx \mathbb{R}(\mathbf{U}^n) + \left.\frac{\partial \mathbb{R}}{\partial \mathbf{U}}\right|_{\mathbf{U}^n} \cdot \Delta\mathbf{U}$$

Here, $\frac{\partial \mathbb{R}}{\partial \mathbf{U}}$ is the Jacobian of the residual evaluated at the current time step.

Starting with the equation for the conservation law in the discretized form:

$$\Omega * \frac{\mathbf{U}^{n+1} - \mathbf{U}^n}{\Delta t} = -\mathbf{R}(\mathbf{U}^n) - \left.\frac{\partial \mathbb{R}}{\partial \mathbf{U}}\right|_{\mathbf{U}^n} \cdot \Delta\mathbf{U} \tag{2.26}$$

$$\frac{\Omega}{\Delta t}\Delta\mathbf{U} = -\mathbf{R}(\mathbf{U}^n) - \left.\frac{\partial \mathbb{R}}{\partial \mathbf{U}}\right|_{\mathbf{U}^n} \cdot \Delta\mathbf{U} \tag{2.27}$$

Rearrange the equation by collecting all terms with $\Delta\mathbf{U}$ to the left and isolating $\mathbf{R}(\mathbf{U}^n)$ on the right side of the equation:

$$\left[\frac{\Omega}{\Delta t}\mathbb{I} + \left.\frac{\partial \mathbb{R}}{\partial \mathbf{U}}\right|_{\mathbf{U}^n}\right] \cdot \Delta\mathbf{U} = -\mathbf{R}(\mathbf{U}^n) \tag{2.28}$$

In this equation, the main challenge when implementing an implicit scheme is the evaluation of the Jacobian $\frac{\partial \mathbf{R}}{\partial \mathbf{U}}(\mathbf{U}^n)$. Using the definition of the residual from equation 2.22, one can evaluate the flux Jacobian $\frac{\partial \mathbf{R}}{\partial \mathbf{U}}$ as:

$$\frac{\partial \mathbf{R}}{\partial \mathbf{U}} = \sum_{j=1}^{N_f} \left[\frac{\partial \left(\vec{\mathbb{F}}_j \cdot \hat{\mathbf{n}}_j \right)}{\partial \mathbf{U}} \right] \Delta \sigma_j \tag{2.29}$$

Assuming that the source term is not a function of flow variables $\mathbf{U}$, plugging equations 2.22 and 2.29 into eq. 2.28, the overall implicit scheme is obtained as:

$$\left[\frac{\Omega}{\Delta t} \mathbb{I} + \sum_{j=1}^{N_f} \left[\frac{\partial \left(\vec{\mathbb{F}}_j \cdot \hat{\mathbf{n}}_j \right)}{\partial \mathbf{U}} \Delta \sigma_j \right] \right] \cdot \Delta \mathbf{U} = - \sum_{j=1}^{N_f} \vec{\mathbb{F}}_j \cdot \hat{\mathbf{n}}_j \Delta \sigma_j + \bar{\mathbf{S}} \Omega \tag{2.30}$$

In this equation, we have combined the residual terms and the Jacobian of the residual terms with respect to the flow variables $\mathbf{U}$. The left-hand side of the equation contains the linearized system of equations, and the right-hand side has the residual terms and the source term $\bar{\mathbf{S}}$.

To solve the system, we need to determine the change in the flow variables $\Delta \mathbf{U}$. This can be done using various linear solvers [29], such as the Gauss-Seidel method, the Jacobi method. Once the $\Delta \mathbf{U}$ values are obtained, The solution can be updated as follows:

$$\mathbf{U}^{n+1} = \mathbf{U}^n + \Delta \mathbf{U}$$

The implicit scheme offers increased stability compared to explicit schemes, especially for problems with large time steps or when the solution exhibits strong gradients. The trade-off is the need to evaluate and invert the Jacobian matrix, which can be computationally expensive. However, the additional computational cost can be justified in many cases due to the improved stability properties of implicit schemes.

CHAPTER 3

LINEARIZED HARMONIC METHOD FOR EULER EQUATIONS

3.1 The Theory of Linearized Harmonic Method

In this section, the underpinning theory of the Linearized Harmonic Method is elaborated. This method is integral to the solver's main task, that is, to infuse harmonic disturbances into the computational domain using harmonic boundary conditions (BCs). The methodology unfolds in several key phases, each of which enhances understanding of its nuanced aspects. Overall scheme and its flowchart can be seen in 3.1

The initial phase entails the transformation of unsteady boundary conditions into harmonic BCs. This process involves transmuting time-variable boundary conditions into their harmonic equivalents. This transformation is typically accomplished by representing these boundary conditions as a collection of sinusoidal functions, often utilizing the Fourier series. The advantage of this transformation is two-fold: it simplifies the task by allowing operations within the frequency domain and replaces the need for dealing with time-dependent variables with harmonic variables.

Upon establishment of the harmonic BCs, the resolution of conserved harmonic variables within the domain proceeds. An implicit scheme, which considers both the harmonic and the flux terms (derived from the transformed boundary conditions), is employed to solve for these variables throughout the domain. The resolution of the linear system of equations thus formed results in the conserved harmonic flow variables at every point within the domain.

Following the resolution of the linear system, the conserved harmonic flow variables throughout the domain are attained. These variables embody the perturbations in the

flow quantities due to the imposed harmonic BCs. However, it's essential to note that these variables still exist in the frequency domain, making them unsuitable for direct application to time-domain analysis.

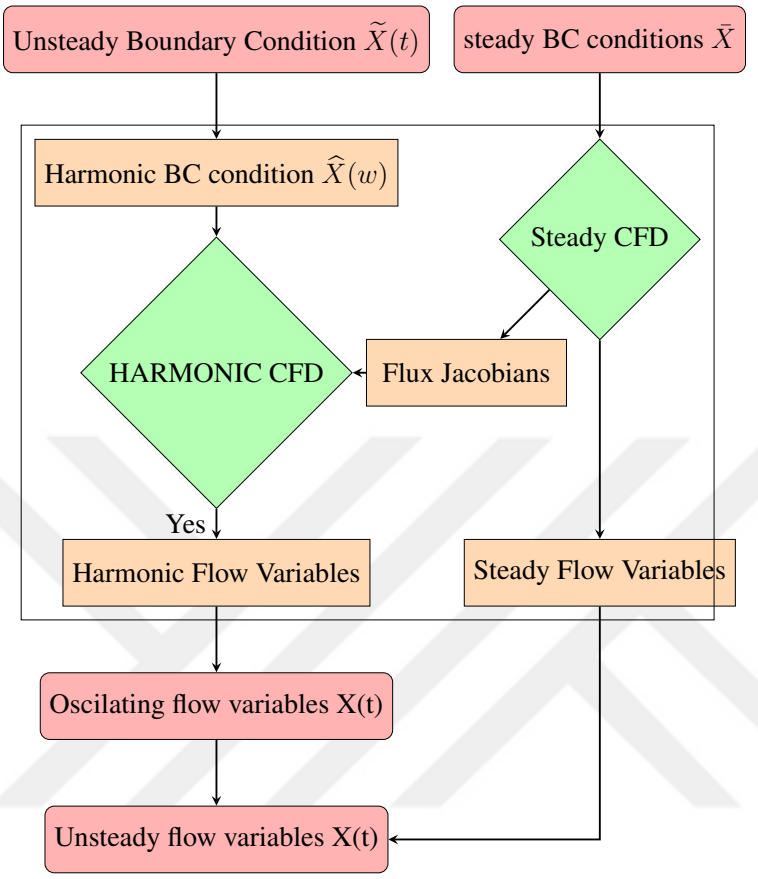

Figure 3.1: Harmonic Solver Flow Chart

The final phase involves converting the procured harmonic flow variables back into the time domain. This is achieved through the inverse transformation of the process applied initially. By translating the harmonic flow variables back into the time domain, the desired unsteady flow variables are obtained, enabling their use for further analysis or simulations. Further sections will provide an in-depth exploration of these steps, emphasizing their critical role in the Linearized Harmonic Method.

3.2 Formulations of Perturbed Flow Variables

In the linearized harmonic method, we express unsteady flow variables as the sum of their mean and unsteady components. This approach allows us to study the behavior of small disturbances around a steady state or a time-averaged mean flow. The harmonic schemes layout follows the scheme proposed by Arash(2019) [2]. The decomposition of the primitive flow variables is given by:

$$\begin{aligned}
\widehat{\rho}(x,y,z,t) &= \bar{\rho}(x,y,z) + \widetilde{\rho}(x,y,z,t) \\
\widehat{\mathbf{V}}(x,y,z,t) &= \bar{\mathbf{V}}(x,y,z) + \widetilde{\mathbf{V}}(x,y,z,t) \\
\widehat{p}(x,y,z,t) &= \bar{p}(x,y,z) + \widetilde{p}(x,y,z,t) \\
\widehat{T}(x,y,z,t) &= \bar{T}(x,y,z) + \widetilde{T}(x,y,z,t)
\end{aligned}$$

The primitive variables defined here are the independent flow variables describing the fluid state. The illustrative representation of the decomposition is also shown in figure 3.2.

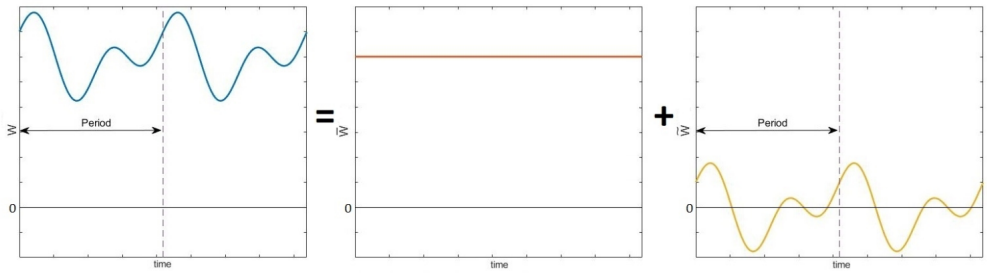

Figure 3.2: Mean and Perturbation Components Decomposition [2]

There are also dependent flow variables describing other physical properties of the fluid, they are derived from the independent primitive variables.

3.2.1 Formulation of Flow Speed Perturbation $\widetilde{|\vec{V}|}$

The flow speed perturbation is a function of steady flow speed $|\vec{V}|$ steady flow velocity $\vec{V}$ and perturbed flow velocity $\widetilde{V}$:

$$|\vec{V}| = \sqrt{\vec{V} \cdot \vec{V}}$$
$$\widetilde{|\vec{V}|} = \frac{1}{2\sqrt{\bar{V} \cdot \bar{V}}}(\bar{V} \cdot \widetilde{V} + \widetilde{V} \cdot \bar{V})$$

$$\widetilde{|\vec{V}|} = \frac{\bar{V} \cdot \widetilde{V}}{|\vec{V}|} \tag{3.1}$$

3.2.2 Formulation of Pressure Perturbation $\widetilde{p}$

Using the ideal gas assumption the pressure perturbations are found to be a function of steady density $\bar{\rho}$, steady temperature $\bar{T}$, perturbed density $\tilde{\rho}$ and perturbed temperature $\tilde{T}$:

$$\widehat{p} = \widehat{\rho} R \widehat{T}$$
$$(\bar{p} + \tilde{p}) = (\bar{\rho} + \tilde{\rho}) R (\bar{T} + \tilde{T})$$
$$(\bar{p} + \tilde{p}) = \cancel{\bar{\rho} R \bar{T}} + \bar{\rho} R \bar{T} + \tilde{\rho} R \bar{T} + \cancel{\tilde{\rho} R \tilde{T}}$$

$$\tilde{p} = \bar{\rho} R \tilde{T} + \tilde{\rho} R \bar{T} \tag{3.2}$$

3.2.3 Formulation of Momentum Perturbation $\widetilde{\mathbf{M}_{tot}}$

Momentum perturbation is derived as:

$$\mathbf{M}_{tot} = \rho \, \vec{V}$$

$$\widetilde{\mathbf{M}_{tot}} = \widetilde{\rho} \bar{V} + \bar{\rho} \widetilde{V} \tag{3.3}$$

3.2.4 Formulation of Total Energy Perturbation $\widetilde{E}_{tot}$

Total energy perturbation is derived as:

$$
\begin{aligned}
E_{tot} &= \rho \left(\frac{RT}{k-1} + \frac{|\vec{V}|}{2} \right) \\
\widetilde{E}_{tot} &= \widetilde{\rho}\bar{E}_{tot} + \bar{\rho} \left(\frac{R\widetilde{T}}{k-1} + \frac{\widetilde{|\vec{V}|}}{2} \right) \\
\widetilde{E}_{tot} &= \widetilde{\rho}\bar{E}_{tot} + \bar{\rho} \left(\frac{R\widetilde{T}}{k-1} + \frac{\bar{V} \cdot \widetilde{V}}{2|\bar{V}|} \right)
\end{aligned} \tag{3.4}
$$

3.3 Formulation of Harmonic Governing Equations

The governing equations for the conserved unsteady flow variables can be written in the integral form using the 2.18:

$$\frac{\partial}{\partial t}\int_{\Omega}\widehat{\mathbf{U}}d\Omega = -\oint_{\partial\Omega}\widehat{\mathbf{F}}\cdot\hat{\mathbf{n}}d\sigma + \int_{\Omega}\widehat{\mathbf{S}}d\Omega$$

The conserved unsteady flow variables vector, $\widehat{\mathbf{U}}$, is composed of the mean flow variables, $\bar{\mathbf{U}}$, and their unsteady counterparts, $\widetilde{\mathbf{U}}$:

$$\widehat{\mathbf{U}} \;=\; \bar{\mathbf{U}} \;+\; \widetilde{\mathbf{U}} \tag{3.5}$$

$$\begin{bmatrix}\hat{\mathbf{U}}_1\\ \hat{\mathbf{U}}_2\\ \hat{\mathbf{U}}_3\\ \hat{\mathbf{U}}_4\\ \hat{\mathbf{U}}_5\end{bmatrix} = \begin{bmatrix}\bar{\rho}\\ \rho\bar{u}\\ \rho\bar{v}\\ \rho\bar{w}\\ \rho\bar{e}\end{bmatrix} + \begin{bmatrix}\tilde{\rho}\\ \rho\tilde{u}+\tilde{\rho}\bar{u}\\ \tilde{\rho}\bar{v}+\tilde{v}\bar{\rho}\\ \tilde{\rho}\bar{w}+\tilde{w}\bar{\rho}\\ \tilde{\rho}\bar{e}+\tilde{e}\bar{\rho}\end{bmatrix} \tag{3.6}$$

In the above equation, the vector $\widehat{\mathbf{U}}$ constitutes both the mean flow variables, $\bar{\mathbf{U}}$, denoting the time-averaged behavior of the flow, and the unsteady flow variables, $\widetilde{\mathbf{U}}$, capturing the fluctuations around this mean state. The intention behind the linearized harmonic method is to examine the flow's response to minor disturbances, symbolized by the unsteady variables. This decomposition of flow variables fosters the analysis of interactions between the mean flow and the disturbances.

To advance further, the unsteady flux vector, $\widehat{\mathbf{F}}$, is linearized by expanding it around the mean flux vector, $\vec{\mathbb{F}}$, utilizing a Taylor series expansion. This strategy permits the approximation of the unsteady flux vector's behavior based on the mean state of the flow and the unsteady flow variables, $\widetilde{\mathbf{U}}$:

$$\widehat{\mathbf{F}} \;=\; \vec{\mathbb{F}} + \frac{\partial\vec{\mathbb{F}}}{\partial\mathbf{U}}\cdot\widetilde{\mathbf{U}} + O(\widetilde{\mathbf{U}}^2) \;\approx\; \vec{\mathbb{F}} + \frac{\partial\vec{\mathbb{F}}}{\partial\mathbf{U}}\cdot\widetilde{\mathbf{U}} \tag{3.7}$$

By substituting this linearized flux vector into the governing equation, one can obtain:

$$\frac{\partial}{\partial t}\int_{\Omega}\left(\bar{\mathbf{U}}+\widetilde{\mathbf{U}}\right)\,d\Omega=-\oint_{\partial\Omega}\left(\vec{\mathbb{F}}+\frac{\partial\vec{\mathbb{F}}}{\partial\mathbf{U}}\cdot\widetilde{\mathbf{U}}\right)\cdot\hat{\mathbf{n}}d\sigma+\int_{\Omega}\widehat{\mathbf{S}}d\Omega \tag{3.8}$$

The unsteady flux vector will be denoted as:

$$\widetilde{\mathbf{F}}=\left.\frac{\partial\vec{\mathbb{F}}}{\partial\mathbf{U}}\right|_{\bar{\mathbf{U}}}\widetilde{\mathbf{U}}=\left[\bar{\mathbf{J}}\right]\widetilde{\mathbf{U}} \tag{3.9}$$

Here, $\left[\bar{\mathbf{J}}\right]$ is the flux Jacobian matrix obtained from the steady flux terms, leading to linearized Euler equation:

$$\frac{\partial}{\partial t}\int_{\Omega}\left(\bar{\mathbf{U}}+\widetilde{\mathbf{U}}\right)\,d\Omega=-\oint_{\partial\Omega}\left(\vec{\mathbb{F}}+\widetilde{\mathbf{F}}\right)\cdot\hat{\mathbf{n}}d\sigma+\int_{\Omega}\widehat{\mathbf{S}}d\Omega \tag{3.10}$$

It is assumed that the perturbations imposed on the steady flow have a negligible effect on the mean state of the flow. This key assumption allows decoupling of the the mean and perturbed terms, making it possible solve them separately:

$$\frac{\partial}{\partial t}\int_{\Omega}\bar{\mathbf{U}}\,d\Omega=-\oint_{\partial\Omega}\vec{\mathbb{F}}\cdot\hat{\mathbf{n}}d\sigma+\int_{\Omega}\widehat{\mathbf{S}}d\Omega \tag{3.11}$$

$$\frac{\partial}{\partial t}\int_{\Omega}\widetilde{\mathbf{U}}\,d\Omega=-\oint_{\partial\Omega}\widetilde{\mathbf{F}}\cdot\hat{\mathbf{n}}d\sigma \tag{3.12}$$

The steady flow state, which is assumed to remain unaltered and taken as the mean flow state, is governed by:

$$\frac{\partial}{\partial t}\int_{\Omega}\bar{\mathbf{U}}\,d\Omega=-\oint_{\partial\Omega}\vec{\mathbb{F}}\cdot\hat{\mathbf{n}}d\sigma+\int_{\Omega}\widehat{\mathbf{S}}d\Omega$$

Using equation 3.9, calculating the harmonic fluxes from the mean state flux Jacobian:

$$\frac{\partial}{\partial t}\int_{\Omega}\widetilde{\mathbf{U}}\,d\Omega=-\oint_{\partial\Omega}\left(\left.\frac{\partial\vec{\mathbb{F}}}{\partial\mathbf{U}}\right|_{\bar{\mathbf{U}}}\widetilde{\mathbf{U}}\right)\cdot\hat{\mathbf{n}}d\sigma \tag{3.13}$$

Now the final simplification is made by modeling the perturbations as solely harmonic oscillations with a known frequency. Any perturbation $\widetilde{\mathbf{X}}$ will therefore be modeled as:

$$\widetilde{\mathbf{X}} = \widehat{\mathbf{X}} e^{i\omega t} \tag{3.14}$$

where:

$$\widehat{\mathbf{X}} = \mathbf{X}_{real} + i\, \mathbf{X}_{imag} = \mathbf{A}_X e^{i\Psi}$$

Using the harmonic perturbation assumption, rewriting equation 3.13 as:

$$\frac{\partial}{\partial t} \int_\Omega \widehat{\mathbf{U}} e^{i\omega t}\, d\Omega = - \oint_{\partial\Omega} \left(\frac{\partial \vec{\mathbb{F}}}{\partial \mathbf{U}} \bigg|_{\bar{\mathbf{U}}} \widehat{\mathbf{U}} e^{i\omega t} \right) \cdot \hat{\mathbf{n}} d\sigma \tag{3.15}$$

To simplify the equation, differentiating the left-hand side with respect to time using the chain rule:

$$\left(\frac{\partial}{\partial t} \int_\Omega \widehat{\mathbf{U}}\, d\Omega \right) e^{i\omega t} + \left(\int_\Omega \widehat{\mathbf{U}}\, d\Omega \right) iw\, e^{i\omega t} = - \oint_{\partial\Omega} \left(\frac{\partial \vec{\mathbb{F}}}{\partial \mathbf{U}} \bigg|_{\bar{\mathbf{U}}} \widehat{\mathbf{U}} \right) \cdot \hat{\mathbf{n}} d\sigma\, e^{i\omega t} \tag{3.16}$$

By eliminating the $e^{i\omega t}$ terms from both sides and rearranging the equations:

$$\frac{\partial}{\partial t} \int_\Omega \widehat{\mathbf{U}}\, d\Omega = -iw \int_\Omega \widehat{\mathbf{U}}\, d\Omega - \oint_{\partial\Omega} \left(\frac{\partial \vec{\mathbb{F}}}{\partial \mathbf{U}} \bigg|_{\bar{\mathbf{U}}} \widehat{\mathbf{U}} \right) \cdot \hat{\mathbf{n}} d\sigma \tag{3.17}$$

The right side of the equation forms the harmonic residual vector $\widetilde{\mathbf{R}}(\widehat{\mathbf{U}})$. The harmonic scheme can therefore be expressed as:

$$\frac{\partial}{\partial t} \int_\Omega \widehat{\mathbf{U}}\, d\Omega = -\widetilde{\mathbf{R}}(\widehat{\mathbf{U}}) \tag{3.18}$$

the harmonic residual vector $\widetilde{\mathbf{R}}(\widehat{\mathbf{U}})$ consists of two main components:

$$\widetilde{\mathbf{R}}(\widehat{\mathbf{U}}) = iw\int_{\Omega} \widehat{\mathbf{U}}\, d\Omega + \oint_{\partial\Omega} \left(\frac{\partial \vec{\mathbb{F}}}{\partial \mathbf{U}}\bigg|_{\bar{\mathbf{U}}} \widehat{\mathbf{U}} \right) \cdot \hat{\mathbf{n}} d\sigma \tag{3.19}$$

Upon a closer inspection, the two parts of the RHS vector each carry on a relevant physical meaning.

The first term shown in eq 3.20 represents the oscillatory nature of the conserved flow variables due to their harmonic behavior, with w being the frequency of oscillation. The imaginary unit i signifies that the oscillation is out of phase with the real part.

$$iw\int_{\Omega} \widehat{\mathbf{U}}\, d\Omega \tag{3.20}$$

The second term as shown in eq 3.21 represents the interaction between the perturbations and the mean flow state. It expresses how the flow perturbations are carried in the flow domain, by the same flux jacobians as the mean flow.

$$\oint_{\partial\Omega} \left(\frac{\partial \vec{\mathbb{F}}}{\partial \mathbf{U}}\bigg|_{\bar{\mathbf{U}}} \widehat{\mathbf{U}} \right) \cdot \hat{\mathbf{n}} d\sigma \tag{3.21}$$

Overall, The harmonic scheme described in equation (3.18) captures the balance between the time rate of change of the perturbation and the combined effects of the perturbation's oscillation and interaction with the mean flow. This mathematical framework allows for the study of the dynamic behavior of perturbations in a steady flow, providing solutions for the response of the flow to disturbances.

3.4 Discretization of harmonic governing equations

In this section, the discretization of the harmonic governing equations is examined, aimed at obtaining a numerical solution for the perturbation variables. The continuous equation (3.18) undergoes transformation into a discrete form, where the spatial and time discretizations are considered independently.

Initially, the spatial discretization of equation (3.18) is conducted, yielding:

$$\frac{\Delta\widehat{\mathbf{U}}\,\Omega}{\Delta t} = -\widetilde{\mathbf{R}}(\widehat{\mathbf{U}}) \tag{3.22}$$

where the discrete harmonic residual vector is given by:

$$\widetilde{\mathbf{R}}(\widehat{\mathbf{U}_\mathbf{i}}) = iw\Omega\widehat{\mathbf{U}_i} + \sum_{j=1}^{N_f}\left(\left.\frac{\partial\vec{\mathbb{F}}}{\partial\mathbf{U}}\right|_{\bar{\mathbf{U}}}\widehat{\mathbf{U}}_i\right)\cdot\hat{\mathbf{n}}_i\Delta\sigma_i \tag{3.23}$$

3.4.1 Explicit Temporal Discritization

Subsequently, the time derivative is discretized using a suitable time integration scheme, such as forward Euler, backward Euler, or a higher-order method like Runge-Kutta. For instance, utilizing the forward Euler method, the discretized equation is represented as:

$$\frac{\widehat{\mathbf{U}}i^{n+1} - \widehat{\mathbf{U}}i^{n}}{\Delta t}\Omega_i = -\widetilde{\mathbf{R}}(\widehat{\mathbf{U}})^n \tag{3.24}$$

In this equation, Δt represents the time step size, while the superscripts n and $n+1$ denote the values at the current and next time levels, respectively. The discretized equation is then solved for $\widehat{\mathbf{U}}i^{n+1}$, yielding:

$$\widehat{\mathbf{U}}i^{n+1} = \widehat{\mathbf{U}}i^{n} - \frac{\Delta t}{\Omega_i}\left[iw\Omega\widehat{\mathbf{U}}_i^n + \sum_{j=1}^{N_f}\left(\left.\frac{\partial\vec{\mathbb{F}}}{\partial\mathbf{U}}\right|_{\bar{\mathbf{U}}}\cdot\hat{\mathbf{n}}_i\Delta\sigma_i\right)\widehat{\mathbf{U}}_i^n\right] \tag{3.25}$$

Explicit time integration schemes, such as the forward Euler method, exhibit straightforward implementation and afford a convenient pathway to advance the solution in time. However, they introduce specific limitations, including the necessity for a sufficiently small time step to sustain stability. This requirement may amplify computational costs, especially for issues exhibiting high-frequency oscillations or stiff systems.

3.4.2 Implicit Temporal Discritization

With an implicit time integration scheme, the residual is evaluated at the subsequent time step, $t = n + 1$. This methodology possesses the advantage of unconditional stability, which allows for larger time steps relative to explicit schemes. Nevertheless, it demands the resolution of a system of equations at each time step, which may be computationally intensive.

To discretize the temporal derivative using an implicit scheme, the spatially discretized conservation equation is formulated as follows:

$$\frac{\Delta\widetilde{\mathbf{U}}_i}{\Delta t}\Omega_i = -\widetilde{\mathbf{R}}(\widehat{\mathbf{U}})^{n+1} \tag{3.26}$$

The challenge presented by the implementation of an implicit scheme resides in expressing the residual $\widetilde{\mathbf{R}}(\widehat{\mathbf{U}})^{n+1}$ in terms of flow variables at the current time step, $\widehat{\mathbf{U_i}^n}$. A Taylor expansion of the residual surrounding the current time step "n" is employed to approximate this expression:

$$\widetilde{\mathbf{R}}(\widehat{\mathbf{U}})^{n+1} = \widetilde{\mathbf{R}}(\widehat{\mathbf{U}})^{n} + \left.\frac{\partial\widetilde{\mathbf{R}}}{\partial\widehat{\mathbf{U}}}\right|_{\widehat{\mathbf{U}}^n} \cdot \Delta\widehat{\mathbf{U}} + O(\Delta\widehat{\mathbf{U}}^2) \tag{3.27}$$

$$\approx \widetilde{\mathbf{R}}(\widehat{\mathbf{U}})^{n} + \left.\frac{\partial\widetilde{\mathbf{R}}}{\partial\widehat{\mathbf{U}}}\right|_{\widehat{\mathbf{U}}^n} \cdot \Delta\widehat{\mathbf{U}} \tag{3.28}$$

By substituting this expression into the spatially discretized conservation equation and rearranging the terms, a system of equations is derived:

Plugging the equation 3.28 to equation 3.26 we obtain:

$$\frac{\Omega_i}{\Delta t}\Delta\widetilde{\mathbf{U}}_i = -\widetilde{\mathbf{R}}(\widehat{\mathbf{U}})^{n} - \left.\frac{\partial\widetilde{\mathbf{R}}}{\partial\widehat{\mathbf{U}}}\right|_{\widehat{\mathbf{U}}^n} \cdot \Delta\widehat{\mathbf{U}} \tag{3.29}$$

To collect all the terms with $\Delta\mathbf{U}$ to the left and isolate $\left.\frac{\partial\widetilde{\mathbf{R}}}{\partial\widehat{\mathbf{U}}}\right|_{\widehat{\mathbf{U}}^n}$) on the right side of the equation

$$\left[\frac{\Omega}{\Delta t}\mathbb{I} + \left.\frac{\partial\widetilde{\mathbf{R}}}{\partial\widehat{\mathbf{U}}}\right|_{\widehat{\mathbf{U}}^n}\right] \cdot \Delta\widehat{\mathbf{U}} = -\widetilde{\mathbf{R}}(\widehat{\mathbf{U}}^n) \tag{3.30}$$

The primary challenge of the implicit scheme implementation is evaluating the Jacobian $\frac{\partial \mathbf{R}}{\partial \mathbf{U}}(\mathbf{U}^n)$. This term signifies how the residual changes with respect to the flow variables $\mathbf{U}$. To compute the Jacobian, it is expanded using the definition of the residual from equation 3.23:

$$\frac{\partial \widetilde{\mathbf{R}}}{\partial \widehat{\mathbf{U}}} = \frac{\partial (iw\Omega \widehat{\mathbf{U}})}{\partial \widehat{\mathbf{U}}} + \frac{\partial \left(\sum_{j=1}^{N_f} \left(\frac{\partial \vec{\mathbb{F}}}{\partial \mathbf{U}} \Big|_{\bar{\mathbf{U}}} \widehat{\mathbf{U}} \right) \cdot \hat{\mathbf{n}} \Delta\sigma \right)}{\partial \widehat{\mathbf{U}}} \tag{3.31}$$

$$\frac{\partial \widetilde{\mathbf{R}}}{\partial \widehat{\mathbf{U}}} = (iw\Omega)\mathbb{I} + \sum_{j=1}^{N_f} \frac{\partial \vec{\mathbb{F}}}{\partial \mathbf{U}} \Big|_{\bar{\mathbf{U}}} \cdot \hat{\mathbf{n}} \Delta\sigma \tag{3.32}$$

In the harmonic implicit scheme, we have now combined the expanded Jacobian with the original implicit scheme equation to form a linear system. The equation 3.33 represents this linear system, which is a key step in the time-marching process:

$$\left[\frac{\Omega}{\Delta t}\mathbb{I} + (iw\Omega)\mathbb{I} + \sum_{j=1}^{N_f} \frac{\partial \vec{\mathbb{F}}}{\partial \mathbf{U}} \Big|_{\bar{\mathbf{U}}} \hat{\mathbf{n}} \Delta\sigma \right] \cdot \Delta\mathbf{U} = -iw\Omega \widehat{\mathbf{U}}_i^n - \sum_{j=1}^{N_f} \left(\frac{\partial \vec{\mathbb{F}}}{\partial \mathbf{U}} \Big|_{\bar{\mathbf{U}}} \widehat{\mathbf{U}}_i^n \right) \hat{\mathbf{n}}_i \Delta\sigma_i \tag{3.33}$$

This equation represents a matrix equation. The left-hand side consists of a linear combination of the time step Δt, the identity matrix $\mathbb{I}$, the harmonic term $(iw\Omega)$, and the sum of the flux terms that depend on the contributions from each face. The right-hand side consists of the harmonic term and the sum of the flux terms, both of which are calculated at the previous time step n.

The subsequent step involves solving this linear system to obtain the $\Delta\widehat{\mathbf{U}}$ values, representing the changes in the flow variables between consecutive time steps. This system's solution can be achieved using various linear algebra techniques, such as direct methods (e.g., LU decomposition) or iterative methods (e.g., conjugate gradient).

Once the $\Delta\widehat{\mathbf{U}}$ values are obtained, the solution can be updated to advance in time as follows:

$$\widehat{\mathbf{U}}^{n+1} = \widehat{\mathbf{U}}^n + \Delta\widehat{\mathbf{U}}$$

3.5 Theory for Boundary Conditions

3.5.1 Moving Wall Boundary Conditions

The moving wall boundary condition is a technique applied to enforce the no-penetration condition for fluid flow at the surface of a moving object, such as an airfoil. The no-penetration condition guarantees that there is no mass flow through the surface. The harmonic implementation follows the same methodology as the one introduced by Hall [7].

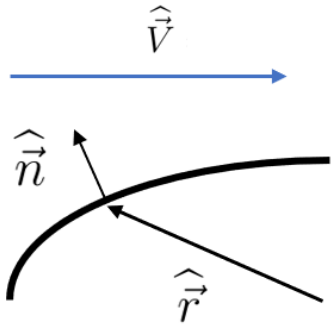

Figure 3.3: Moving Wall Variables

Mathematically, this condition can be expressed as:

$$\widehat{\vec{V}} \cdot \widehat{\vec{n}} - \frac{\partial \widehat{\vec{r}}}{\partial t} \cdot \widehat{\vec{n}} = 0 \tag{3.34}$$

As shown in 3.3, $\vec{r}$ represents the position vector that describes the location of the airfoil surface, $\vec{V}$ is the flow velocity vector, and $\vec{n}$ is the surface unit normal vector.

we first decompose the velocity, position, and normal vectors into their mean and perturbation components:

$$\widehat{\vec{V}} = \bar{\vec{V}} + \widetilde{\vec{V}}$$
$$\widehat{\vec{r}} = \bar{\vec{r}} + \widetilde{\vec{r}}$$
$$\widehat{\vec{n}} = \bar{\vec{n}} + \widetilde{\vec{n}}$$

Substituting these decomposed vectors into the no-penetration condition equation, we obtain:

$$(\bar{\vec{V}} + \widetilde{\vec{V}}) \cdot (\bar{\vec{n}} + \widetilde{\vec{n}}) = \frac{\partial(\bar{\vec{r}} + \widetilde{\vec{r}})}{\partial t} \cdot (\bar{\vec{n}} + \widetilde{\vec{n}}) \tag{3.35}$$

$$\cancel{\bar{\vec{V}} \cdot \bar{\vec{n}}} + \widetilde{\vec{V}} \cdot \bar{\vec{n}} + \bar{\vec{V}} \cdot \widetilde{\vec{n}} + \widetilde{\vec{V}} \cdot \widetilde{\vec{n}} = \cancel{\frac{\partial \bar{\vec{r}}}{\partial t} \cdot \bar{\vec{n}}} + \frac{\partial \widetilde{\vec{r}}}{\partial t} \cdot \bar{\vec{n}} + \frac{\partial \bar{\vec{r}}}{\partial t} \cdot \widetilde{\vec{n}} \tag{3.36}$$

$$\widetilde{\vec{V}} \cdot \bar{\vec{n}} + \bar{\vec{V}} \cdot \widetilde{\vec{n}} = \frac{\partial \widetilde{\vec{r}}}{\partial t} \cdot \bar{\vec{n}} + \cancel{\frac{\partial \bar{\vec{r}}}{\partial t} \cdot \widetilde{\vec{n}}} \tag{3.37}$$

Our goal is to find the perturbation velocity component $\widetilde{\vec{V}}$ that satisfies this equation. Rearranging the terms, we arrive at the expression for the perturbation velocity component:

$$\widetilde{\vec{V}} \cdot \bar{\vec{n}} = \frac{\partial \widetilde{\vec{r}}}{\partial t} \cdot \bar{\vec{n}} - \bar{\vec{V}} \cdot \widetilde{\vec{n}} + \cancel{\frac{\partial \bar{\vec{r}}}{\partial t} \cdot \widetilde{\vec{n}}} \tag{3.38}$$

$$\widetilde{\vec{V}} \cdot \bar{\vec{n}} \cdot \bar{\vec{n}} = (\frac{\partial \widetilde{\vec{r}}}{\partial t} \cdot \bar{\vec{n}} - (\bar{\vec{V}} \cdot \widetilde{\vec{n}})) \cdot \bar{\vec{n}} \tag{3.39}$$

$$\widetilde{\vec{V}} = \frac{\frac{\partial \widetilde{\vec{r}}}{\partial t} \cdot \cancel{(\bar{\vec{n}} \cdot \bar{\vec{n}})}}{\cancel{(\bar{\vec{n}} \cdot \bar{\vec{n}})}} - \frac{(\bar{\vec{V}} \cdot \widetilde{\vec{n}}) \cdot \bar{\vec{n}}}{(\bar{\vec{n}} \cdot \bar{\vec{n}})} \tag{3.40}$$

$$\widetilde{\vec{V}} = \frac{\partial \widetilde{\vec{r}}}{\partial t} - \frac{(\bar{\vec{V}} \cdot \widetilde{\vec{n}})}{(\bar{\vec{n}} \cdot \bar{\vec{n}})} \cdot \bar{\vec{n}} \tag{3.41}$$

We model perturbations as harmonic oscilations, hence use the expressions $\widetilde{\vec{r}} = \widehat{\vec{r}} e^{i\omega t}$, $\widetilde{\vec{V}} = \widehat{\vec{V}} e^{i\omega t}$, and $\widetilde{\vec{n}} = \widehat{\vec{n}} e^{i\omega t}$. Substituting these expressions into equation 3.41, we obtain:

$$\widehat{\vec{V}} e^{i\omega t} = \frac{\partial(\widehat{\vec{r}} e^{i\omega t})}{\partial t} - \frac{(\bar{\vec{V}} \cdot \widehat{\vec{n}} e^{i\omega t})}{(\bar{\vec{n}} \cdot \bar{\vec{n}})} \cdot \bar{\vec{n}} \tag{3.42}$$

Taking the time derivative and simplifying, we arrive at the following expression for the complex velocity $\widehat{\vec{V}}$:

$$\widehat{\vec{V}} e^{i\omega t} = iw\widehat{\vec{r}} e^{i\omega t} - \frac{(\bar{\vec{V}} \cdot \widehat{\vec{n}})}{(\bar{\vec{n}} \cdot \bar{\vec{n}})} \cdot \bar{\vec{n}} e^{i\omega t} \tag{3.43}$$

$$\widehat{\vec{V}} = iw\widehat{\vec{r}} - \frac{(\bar{\vec{V}} \cdot \widehat{\vec{n}})}{(\bar{\vec{n}} \cdot \bar{\vec{n}})} \cdot \bar{\vec{n}} \tag{3.44}$$

In this expression, w symbolizes the angular frequency of the harmonic perturbation, i is the imaginary unit, and $e^{i\omega t}$ represents the complex exponential function. The complex velocity $\widehat{\vec{V}}$ describes the velocity we wish to impose on the boundary faces that are undergoing harmonic motion.

The two terms on the right side of the equation have distinct physical interpretations.

The first term which is $iw\widehat{\vec{r}}$, accounts for the velocity of the boundary due to its harmonic movement. This term captures the effect of the boundary face oscillation impinging on the flow field. This term is also named as the direct velocity component.

$$\widehat{\vec{V}}^{direct} = \frac{\partial \widehat{\vec{r}}}{\partial t}$$

the second term which is $\frac{(\bar{\vec{V}} \cdot \widehat{\vec{n}})}{(\bar{\vec{n}} \cdot \bar{\vec{n}})} \cdot \bar{\vec{n}}$, represents the component of the mean flow velocity $\bar{\vec{V}}$ projected onto the perturbation of normal vector. $\widehat{\vec{n}}$, representing the effect the change in face normal has on the flow.

$$\widehat{\vec{V}}^{\Delta \vec{n}} = \frac{(\bar{\vec{V}} \cdot \widehat{\vec{n}})}{(\bar{\vec{n}} \cdot \bar{\vec{n}})} \cdot \bar{\vec{n}}$$

CHAPTER 4

LINEARIZED HARMONIC METHOD NUMERICAL IMPLEMENTATION

4.1 Conserved Harmonic Flow Variables

The primitive variable vector, denoted as $\widetilde{\mathbf{W}}$, consists of 10 variables. The first half, $\widetilde{\mathbf{W}}re$, comprises the real part of the primitive variables, while the remaining five, $\widetilde{\mathbf{W}}im$, contain the imaginary part of these variables.These primitive variables are defined based on the equation 3.6, with each element having both a real and an imaginary part to account for the complex nature of harmonic variables.

$$\widetilde{\mathbf{U}} = \begin{bmatrix} \widetilde{\mathbf{U}}_1 \\ \widetilde{\mathbf{U}}_2 \\ \widetilde{\mathbf{U}}_3 \\ \widetilde{\mathbf{U}}_4 \\ \widetilde{\mathbf{U}}_5 \end{bmatrix} = \begin{bmatrix} \widehat{\mathbf{U}}_1 \\ \widehat{\mathbf{U}}_2 \\ \widehat{\mathbf{U}}_3 \\ \widehat{\mathbf{U}}_4 \\ \widehat{\mathbf{U}}_5 \end{bmatrix} e^{i\omega t} = \begin{bmatrix} \tilde{\rho} \\ \rho\tilde{u} + \tilde{\rho}\bar{u} \\ \tilde{\rho}\bar{v} + \tilde{v}\bar{\rho} \\ \tilde{\rho}\bar{w} + \tilde{w}\bar{\rho} \\ \tilde{\rho}\bar{e} + \tilde{e}\bar{\rho} \end{bmatrix} e^{i\omega t} \tag{4.1}$$

However, due to their complex nature, these harmonic variables can pose challenges for numerical computations. Therefore, it's necessary to decompose them into their real and imaginary components to ease the process of numerical implementation. This decomposition allows us to handle these variables in a real-number framework, simplifying numerical operations and potentially improving computational efficiency.

$$\widehat{\mathbf{U}} = \begin{bmatrix} \widehat{\mathbf{U}}_1 \\ \widehat{\mathbf{U}}_2 \\ \widehat{\mathbf{U}}_3 \\ \widehat{\mathbf{U}}_4 \\ \widehat{\mathbf{U}}_5 \end{bmatrix} = \begin{bmatrix} \widehat{\mathbf{U}}_1^{real} + i\,\widehat{\mathbf{U}}_1^{imag} \\ \widehat{\mathbf{U}}_2^{real} + i\,\widehat{\mathbf{U}}_2^{imag} \\ \widehat{\mathbf{U}}_3^{real} + i\,\widehat{\mathbf{U}}_3^{imag} \\ \widehat{\mathbf{U}}_4^{real} + i\,\widehat{\mathbf{U}}_4^{imag} \\ \widehat{\mathbf{U}}_5^{real} + i\,\widehat{\mathbf{U}}_5^{imag} \end{bmatrix} \tag{4.2}$$

For the numerical scheme implementation, the vector of 5 complex variables is converted into a vector of 10 variables as follows:

$$\widehat{\mathbf{U}} = \left\{ \begin{array}{l} \left\{ \begin{array}{l} \widehat{\mathbf{U}}_1^{real} \\ \widehat{\mathbf{U}}_2^{real} \\ \widehat{\mathbf{U}}_3^{real} \\ \widehat{\mathbf{U}}_4^{real} \\ \widehat{\mathbf{U}}_5^{real} \end{array} \right\} \\ i \left\{ \begin{array}{l} \widehat{\mathbf{U}}_1^{imag} \\ \widehat{\mathbf{U}}_2^{imag} \\ \widehat{\mathbf{U}}_3^{imag} \\ \widehat{\mathbf{U}}_4^{imag} \\ \widehat{\mathbf{U}}_5^{imag} \end{array} \right\} \end{array} \right\} \tag{4.3}$$

This representation allows us to track the real and imaginary parts of the complex variables separately throughout the solution process. It simplifies computations and facilitates the implementation of the harmonic solver scheme. The solver will use this definition of conserved variables to analyze how the real and imaginary parts of the complex variables change as the solution evolves.

4.2 Linearized Harmonic Solution methodology

The harmonic solver is a numerical method used to solve fluid flow problems. It operates by first obtaining a steady-state solution, which provides the steady flux Jacobians. These are then used to calculate harmonic intercell fluxes, which represent the exchange of quantities between neighboring cells in the computational domain. The flow variables are updated iteratively using one of two temporal schemes: explicit or implicit.

The structure of the harmonic solver can be visualized in the given figure, which represents the steps in the solver process.

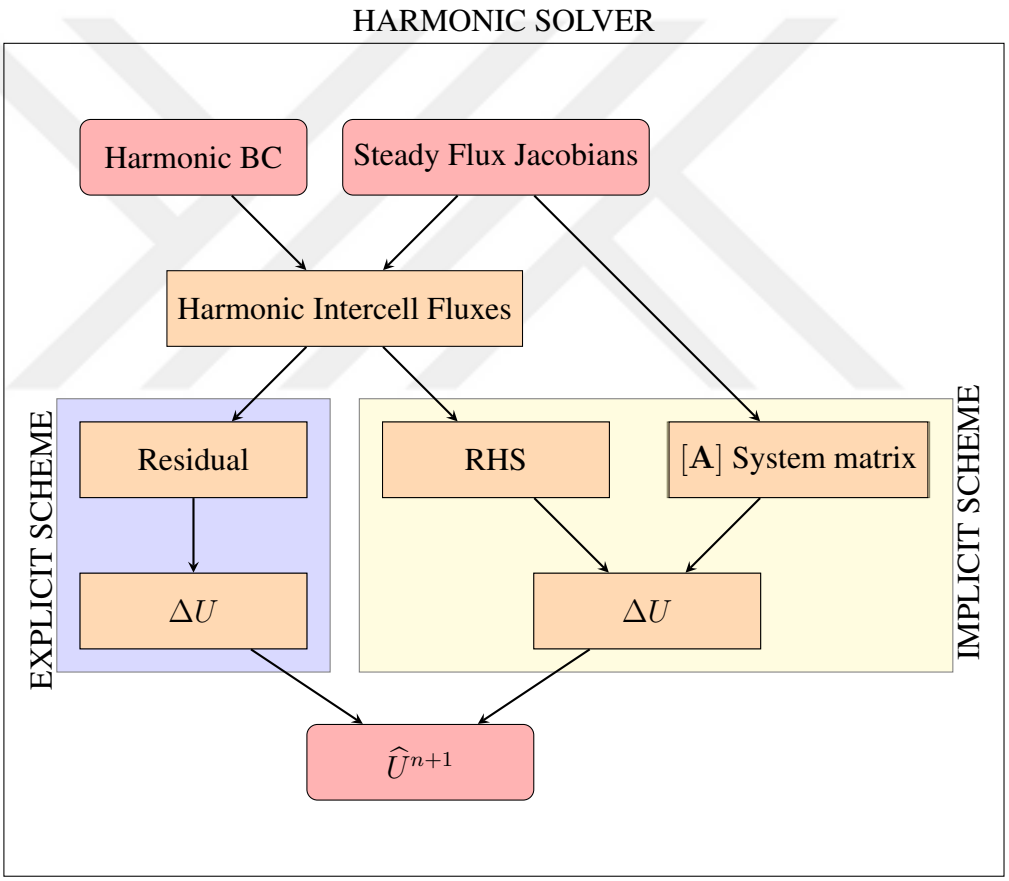

Figure 4.1: A caption for my figure.

- Harmonic BC: Boundary conditions are imposed on the computational domain.
- Steady Flux Jacobians: These are derived from the steady-state solution, providing information about the flow's sensitivity to changes in the conserved variables.
- Harmonic Intercell Fluxes: These are computed using the harmonic boundary conditions and steady flux Jacobians to describe the exchange of quantities between neighboring cells.

Depending on the chosen temporal scheme, the next steps differ. In explicit schemes:

- Residual: The difference between the harmonic intercell fluxes and the current flow state is calculated.
- ΔU: The flow variables are updated directly using the residual, which represents the rate of change of the conserved variables.

But in implicit schemes:

- RHS: The right-hand side of the linear system of equations is calculated using the harmonic intercell fluxes.
- $[\mathbf{A}]$ System matrix: The harmonic system matrix, representing the linear relationship between the flow variables and their rates of change, is assembled.
- ΔU: The linear system is solved iteratively to obtain the changes in the flow variables.

Finally, the updated flow variables are combined to obtain the new flow state, $\widehat{U}^{n+1}$, for the next iteration. This process is repeated until convergence is achieved or a specified number of iterations is reached.

4.3 Explicit Scheme Implementation

In this section, the explicit scheme implementation for the harmonic solver is explained. The explicit scheme updates the flow variables directly based on the current flow state. The equation for the explicit scheme is given as follows:

$$\widehat{\mathbf{U}}i^{n+1} = \widehat{\mathbf{U}}i^{n} - \frac{\Delta t}{\Omega_i}\widetilde{\mathbf{R}}(\widehat{\mathbf{U}})^{n}$$

$$\widehat{\mathbf{U}}i^{n+1} = \widehat{\mathbf{U}}i^{n} - \frac{\Delta t}{\Omega_i}\left[iw\Omega\widehat{\mathbf{U}}_i^{n} + \sum_{j=1}^{N_f}\left(\frac{\partial\vec{\mathbb{F}}}{\partial\mathbf{U}}\bigg|_{\bar{\mathbf{U}}}\widehat{\mathbf{U}}_i^{n}\right)\cdot\hat{\mathbf{n}}_i\Delta\sigma_i\right]$$

In this equation, $\widehat{\mathbf{U}}i^{n+1}$ represents the updated harmonic conserved variables at the $(n+1)$-th time step, while $\widehat{\mathbf{U}}i^{n}$ denotes the variables at the n th time step. Δt is the time step, and Ω_i is the cell volume. The Residual term consists of two parts:

The first part as shown in eq 4.4 accounts for the harmonic oscillation in the flow variables due to the frequency w.

$$iw\Omega\widehat{\mathbf{U}}_i^{n} \tag{4.4}$$

The second part as shown in eq 4.5 represents the contribution of the harmonic inter-cell fluxes.

$$\sum_{j=1}^{N_f}\left(\frac{\partial\vec{\mathbb{F}}}{\partial\mathbf{U}}\bigg|\bar{\mathbf{U}}\widehat{\mathbf{U}}i^{n}\right)\cdot\hat{\mathbf{n}}_i\Delta\sigma i \tag{4.5}$$

The harmonic conserved variable vector $\widehat{\mathbf{U}}_i^{n}$ is a complex vector with real and imaginary parts as defined in eq 4.3. The harmonic flux Jacobian, derived from the steady flux Jacobians, is a 10x10 matrix that can be split into two 5x5 blocks, one for the real part and another for the imaginary part.

$$\left[\mathbf{Jacobian}\right]_{10x10} = \begin{bmatrix} \left[\frac{\partial\vec{\mathbb{F}}}{\partial\bar{\mathbf{U}}}\bigg|_{\bar{\mathbf{U}}}\cdot\hat{\mathbf{n}}_i\Delta\sigma_i\right]_{5x5} & \begin{bmatrix} 0 & \cdots \\ \cdots & 0 \end{bmatrix}_{5x5} \\ \begin{bmatrix} 0 & \ddots \\ \cdots & 0 \end{bmatrix}_{5x5} & \left[\frac{\partial\vec{\mathbb{F}}}{\partial\bar{\mathbf{U}}}\bigg|_{\bar{\mathbf{U}}}\cdot\hat{\mathbf{n}}_i\Delta\sigma_i\right]_{5x5} \end{bmatrix}_{10x10} \tag{4.6}$$

The implementation of explicit harmonic scheme, from the eq. 3.25 can then be obtained as follows:

$$\left\{\begin{array}{c}\left\{\begin{array}{c}\vdots\\ \widehat{\mathbf{U}}^{re}\\ \vdots\end{array}\right\}\\ i\left\{\begin{array}{c}\vdots\\ \widehat{\mathbf{U}}^{im}\\ \vdots\end{array}\right\}\end{array}\right\}^{\boldsymbol{n+1}} = \left\{\begin{array}{c}\left\{\begin{array}{c}\vdots\\ \widehat{\mathbf{U}}^{re}\\ \vdots\end{array}\right\}\\ i\left\{\begin{array}{c}\vdots\\ \widehat{\mathbf{U}}^{im}\\ \vdots\end{array}\right\}\end{array}\right\}^{\boldsymbol{n}} - \frac{\Delta t}{\Omega}\left[\begin{array}{c} iw\Omega\left\{\begin{array}{c}\left\{\begin{array}{c}\vdots\\ \widehat{\mathbf{U}}^{re}\\ \vdots\end{array}\right\}\\ i\left\{\begin{array}{c}\vdots\\ \widehat{\mathbf{U}}^{im}\\ \vdots\end{array}\right\}\end{array}\right\}^{\boldsymbol{n}} + \left[\mathbf{Jacobian}\right]\left\{\begin{array}{c}\left\{\begin{array}{c}\vdots\\ \widehat{\mathbf{U}}^{re}\\ \vdots\end{array}\right\}\\ i\left\{\begin{array}{c}\vdots\\ \widehat{\mathbf{U}}^{im}\\ \vdots\end{array}\right\}\end{array}\right\}^{\boldsymbol{n}}\end{array}\right] \tag{4.7}$$

$$\left\{\begin{array}{c}\left\{\begin{array}{c}\vdots\\ \widehat{\mathbf{U}}^{re}\\ \vdots\end{array}\right\}\\ i\left\{\begin{array}{c}\vdots\\ \widehat{\mathbf{U}}^{im}\\ \vdots\end{array}\right\}\end{array}\right\}^{\boldsymbol{n+1}} = \left\{\begin{array}{c}\left\{\begin{array}{c}\vdots\\ \widehat{\mathbf{U}}^{re}\\ \vdots\end{array}\right\}\\ i\left\{\begin{array}{c}\vdots\\ \widehat{\mathbf{U}}^{im}\\ \vdots\end{array}\right\}\end{array}\right\}^{\boldsymbol{n}} - \frac{\Delta t}{\Omega}\left[\begin{array}{c} w\Omega\left\{\begin{array}{c}-\left[\begin{array}{c}\vdots\\ \widehat{\mathbf{U}}^{im}\\ \vdots\end{array}\right]\\ i\left[\begin{array}{c}\vdots\\ \widehat{\mathbf{U}}^{re}\\ \vdots\end{array}\right]\end{array}\right\}^{\boldsymbol{n}} + \left[\mathbf{Jacobian}\right]\left\{\begin{array}{c}\left\{\begin{array}{c}\vdots\\ \widehat{\mathbf{U}}^{re}\\ \vdots\end{array}\right\}\\ i\left\{\begin{array}{c}\vdots\\ \widehat{\mathbf{U}}^{im}\\ \vdots\end{array}\right\}\end{array}\right\}^{\boldsymbol{n}}\end{array}\right] \tag{4.8}$$

This leads us to the solution algorithm for acquiring the harmonic conserved variables at the subsequent time step.

$$\left\{\begin{array}{c}\vdots\\ \widehat{\mathbf{U}}^{re}\\ \vdots\end{array}\right\}^{\boldsymbol{n+1}} = \left\{\begin{array}{c}\vdots\\ \widehat{\mathbf{U}}^{re}\\ \vdots\end{array}\right\}^{\boldsymbol{n}} - \frac{\Delta t}{\Omega}\left[\begin{array}{c} -w\Omega\left\{\begin{array}{c}\vdots\\ \widehat{\mathbf{U}}^{im}\\ \vdots\end{array}\right\}^{\boldsymbol{n}} + \left[\left.\frac{\partial\vec{\mathbb{F}}}{\partial\mathbf{U}}\right|_{\bar{\mathbf{U}}}\cdot\hat{\mathbf{n}}_i\Delta\sigma_i\right]\left\{\begin{array}{c}\vdots\\ \widehat{\mathbf{U}}^{re}\\ \vdots\end{array}\right\}^{\boldsymbol{n}}\end{array}\right] \tag{4.9}$$

$$\left\{\begin{array}{c}\vdots\\ \widehat{\mathbf{U}}^{im}\\ \vdots\end{array}\right\}^{\boldsymbol{n+1}} = \left\{\begin{array}{c}\vdots\\ \widehat{\mathbf{U}}^{im}\\ \vdots\end{array}\right\}^{\boldsymbol{n}} - \frac{\Delta t}{\Omega}\left[\begin{array}{c} w\Omega\left\{\begin{array}{c}\vdots\\ \widehat{\mathbf{U}}^{re}\\ \vdots\end{array}\right\}^{\boldsymbol{n}} + \left[\left.\frac{\partial\vec{\mathbb{F}}}{\partial\mathbf{U}}\right|_{\bar{\mathbf{U}}}\cdot\hat{\mathbf{n}}_i\Delta\sigma_i\right]\left\{\begin{array}{c}\vdots\\ \widehat{\mathbf{U}}^{im}\\ \vdots\end{array}\right\}^{\boldsymbol{n}}\end{array}\right] \tag{4.10}$$

4.4 Implicit Scheme implementation

The implicit scheme implementation aims to overcome the stability limitations of the explicit scheme by incorporating the time step Δt into the equation directly. From equation 3.33:

$$\left[\frac{\Omega}{\Delta t}\mathbb{I} + \left.\frac{\partial \widetilde{\mathbf{R}}}{\partial \widehat{\mathbf{U}}}\right|_{\widehat{\mathbf{U}}^n}\right] \cdot \Delta\widehat{\mathbf{U}} = -\widetilde{\mathbf{R}}(\widehat{\mathbf{U}}^n)$$

$$\left[\frac{\Omega}{\Delta t}\mathbb{I} + (iw\Omega)\mathbb{I} \;+\; \sum_{j=1}^{N_f} \left.\frac{\partial \vec{\mathbb{F}}}{\partial \mathbf{U}}\right|_{\bar{\mathbf{U}}} \cdot \hat{\mathbf{n}}\Delta\sigma\right] \cdot \Delta\widehat{\mathbf{U}} = -iw\Omega\widehat{\mathbf{U}}_i^n - \sum_{j=1}^{N_f}\left(\left.\frac{\partial \vec{\mathbb{F}}}{\partial \mathbf{U}}\right|_{\bar{\mathbf{U}}} \widehat{\mathbf{U}}_i^n\right) \cdot \hat{\mathbf{n}}_i\Delta\sigma_i$$

This can be written as a linear system:

$$[\mathbf{A}] \cdot \left\{\Delta\widehat{\mathbf{U}}\right\} = \left\{\widehat{RHS}\right\} \tag{4.11}$$

Where system matrix $[\mathbf{A}]$ is:

$$[\mathbf{A}] = \left[\frac{\Omega}{\Delta t}\mathbb{I} + (iw\Omega)\mathbb{I} \;+\; \sum_{j=1}^{N_f} \left.\frac{\partial \vec{\mathbb{F}}}{\partial \mathbf{U}}\right|_{\bar{\mathbf{U}}} \cdot \hat{\mathbf{n}}\Delta\sigma\right] \tag{4.12}$$

Right hand side vector is:

$$\left\{\widehat{RHS}\right\} = -iw\Omega\widehat{\mathbf{U}}_i^n - \sum_{j=1}^{N_f}\left(\left.\frac{\partial \vec{\mathbb{F}}}{\partial \mathbf{U}}\right|_{\bar{\mathbf{U}}} \widehat{\mathbf{U}}_i^n\right) \cdot \hat{\mathbf{n}}_i\Delta\sigma_i \tag{4.13}$$

4.4.1 Implementation of System Matrix [A]

The discretization of System Matrix A is derived from equation 4.12. Starting with the left hand side of the equation:

$$[\mathbf{A}]\left\{\Delta\mathbf{U}\right\} = \left[\frac{\Omega}{\Delta t}\begin{bmatrix}[I] & \ddots \\ \ddots & [I]\end{bmatrix} + (iw\Omega)\begin{bmatrix}[I] & \ddots \\ \ddots & [I]\end{bmatrix} + \left[\mathbf{Jacobian}\right]\right] \cdot \left\{\begin{array}{c}\left\{\begin{array}{c}\vdots \\ \Delta\widehat{\mathbf{U}}^{re} \\ \vdots\end{array}\right\} \\ i\left\{\begin{array}{c}\vdots \\ \Delta\widehat{\mathbf{U}}^{im} \\ \vdots\end{array}\right\}\end{array}\right\} \tag{4.14}$$

$$[\mathbf{A}]\left\{\Delta\mathbf{U}\right\} = \left[\frac{\Omega}{\Delta t}\begin{bmatrix}[I] & \ddots \\ \ddots & [I]\end{bmatrix} + (w\Omega)\begin{bmatrix}\ddots & -[I] \\ [I] & \ddots\end{bmatrix} + \left[\mathbf{Jacobian}\right]\right] \cdot \left\{\begin{array}{c}\left\{\begin{array}{c}\vdots \\ \Delta\widehat{\mathbf{U}}^{re} \\ \vdots\end{array}\right\} \\ i\left\{\begin{array}{c}\vdots \\ \Delta\widehat{\mathbf{U}}^{im} \\ \vdots\end{array}\right\}\end{array}\right\} \tag{4.15}$$

To simplify the implementation, we move the off-diagonal terms to the outside of the system matrix using values from the previous time step. This decouples the real parts of the system matrix from the imaginary parts, allows solving two decoupled systems of size 5x5 instead of one 10x10 system.

$$[\mathbf{A}]\left\{\Delta\mathbf{U}\right\}^{n} = \left[\frac{\Omega}{\Delta t}\begin{bmatrix}[I] & \ddots \\ \ddots & [I]\end{bmatrix} + \left[\mathbf{Jacobian}\right]\right]\left\{\begin{array}{c}\left\{\begin{array}{c}\vdots \\ \Delta\widehat{\mathbf{U}}^{re} \\ \vdots\end{array}\right\} \\ i\left\{\begin{array}{c}\vdots \\ \Delta\widehat{\mathbf{U}}^{im} \\ \vdots\end{array}\right\}\end{array}\right\}^{n} + w\Omega\left\{\begin{array}{c}\left\{\begin{array}{c}\vdots \\ -\Delta\widehat{\mathbf{U}}^{im} \\ \vdots\end{array}\right\} \\ i\left\{\begin{array}{c}\vdots \\ \Delta\widehat{\mathbf{U}}^{re} \\ \vdots\end{array}\right\}\end{array}\right\}^{n-1} \tag{4.16}$$

The underlined portion will be moved to the RHS of the equation. What we essentially achieved is a significant reduction in computational times (up to 40 percent) by solving the real and imaginary 5x5 systems sequentially instead of solving a fully coupled 10x10 system.

$$\begin{bmatrix} \begin{bmatrix} A_{diagonal} \end{bmatrix} & -\begin{bmatrix} w\Omega\,[I] \end{bmatrix} \\ \begin{bmatrix} w\Omega\,[I] \end{bmatrix} & \begin{bmatrix} A_{diagonal} \end{bmatrix} \end{bmatrix} \left\{\Delta\hat{\mathbf{U}}\right\} = \left\{\widehat{RHS}\right\}$$

$$\begin{bmatrix} \begin{bmatrix} A_{diagonal} \end{bmatrix} & \ddots \\ \ddots & \begin{bmatrix} A_{diagonal} \end{bmatrix} \end{bmatrix} \left\{\Delta\hat{\mathbf{U}}\right\} = \left\{\widehat{RHS}\right\} + (Simplification\ Term)$$

Hence, the simplified System Matrix A is obtained as:

$$[A_{simplified}] = \begin{bmatrix} \begin{bmatrix} A_{diagonal} \end{bmatrix} & \ddots \\ \ddots & \begin{bmatrix} A_{diagonal} \end{bmatrix} \end{bmatrix}$$

$$[A_{simplified}] = \begin{bmatrix} \dfrac{\Omega}{\Delta t} \begin{bmatrix} [I] & \ddots \\ \ddots & [I] \end{bmatrix} + \begin{bmatrix} \left[\dfrac{\partial\vec{\mathbb{F}}}{\partial\mathbf{U}}\Big|_{\bar{\mathbf{U}}} \cdot \hat{\mathbf{n}}_i \Delta\sigma_i\right] & \ddots \\ \ddots & \left[\dfrac{\partial\vec{\mathbb{F}}}{\partial\mathbf{U}}\Big|_{\bar{\mathbf{U}}} \cdot \hat{\mathbf{n}}_i \Delta\sigma_i\right] \end{bmatrix} \end{bmatrix} \tag{4.17}$$

4.4.2 Implementation of RHS Vector

The discretization of the RHS vector follows the same methods as the discretization for the explicit method. However, it additionally includes the simplification term from the system matrix:

$$[A_{simplified}] \cdot \left\{\Delta\widehat{\mathbf{U}}\right\} = \left\{\widehat{RHS}\right\} + (Simplification\ Term)$$

The RHS vector includes two components:

- The Residual Term: Same as the one from the Explicit Scheme
- The simplification term: Calculated from the previous solution step, accounting for the off-diagonal terms moved to the RHS from the system matrix:

$$\left\{RHS\right\} = w\Omega \begin{Bmatrix} \\ -\begin{bmatrix} \vdots \\ \widehat{\mathbf{U}}^{im} \\ \vdots \end{bmatrix} \\ \\ i\begin{bmatrix} \vdots \\ \widehat{\mathbf{U}}^{re} \\ \vdots \end{bmatrix} \\ \\ \end{Bmatrix}^{\boldsymbol{n}} + \begin{bmatrix}\textbf{Jacobian}\end{bmatrix} \begin{Bmatrix} \\ \begin{Bmatrix} \vdots \\ \widehat{\mathbf{U}}^{re} \\ \vdots \end{Bmatrix} \\ \\ i\begin{Bmatrix} \vdots \\ \widehat{\mathbf{U}}^{im} \\ \vdots \end{Bmatrix} \\ \\ \end{Bmatrix}^{\boldsymbol{n}} + w\Omega \begin{Bmatrix} \\ -\begin{Bmatrix} \vdots \\ \Delta\widehat{\mathbf{U}}^{im} \\ \vdots \end{Bmatrix} \\ \\ i\begin{Bmatrix} \vdots \\ \Delta\widehat{\mathbf{U}}^{re} \\ \vdots \end{Bmatrix} \\ \\ \end{Bmatrix}^{n-1}$$

$$\left\{RHS_{real}\right\}^n = -w\Omega \begin{Bmatrix} \vdots \\ \widehat{\mathbf{U}}^{im} \\ \vdots \end{Bmatrix}^{\boldsymbol{n}} + \left[\left.\frac{\partial\vec{\mathbb{F}}}{\partial\mathbf{U}}\right|_{\bar{\mathbf{U}}} \cdot \hat{\mathbf{n}}_i\Delta\sigma_i\right] \begin{Bmatrix} \vdots \\ \widehat{\mathbf{U}}^{re} \\ \vdots \end{Bmatrix}^{\boldsymbol{n}} - w\Omega \begin{Bmatrix} \vdots \\ \Delta\widehat{\mathbf{U}}^{im} \\ \vdots \end{Bmatrix}^{n-1} \tag{4.18}$$

$$\left\{RHS_{imag}\right\}^n = w\Omega \begin{Bmatrix} \vdots \\ \widehat{\mathbf{U}}^{re} \\ \vdots \end{Bmatrix}^{\boldsymbol{n}} + \left[\left.\frac{\partial\vec{\mathbb{F}}}{\partial\mathbf{U}}\right|_{\bar{\mathbf{U}}} \cdot \hat{\mathbf{n}}_i\Delta\sigma_i\right] \begin{Bmatrix} \vdots \\ \widehat{\mathbf{U}}^{im} \\ \vdots \end{Bmatrix}^{\boldsymbol{n}} + w\Omega \begin{Bmatrix} \vdots \\ \Delta\widehat{\mathbf{U}}^{re} \\ \vdots \end{Bmatrix}^{n-1} \tag{4.19}$$

By including the simplification term, it ensures that the decoupled real and imaginary parts of the system are accounted for, while maintaining computational efficiency. The separation of the RHS vector into real and imaginary components allows to sequentially solving the two decoupled systems, which significantly reduces computational time.

4.4.3 Final Decoupled Numerical Scheme

The full system can be represented as follows:

$$\begin{bmatrix} \begin{bmatrix} A_{diagonal} \end{bmatrix} & & \ddots \\ & \ddots & & \begin{bmatrix} A_{diagonal} \end{bmatrix} \end{bmatrix}_{10x10} \cdot \begin{Bmatrix} \begin{Bmatrix} \vdots \\ \Delta\widehat{\mathbf{U}}^{re} \\ \vdots \end{Bmatrix} \\ i \begin{Bmatrix} \vdots \\ \Delta\widehat{\mathbf{U}}^{im} \\ \vdots \end{Bmatrix} \end{Bmatrix} = \begin{Bmatrix} \begin{Bmatrix} \vdots \\ \{RHS_{real}\} \\ \vdots \end{Bmatrix} \\ i \begin{Bmatrix} \vdots \\ \{RHS_{real}\} \\ \vdots \end{Bmatrix} \end{Bmatrix} \tag{4.20}$$

However, to reduce computational complexity and improve efficiency, we decouple the system into two separate 5x5 systems, one for the real part and another for the imaginary part:

$$\begin{bmatrix} \\ A_{diag} \\ \\ \end{bmatrix}_{5x5} \begin{Bmatrix} \vdots \\ \Delta\widehat{\mathbf{U}}^{re} \\ \vdots \end{Bmatrix} = -w\Omega \begin{Bmatrix} \vdots \\ \widehat{\mathbf{U}}^{im} \\ \vdots \end{Bmatrix}^{\boldsymbol{n}} + \left[\frac{\partial \vec{\mathbb{F}}}{\partial \mathbf{U}}\bigg|_{\bar{\mathbf{U}}} \cdot \hat{\mathbf{n}}_i \Delta\sigma_i \right] \begin{Bmatrix} \vdots \\ \widehat{\mathbf{U}}^{re} \\ \vdots \end{Bmatrix}^{\boldsymbol{n}} - w\Omega \begin{Bmatrix} \vdots \\ \Delta\widehat{\mathbf{U}}^{im} \\ \vdots \end{Bmatrix}^{n-1} \tag{4.21}$$

$$\begin{bmatrix} \\ A_{diag} \\ \\ \end{bmatrix}_{5x5} \begin{Bmatrix} \vdots \\ \Delta\widehat{\mathbf{U}}^{im} \\ \vdots \end{Bmatrix} = w\Omega \begin{Bmatrix} \vdots \\ \widehat{\mathbf{U}}^{re} \\ \vdots \end{Bmatrix}^{\boldsymbol{n}} + \left[\frac{\partial \vec{\mathbb{F}}}{\partial \mathbf{U}}\bigg|_{\bar{\mathbf{U}}} \cdot \hat{\mathbf{n}}_i \Delta\sigma_i \right] \begin{Bmatrix} \vdots \\ \widehat{\mathbf{U}}^{re} \\ \vdots \end{Bmatrix}^{\boldsymbol{n}} + w\Omega \begin{Bmatrix} \vdots \\ \Delta\widehat{\mathbf{U}}^{im} \\ \vdots \end{Bmatrix}^{n-1} \tag{4.22}$$

By solving these decoupled systems, we can efficiently compute the real and imaginary parts of the fluid state updates, $\Delta\widehat{U}^{real}$ and $\Delta\widehat{U}^{imag}$, respectively.

Once updated, they are used to update the real and imaginary parts of the solution at the next time step, as shown in the following equations:

$$\begin{Bmatrix} \vdots \\ \widehat{\mathbf{U}}^{re} \\ \vdots \end{Bmatrix}^{\boldsymbol{n+1}} = \begin{Bmatrix} \vdots \\ \widehat{\mathbf{U}}^{re} \\ \vdots \end{Bmatrix}^{\boldsymbol{n}} + \begin{Bmatrix} \vdots \\ \Delta\widehat{\mathbf{U}}^{re} \\ \vdots \end{Bmatrix} \tag{4.23}$$

$$\begin{Bmatrix} \vdots \\ \widehat{\mathbf{U}}^{im} \\ \vdots \end{Bmatrix}^{\boldsymbol{n+1}} = \begin{Bmatrix} \vdots \\ \widehat{\mathbf{U}}^{im} \\ \vdots \end{Bmatrix}^{\boldsymbol{n}} + \begin{Bmatrix} \vdots \\ \Delta\widehat{\mathbf{U}}^{im} \\ \vdots \end{Bmatrix} \tag{4.24}$$

By decoupling the system and solving the smaller 5x5 systems sequentially, we significantly reduce the compute time while still accounting for the complex behavior of the system. This approach is an efficient way to model the dynamics of the fluid, capturing both the real and imaginary components of the state variables.

4.5 Oscilating Wall BC Implementation

The solver's primary aim is the imposition of a harmonic perturbation on the domain through the harmonic boundary conditions (BC). The initial step involves the representation of the unsteady boundary conditions as harmonic boundary conditions. The following stage is to calculate the conserved harmonic variables for the domain, resulting in the final conserved harmonic flow variables. Finally, these harmonic flow values are converted back into the time domain, providing the ultimate solution desired.

For the solver, we map the time domain to the frequency domain, referencing everything to a pure sine wave. This means the unsteady flow starts from the mean flow at time=0. The frequency domain solutions are converted back to the time domain solution using the sine convention. Following the convention this requires imposing the harmonic boundaries, referencing to a pure sine wave. The phase of the boundary condition imposed will be obtained from its difference compared to a pure sine wave.

$$\widetilde{\mathbf{X}} = \widehat{\mathbf{X}} e^{i\omega t} = (\mathbf{X} * cos(\Psi) + i\ \mathbf{X} * sin(\Psi)) e^{i\omega t}$$
$$\widetilde{\mathbf{X}} = \widehat{\mathbf{X}} e^{i\omega t} = (\mathbf{X}_{real} + i\ \mathbf{X}_{imag}) e^{i\omega t}$$

$$\widehat{\mathbf{X}} = (\mathbf{X}_{real} + i\ \mathbf{X}_{imag})$$

The above equations describe the conversion from the time domain to the frequency domain, represented by the complex phasor notation, where $\widetilde{\mathbf{X}}$ represents the phasor and $\widehat{\mathbf{X}}$ represents the complex harmonic variables.

Conserved harmonic variables that will be imposed on the boundary, are defined as:

$$\widehat{\mathbf{X}} = \left\{ \begin{array}{l} cos(\Psi) * \left\{ \begin{array}{c} \vdots \\ \left|\widehat{U}_{BC}\right| \\ \vdots \end{array} \right\} \\ \\ sin(\Psi) * \left\{ \begin{array}{c} \vdots \\ \left|\widehat{U}_{BC}\right| \\ \vdots \end{array} \right\} \end{array} \right\} \tag{4.25}$$

Here, the conserved harmonic variables are separated into real and imaginary parts, with each part multiplied by the cosine and sine of the phase, respectively. This formulation allows us to impose the oscillating wall boundary conditions in the frequency domain, taking into account both the amplitude and phase of the harmonic perturbation.

4.5.1 Implementation of $\widetilde{\vec{r}}$ and $\widetilde{\vec{n}}$ Terms

The perturbed harmonic velocity that will be imposed is given by Equation 3.41:

$$\widetilde{\vec{V}}_{BC} = \frac{\partial \widetilde{\vec{r}}}{\partial t} - \frac{(\bar{\vec{V}} \cdot \widetilde{\vec{n}})}{(\bar{\vec{n}} \cdot \bar{\vec{n}})} \cdot \bar{\vec{n}}$$

$\widetilde{\vec{r}}$ represents the position vector in the frequency domain, considering both the real and imaginary parts with respect to the phase, Ψ. Similarly, $\widetilde{\vec{n}}$ represents the normal vector in the frequency domain, again considering both real and imaginary parts with respect to the phase. $\widetilde{\vec{r}}$ and $\widetilde{\vec{n}}$ are defined as follows:

$$\begin{aligned} \widetilde{\vec{r}}(t) &= \vec{r} e^{i(wt-\Psi)} = \vec{r} e^{-i\Psi} e^{i\omega t} = \widehat{\vec{r}} e^{i\omega t} \\ \widetilde{\vec{r}}(t) &= (\vec{r} * cos(-\Psi) + i\, \vec{r} * sin(-\Psi)) e^{i\omega t} \\ \widetilde{\vec{r}} &= (\widehat{\vec{r}}_{real} + i\, \widehat{\vec{r}}_{imag}) e^{i\omega t} \end{aligned}$$

Obtaining the harmonic position vector r, decomposed into its real and imaginary

parts as:

$$\widehat{\vec{r}} = \left\{ \begin{array}{l} \left\{ \begin{array}{l} \widehat{r}_x^{re} \\ \widehat{r}_y^{re} \\ \widehat{r}_z^{re} \end{array} \right\} \\ i \left\{ \begin{array}{l} \widehat{r}_x^{im} \\ \widehat{r}_y^{im} \\ \widehat{r}_z^{im} \end{array} \right\} \end{array} \right\} = \left\{ \begin{array}{l} \vec{r} cos(-\Psi) \\ \\ i\ \vec{r} sin(-\Psi) \end{array} \right\} \tag{4.26}$$

The $\widehat{\vec{n}}$ term represents the harmonic change in the normal direction as it is shown in figure 4.2.

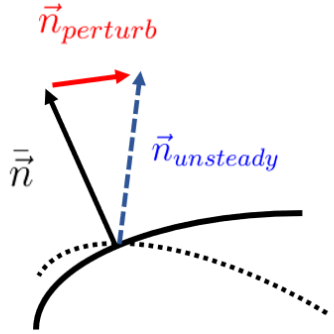

Figure 4.2: Normal Change Term

It is calculated as shown:

$$\widetilde{\vec{n}}(t) = \vec{n}_{perturb}\, e^{-i\Psi} e^{i\omega t}$$
$$\widetilde{\vec{n}}(t) = (\vec{n}_{perturb} \cos\Psi - i\vec{n}_{perturb} \sin\Psi) e^{i\omega t}$$
$$\widetilde{\vec{n}}(t) = \widehat{\vec{n}} e^{i\omega t}$$

The perturbed normal vector, $\vec{n}_{perturb}$, is defined as the difference between the final normal vector which depends on the rotation matrix and the average normal vector:

$$\vec{n}_{perturb} = \vec{n}_{unsteady} - \bar{\vec{n}}$$

To find $\vec{n}_{perturb}$, we first calculate the final normal vector, $\vec{n}_{unsteady}$, using a rotation matrix, $\mathbb{R}$:

$$\vec{n}_{unsteady} = [\mathbb{R}]\, \bar{\vec{n}}$$

The rotation matrix about the z-axis in 3D is given by:

$$\mathbb{R}_z(\theta) = \begin{bmatrix} \cos\theta & -\sin\theta & 0 \\ \sin\theta & \cos\theta & 0 \\ 0 & 0 & 1 \end{bmatrix}$$

This gives the net perturbed normal vector as:

$$\vec{n}_{perturb} = [[\mathbb{R}] - \mathbb{I}] \cdot \bar{\vec{n}}$$

Here, $\mathbb{R}$ represents the rotation matrix that changes the normal direction.

Using the above definitions, one can now express the perturbed normal vector in the frequency domain:

$$\widetilde{\vec{n}}(t) = \vec{n}_{perturb}\, e^{-i\Psi} e^{i\omega t} = \widehat{\vec{n}} e^{i\omega t}$$
$$\widetilde{\vec{n}}(t) = (\vec{n}_{perturb} * \cos(-\Psi) + i\, \vec{n}_{perturb} * \sin(-\Psi)) e^{i\omega t}$$

$$\widetilde{\vec{n}}(t) = \left\{ \begin{array}{l} \left\{ \vec{n}_{perturb} \cos(-\Psi) \right\} \\ \\ i \left\{ \vec{n}_{perturb} \sin(-\Psi) \right\} \end{array} \right\} e^{i\omega t} \tag{4.27}$$

$$\widetilde{\vec{n}}(t) = \left\{ \begin{array}{l} \left\{ \left[[R] - \left[I \right] \right] \bar{\vec{n}} \cos(-\Psi) \right\} \\ \\ i \left\{ \left[[R] - \left[I \right] \right] \bar{\vec{n}} \sin(-\Psi) \right\} \end{array} \right\} e^{i\omega t} \tag{4.28}$$

4.5.2 Harmonic Plunging Motion

In this section, plunging motion of an impermeable wall, as shown in the figure, is investigated:

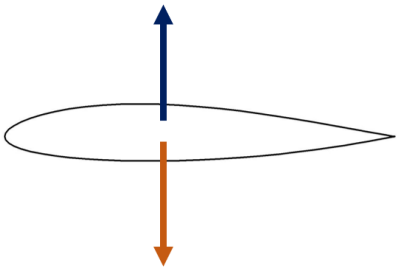

Figure 4.3: plungingMotion

During plunging motion, the normal vector remains unchanged, and only the induced velocity on the surface due to relative motion is considered. Therefore the phenomena solely involves imposed velocity on the surface. One can express the complex velocity vector as:

$$\widehat{\vec{V}}_{BC} = iw\widehat{\vec{r}} - \cancel{\frac{(\vec{\bar{V}} \cdot \vec{\widehat{n}})}{(\vec{\bar{n}} \cdot \vec{\bar{n}})} \cdot \vec{\bar{n}}} \tag{4.29}$$

Here, $\widehat{\vec{V}}$ represents the complex velocity vector, w is the angular velocity of the plunging motion, and $\widehat{\vec{r}}$ is the complex position vector. The second term, which involves the normal vector, is eliminated as there is no change in the normal direction during the plunging motion.

$$\widehat{\vec{V}}_{BC} = \begin{Bmatrix} \begin{Bmatrix} \widehat{u}^{re} \\ \widehat{v}^{re} \\ \widehat{w}^{re} \end{Bmatrix} \\ i \begin{Bmatrix} \widehat{u}^{im} \\ \widehat{v}^{im} \\ \widehat{w}^{im} \end{Bmatrix} \end{Bmatrix} = iw \begin{Bmatrix} \begin{Bmatrix} \widehat{r}_x^{re} \\ \widehat{r}_y^{re} \\ \widehat{r}_z^{re} \end{Bmatrix} \\ i \begin{Bmatrix} \widehat{r}_x^{im} \\ \widehat{r}_y^{im} \\ \widehat{r}_z^{im} \end{Bmatrix} \end{Bmatrix} = iw \begin{Bmatrix} \vec{r}cos(-\Psi) \\ \\ i\,\vec{r}sin(-\Psi) \end{Bmatrix} \tag{4.30}$$

$$\widehat{\vec{V}}_{BC} = \begin{Bmatrix} \begin{Bmatrix} \widehat{u}^{re} \\ \widehat{v}^{re} \\ \widehat{w}^{re} \end{Bmatrix} \\ i \begin{Bmatrix} \widehat{u}^{im} \\ \widehat{v}^{im} \\ \widehat{w}^{im} \end{Bmatrix} \end{Bmatrix} = w \begin{Bmatrix} - \begin{Bmatrix} \widehat{r}_x^{im} \\ \widehat{r}_y^{im} \\ \widehat{r}_z^{im} \end{Bmatrix} \\ i \begin{Bmatrix} \widehat{r}_x^{re} \\ \widehat{r}_y^{re} \\ \widehat{r}_z^{re} \end{Bmatrix} \end{Bmatrix} = w \begin{Bmatrix} -\vec{r}sin(\Psi) \\ \\ i\,\vec{r}cos(\Psi) \end{Bmatrix} \tag{4.31}$$

Here, Ψ represents the phase angle. The complex velocity vector's real and imaginary parts are multiplied by the sine and cosine of the phase angle, respectively.

Therefore one can represent the complex velocity vector as a matrix:

$$\widehat{\vec{V}}_{BC} = \begin{Bmatrix} \widehat{\vec{V}}_{real} \\ \\ \widehat{\vec{V}}_{imag} \end{Bmatrix} = w * \begin{Bmatrix} -\left\{\vec{r}\,sin(\Psi)\right\} \\ \\ \left\{\vec{r}\,cos(\Psi)\right\} \end{Bmatrix} \tag{4.32}$$

This equation describes the complex velocity vector during the plunging motion in terms of the position vector $\vec{r}$, the angular velocity w, and the phase angle Ψ. Analyzing this expression can help us understand the relationship between the object's motion and the induced velocity on its surface, which is crucial for various applications, such as fluid-structure interactions and aerodynamics.

4.5.3 Harmonic Pitching Motion

The underlying physics of the pitching motion is shown in figure 4.4

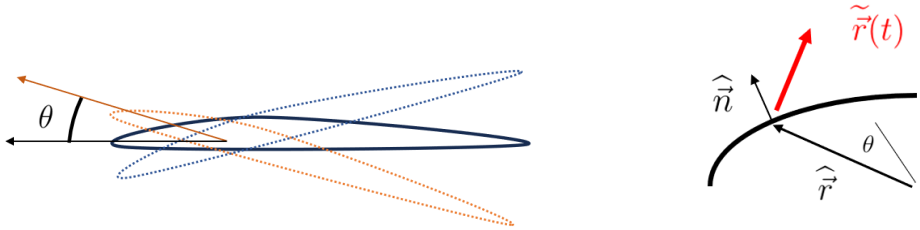

(a) Pitching Motion

(b) Pitching Induced Velocity

Figure 4.4: Physics of Pitching Motion

The position vector $\widetilde{\vec{r}}(t)$, which represents the pitching motion around the k-axis, is defined as:

$$\widetilde{\vec{r}}(t) = (\vec{r} \times \vec{k})\theta(t) \tag{4.33}$$

Here, $\vec{r}$ is the position vector, $\vec{k}$ is the rotation axis, and $\theta(t)$ is the perturbation, which is assumed to be a harmonic oscillation with a phase of Φ:

$$\widetilde{\vec{r}}(t) = (\vec{r} \times \vec{k})\theta e^{i(wt-\Phi)} \tag{4.34}$$

Complex velocity to be imposed on the BC can be decomposed into direct and normal change components:

$$\begin{aligned} \widetilde{\vec{V}}_{BC} &= \frac{\partial \widetilde{\vec{r}}}{\partial t} - \frac{(\bar{\vec{V}} \cdot \widetilde{\vec{n}})}{(\bar{\vec{n}} \cdot \bar{\vec{n}})} \cdot \bar{\vec{n}} \\ \widetilde{\vec{V}}_{BC} &= \hat{\vec{V}}^{direct} e^{i\omega t} + \hat{\vec{V}}^{\Delta \vec{n}} e^{i\omega t} \end{aligned} \tag{4.35}$$

The decomposed components can be dealt with seperately. Starting with the direct velocity term $\widetilde{\vec{V}}^{direct} = \frac{\partial \widetilde{\vec{r}}}{\partial t}$:

$$\widetilde{\vec{V}}^{direct} = \frac{\partial \widetilde{\vec{r}}(t)}{\partial t} = \frac{\partial(\vec{r} \times \vec{k})\theta e^{i(wt-\Phi)}}{\partial t} \tag{4.36}$$

$$\frac{\partial \widetilde{\vec{r}}(t)}{\partial t} = iw(\vec{r} \times \vec{k})\theta e^{-i\Phi} e^{i\omega t} \tag{4.37}$$

$$\frac{\partial \widetilde{\vec{r}}(t)}{\partial t} = iw(\vec{r} \times \vec{k})\theta \cdot (cos(-\Phi) + isin(-\Phi)) \cdot e^{i\omega t} \tag{4.38}$$

$$\begin{Bmatrix} \widehat{\vec{V}}^{(direct)}_{real} \\ \\ \widehat{\vec{V}}^{(direct)}_{imag} \end{Bmatrix} e^{i\omega t} = \widetilde{\vec{V}}^{direct} = \frac{\partial \widetilde{\vec{r}}(t)}{\partial t} = w\theta * \begin{Bmatrix} \left\{(\vec{r} \times \vec{k})\right\} \cdot sin(\Phi) \\ \\ \left\{(\vec{r} \times \vec{k})\right\} \cdot cos(\Phi) \end{Bmatrix} e^{i\omega t} \tag{4.39}$$

Similarly, the Normal change term $\widehat{\vec{V}}^{\Delta\vec{n}} = -\frac{(\bar{\vec{V}} \cdot \widetilde{\vec{n}})}{(\bar{\vec{n}} \cdot \bar{\vec{n}})} \cdot \bar{\vec{n}}$ is obtained as:

$$\widetilde{\vec{V}}^{\Delta\vec{n}} = -\frac{(\bar{\vec{V}} \cdot \widetilde{\vec{n}})}{(\bar{\vec{n}} \cdot \bar{\vec{n}})} \cdot \bar{\vec{n}} \tag{4.40}$$

$$\widetilde{\vec{V}}^{\Delta\vec{n}} = -\left(\frac{\bar{\vec{V}} \cdot (\vec{n}_{unsteady} - \bar{\vec{n}})}{(\bar{\vec{n}} \cdot \bar{\vec{n}})}\right) \cdot \bar{\vec{n}}\, e^{-i\Phi}\, e^{i\omega t} \tag{4.41}$$

$$\widetilde{\vec{V}}^{\Delta\vec{n}} = -\left(\frac{\bar{\vec{V}} \cdot ([\mathbb{R} - \mathbb{I}] \cdot \bar{\vec{n}})}{(\bar{\vec{n}} \cdot \bar{\vec{n}})}\right) \cdot \bar{\vec{n}}\, (cos(-\Phi) + isin(-\phi))\, e^{i\omega t} \tag{4.42}$$

Leading up to:

$$\begin{Bmatrix} \widehat{\vec{V}}^{\Delta\vec{n}}_{real} \\ \\ \widehat{\vec{V}}^{\Delta\vec{n}}_{imag} \end{Bmatrix} e^{i\omega t} = \widetilde{\vec{V}}^{\Delta\vec{n}} = \begin{Bmatrix} -\left\{\left(\frac{\bar{\vec{V}} \cdot ([\mathbb{R}-\mathbb{I}] \cdot \bar{\vec{n}})}{(\bar{\vec{n}} \cdot \bar{\vec{n}})}\right)\right\} \cdot cos(\Phi) \\ \left\{\left(\frac{\bar{\vec{V}} \cdot ([\mathbb{R}-\mathbb{I}] \cdot \bar{\vec{n}})}{(\bar{\vec{n}} \cdot \bar{\vec{n}})}\right)\right\} \cdot sin(\Phi) \end{Bmatrix} \cdot e^{i\omega t} \tag{4.43}$$

Plugging the values for $\widehat{\vec{V}}^{(direct)}_{real}$ and $\widehat{\vec{V}}^{\Delta\vec{n}}$ into 4.35 one can obtain the harmonic velocities at the BC faces as:

$$\widehat{\vec{V}}_{BC} = w\theta * \begin{Bmatrix} \left\{(\vec{r} \times \vec{k})\right\} \cdot sin(\Phi) \\ \\ \left\{(\vec{r} \times \vec{k})\right\} \cdot cos(\Phi) \end{Bmatrix} + \begin{Bmatrix} -\left\{\left(\frac{\bar{\vec{V}} \cdot ([\mathbb{R}-\mathbb{I}] \cdot \bar{\vec{n}})}{(\bar{\vec{n}} \cdot \bar{\vec{n}})}\right)\right\} \cdot cos(\Phi) \\ \\ \left\{\left(\frac{\bar{\vec{V}} \cdot ([\mathbb{R}-\mathbb{I}] \cdot \bar{\vec{n}})}{(\bar{\vec{n}} \cdot \bar{\vec{n}})}\right)\right\} \cdot sin(\Phi) \end{Bmatrix} \tag{4.44}$$

4.5.4 Harmonic Variables at the Ghost Cell

After determining the harmonic velocity to be imposed on the wall, it is crucial to ensure that the necessary flow properties at the moving boundary are maintained. To achieve this, the boundary conditions are applied using ghost cells [30]. To obtain ghost cell flow properties for a moving wall boundary in a compressible conservative CFD solver, the scheme is as follows.

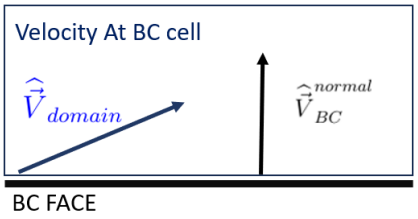

Figure 4.5: Velocity Normal

First the velocity component normal to the boundary $\hat{\vec{V}}_n$ as shown in 4.5, is calculated as:

$$\hat{\vec{V}}_{BC}^{normal} = \hat{\vec{V}}_{BC} \cdot \vec{n} \tag{4.45}$$

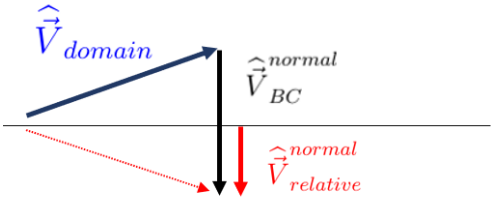

Figure 4.6: Relative Velocity

Next, the BC face relative normal velocity $\hat{\vec{V}}_{relative}^{normal}$, as shown in 4.45 is calculated as:

$$\hat{\vec{V}}_{relative}^{normal} = \left(\hat{\vec{V}}_{domain} - \hat{\vec{V}}_{BC}^{normal}\right) \cdot \vec{n} \tag{4.46}$$

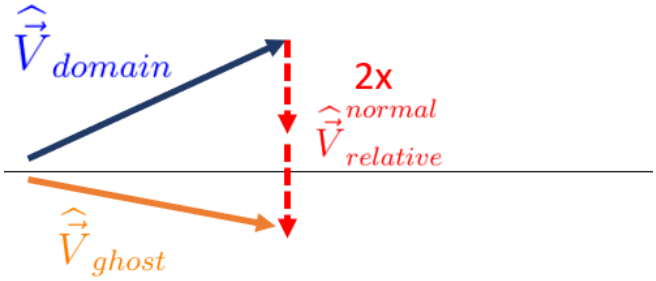

Figure 4.7: Velocity at Ghost Cell

The final step is then to Calculate the ghost cell velocity vector, $\widehat{\vec{V}}_{ghost}$ as:

$$\widehat{\vec{V}}_{ghost} = \widehat{\vec{V}}_{domain} - 2\widehat{\vec{V}}^{normal}_{relative} \tag{4.47}$$

It is assumed that harmonic density and temperature stay the same across the BC, Hence setting them as:

$$\widehat{\rho}_{ghost} = \widehat{\rho}_{domain} \tag{4.48}$$

$$\widehat{T}_{ghost} = \widehat{T}_{domain} \tag{4.49}$$

Using the equation 3.4 and 3.3 one can obtain the conserved Harmonic variables at ghost cell as:

$$\widehat{\mathbf{U}}_{ghost} = \begin{Bmatrix} \widehat{\rho}_{ghost} \\ \begin{Bmatrix} \vdots \\ \widehat{\vec{M}}_{ghost} \\ \vdots \end{Bmatrix} \\ \widehat{E}_{ghost} \end{Bmatrix} = \begin{Bmatrix} \widehat{\rho}_{ghost} \\ \begin{Bmatrix} \vdots \\ \widehat{\rho}\bar{V} + \bar{\rho}\widehat{V} \\ \vdots \end{Bmatrix} \\ \widehat{\rho}\bar{E}_{tot} + \bar{\rho}\left(\frac{R\widehat{T}}{k-1} + \frac{\bar{V}\cdot\widehat{V}}{2|\bar{V}|}\right) \end{Bmatrix} \tag{4.50}$$

CHAPTER 5

FLUTTER ANALYSIS WITH HARMONIC METHODS

5.1 Vibrating Airfoil Governing Equations

The Model being analyzed represents a two-dimensional airfoil placed in a horizontal airflow with a steady speed, in horizontal direction, illustrated in Figure 5.1. This airfoil's movement is characterized by two distinct degrees of freedom: the vertical movement, termed "plunge" (denoted by h and positive downwards), and its rotation, referred to as "pitch" (represented by θ). To describe its structural behavior, we use linear bending and torsional springs located at the airfoil's elastic axis. These springs mimic the counteracting forces exerted by the rest of the structure on the airfoil. Many aeroelasticity textbooks provide the motion equations for such an airfoil. [31]

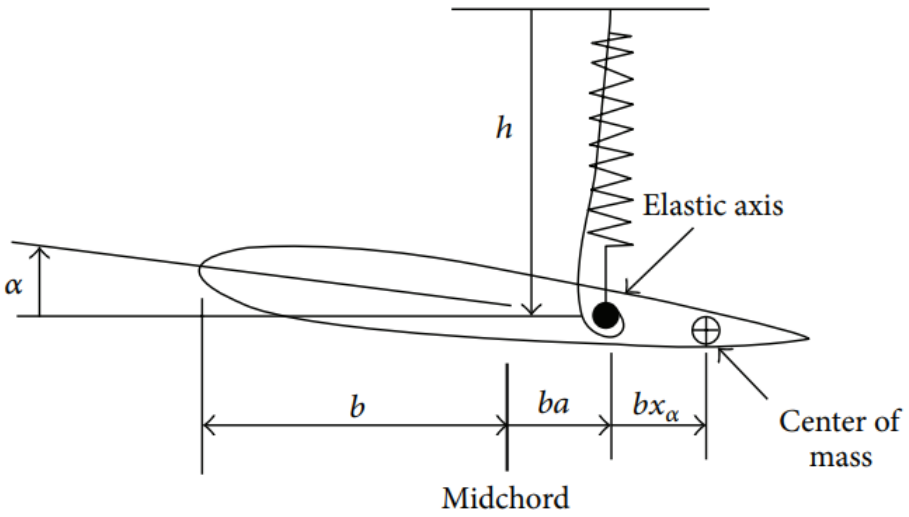

Figure 5.1: Airfoil Vibration Model [3]

In the model, the distance between the pitch axis and the center of mass will be expressed as variable $e = x_a * b$ where b is the half chord of the airfoil. Sum of all the unsteady aerodynamic forces in the vertical direction will be expressed as the 'Lift' variable and the net moment of the unsteady aerodynamic forces will be denoted with 'Moment' term. Using this convention following governing equations of the system can be formulated as:

$$\begin{bmatrix} m & -me \\ -me & I \end{bmatrix} \begin{Bmatrix} \ddot{h} \\ \ddot{\alpha} \end{Bmatrix} + \begin{bmatrix} K & 0 \\ 0 & Kt \end{bmatrix} \begin{Bmatrix} h \\ \alpha \end{Bmatrix} = \begin{Bmatrix} Lift \\ Moment \end{Bmatrix} \tag{5.1}$$

In the represented system, lift and moment forces depend on the motion of the airfoil, while the airfoil motion itself depends on the lift and moment forces. Thereby creating the fluid-structure interaction problem, where the fluid and structure domains are coupled. The following formulation, utilizes methods proposed by Gunes(2023) [32], to obtain solutions for the coupled system.

The unsteady of position and Forcing vectors will be modeled as harmonic oscillations with dissipation or dispersion term, thereby encapsulating the harmonic and dissipative nature of systems response.

$$\begin{Bmatrix} Lift \\ Moment \end{Bmatrix} = \begin{Bmatrix} \widehat{Lift} \\ \widehat{Moment} \end{Bmatrix} e^{(iw+D)t} \tag{5.2}$$

$$\begin{Bmatrix} h \\ \alpha \end{Bmatrix} = \begin{Bmatrix} \widehat{h} \\ \widehat{\alpha} \end{Bmatrix} e^{(iw+D)t} \tag{5.3}$$

$$\begin{Bmatrix} \ddot{h} \\ \ddot{\alpha} \end{Bmatrix} = (iw+D)^2 \begin{Bmatrix} \widehat{h} \\ \widehat{\alpha} \end{Bmatrix} e^{(iw+D)t} \tag{5.4}$$

Depending on the value of the damping term D, the solution will exhibit following oscillatory, dissipative, or dispersive behaviors:

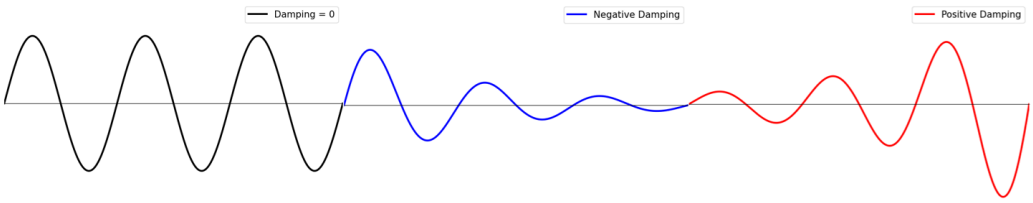

Figure 5.2: Harmonic Solution Behavior with Different Damping Values

For the problem of flutter spesifically, solution space will exhibit oscillatory or dispersive behavior, as these would imply instability. This can cause even infinitesimally small disturbances to lead to large displacements in the structure.

Using the definition from equation 5.1, the governing equation is obtained as:

$$\left(D^2 - w^2 + iw\right)\begin{bmatrix} m & -me \\ -me & I \end{bmatrix}\begin{Bmatrix} \widehat{h} \\ \widehat{\alpha} \end{Bmatrix}\cancel{e^{(iw+D)t}} + \begin{bmatrix} K & 0 \\ 0 & Kt \end{bmatrix}\begin{Bmatrix} \widehat{h} \\ \widehat{\alpha} \end{Bmatrix}\cancel{e^{(iw+D)t}} = \begin{Bmatrix} \widehat{Lift} \\ \widehat{Moment} \end{Bmatrix}\cancel{e^{(iw+D)t}}$$

$$\left[\left(D^2 - w^2 + iwD\right)\begin{bmatrix} m & -me \\ -me & I \end{bmatrix} + \begin{bmatrix} K & 0 \\ 0 & Kt \end{bmatrix}\right]\begin{Bmatrix} \widehat{h} \\ \widehat{\alpha} \end{Bmatrix} = \begin{Bmatrix} \widehat{Lift} \\ \widehat{Moment} \end{Bmatrix} \tag{5.5}$$

The equation 5.5, relates the amplitudes and the phases unsteady Moment/Lift responses, with the harmonic disturbance in plunge and pitch of the airfoil.

The difficulty in obtaining a solution for this system is that, for a given Complex Lift and Moment forcing, we are interested in obtaining the corresponding Damping D, frequency w, and harmonic displacements $\begin{Bmatrix} \widehat{h} \\ \widehat{\alpha} \end{Bmatrix}$, meaning that Lift and Moment forcings are not a linear function of desired unknown variables.

To obtain a solution for this non-linear system, we can represent system 5.5 in a simplified form which is a simple linear relation in the form Ax=b, where:

$$[A] = \left[(D^2 - w^2 + iwD) \begin{bmatrix} m & -me \\ -me & I \end{bmatrix} + \begin{bmatrix} K & 0 \\ 0 & Kt \end{bmatrix} \right] = [A(w, D)] \tag{5.6}$$

$$\left\{ \vec{x} \right\} = \begin{Bmatrix} \widehat{h} \\ \widehat{\alpha} \end{Bmatrix} = \vec{x}(\widehat{h}, \widehat{\alpha}, w, D) \tag{5.7}$$

$$\left\{ \vec{b} \right\} = \begin{Bmatrix} \widehat{Lift} \\ \widehat{Moment} \end{Bmatrix} = \vec{b}(\widehat{h}, \widehat{\alpha}, w, U_\infty) \tag{5.8}$$

To obtain our non-linear system involving the variables we seek to solve for, We express the governing system 5.5 as a functional F, where F=Ax-b and F=0. Leading to:

$$\left\{ F \right\} = [A(w, D)]\, \vec{x}(\widehat{h}, \widehat{\alpha}, w, D) - \vec{b}(\widehat{h}, \widehat{\alpha}, w, U_\infty) = 0 \tag{5.9}$$

$$\left\{ F \right\} = F(\widehat{h}, \widehat{\alpha}, w, D, U_\infty) = 0 \tag{5.10}$$

Hence, utilizing the method proposed by Gunes [32], the solution domain is defined by the vector $\vec{x} = \left\{ \widehat{h}, \widehat{\alpha}, w, D, U_\infty \right\}$, which satisfies the nonlinear function $F(\widehat{h}, \widehat{\alpha}, w, D, U_\infty) = 0$. All possible states of the system reside in this defined solution space, which is expressed as:

$$\{F(\vec{x})\} = \left[\left(D^2 - w^2 + iwD\right) \begin{bmatrix} m & -me \\ -me & I \end{bmatrix} + \begin{bmatrix} K & 0 \\ 0 & Kt \end{bmatrix} \right] \begin{Bmatrix} \widehat{h} \\ \widehat{\alpha} \end{Bmatrix} - \begin{Bmatrix} \widehat{Lift} \\ \widehat{Moment} \end{Bmatrix} = 0 \tag{5.11}$$

5.2 Flutter Harmonic Method Implementation

In the numeric implementation, complex variables are decomposed into their real and imaginary parts.

$$\begin{Bmatrix} \widehat{h} \\ \widehat{\alpha} \end{Bmatrix} = \begin{Bmatrix} h_{real} \\ \alpha_{real} \\ h_{imag} \\ \alpha_{imag} \end{Bmatrix} \tag{5.12}$$

$$\begin{Bmatrix} \widehat{Lift} \\ \widehat{Moment} \end{Bmatrix} = \begin{Bmatrix} L_{real} \\ M_{real} \\ L_{imag} \\ M_{imag} \end{Bmatrix} \tag{5.13}$$

Using this formulation, the governing functional F of the system described in eq. 5.11 is equalavent to:

$$\begin{bmatrix} (D^2 - w^2)\begin{bmatrix} m & -me \\ -me & I \end{bmatrix} + \begin{bmatrix} K & 0 \\ 0 & Kt \end{bmatrix} & -wd\begin{bmatrix} m & -me \\ -me & I \end{bmatrix} \\ wd\begin{bmatrix} m & -me \\ -me & I \end{bmatrix} & (D^2 - w^2)\begin{bmatrix} m & -me \\ -me & I \end{bmatrix} + \begin{bmatrix} K & 0 \\ 0 & Kt \end{bmatrix} \end{bmatrix} \begin{Bmatrix} h_{re} \\ \alpha_{re} \\ h_{im} \\ \alpha_{im} \end{Bmatrix} - \begin{Bmatrix} L_{re} \\ M_{re} \\ L_{im} \\ M_{im} \end{Bmatrix} \tag{5.14}$$

In simpler terms, one can write;

$$F(h_{re}, \alpha_{re}, h_{im}, \alpha_{im}, w, D, U_\infty) = [A(w, D)]\,\vec{x}(h_{re}, \alpha_{re}, h_{im}, \alpha_{im}) - \vec{b}(h_{re}, \alpha_{re}, h_{im}, \alpha_{im}, U_\infty) \tag{5.15}$$

where;

$$F(h_{re}, \alpha_{re}, h_{im}, \alpha_{im}, w, D, U_\infty) = 0$$

The nonlinear functional F, representing the governing equations of the oscillating airfoil problem, has 7 variables and 4 independent equations where the 4 independent equations describe the airfoil's motion, fluid forces, and dynamic structural response. This function captures the coupling between fluid and structural domains. For any given state of 3 variables, there is a unique solution for the system, which allows us to determine critical conditions for flutter-induced instability.

5.3 Iterative Solution Strategy - Newton Method

The nonlinear function $\vec{F}(\vec{x})$, where $\vec{x} = \{h_{re}, \alpha_{re}, h_{im}, \alpha_{im}, w, D, U_\infty\}$. The goal is to find a solution for $\vec{x}$ such that $\vec{F}(\vec{x}) = 0$. Newton-Raphson method provides an iterative approach to converge to a suitable $\vec{x}$:

$$\{\vec{x}_{new}\} = \{\vec{x}\} - \left[\frac{\partial \vec{F}}{\partial \vec{x}}\right]^{-1} \{F(\vec{x})\} \tag{5.16}$$

The main task in this method is to compute the partial derivatives of the system with respect to our unknowns. The Jacobian matrix is obtained as follows:

$$\left[\frac{\partial \vec{F}}{\partial \vec{x}}\right] = \left[\left\{\frac{\partial \vec{F}}{\partial \vec{x}^1}\right\}\left\{\frac{\partial \vec{F}}{\partial \vec{x}^2}\right\}\dots\left\{\frac{\partial \vec{F}}{\partial \vec{x}^n}\right\}\right] \tag{5.17}$$

The Newton-Raphson scheme, starts with an initial guess and iterate towards the solution. Similar schemes for obtaining flutter solutions for airfoils problems had been in the literature [33]. For this problem, initial values for the frequency w and the flow speed U_∞ are straightforward, as the flow speed is often given, and a good initial guess for the frequency w is available from the natural frequency of the system. The remaining initial values are chosen by the user, with various strategies available for selection, which will be discussed later.

5.4 Scheme Implementation - Flutter Onset for a 2 Degree of Freedom Airfoil

In the oscillating airfoil problem, a system with a damping value smaller than zero ($D < 0$) exhibits dissipating oscillatory behavior. For the flutter problem, we are interested in the opposite case, where $D \geq 0$. When the damping is exactly equal to zero ($D = 0$), the system is on the brink of divergent behavior, meaning any infinitesimally small disturbances could lead to large oscillations. The flutter onset point corresponds to the condition where $D = 0$. This idea, along with other insights are utilized in Gunes's proposed method for finding flutter onset point [32].

Therefore for the flutter onset problem, damping value for the desired solution space is already known leading to:

$$\vec{x} = \begin{Bmatrix} h_{re} \\ \alpha_{re} \\ h_{im} \\ \alpha_{im} \\ w \\ \boldsymbol{D = 0} \\ U_{\infty} \end{Bmatrix} \tag{5.18}$$

We can set the phase of the perturbation α to zero and use it as a reference for the phases of all other perturbations in the flow domain, such as plunging oscillations $\widehat{h}$. With the phase Φ for $\widehat{\alpha}$ as the reference, we have:

$$\widehat{\alpha} = |\alpha|(cos(\Phi) + isin(\Phi)) = \alpha_{real} + i\alpha_{imag}$$

Where the imaginary term is zero, since our reference harmonic input is chosen as a sine wave.

$$\alpha_{imag} = 0$$

Lastly, we set one of the deflection perturbations to an infinitesimally small value. This is valid for the flutter problem because we seek a point where the system enters a non-dissipative oscillatory state, where any small perturbation leads to unending oscillations.

$$\alpha = \alpha_{real} = 0.1\ degrees \tag{5.19}$$

With these final steps, our solution space becomes:

$$\vec{x} = \begin{Bmatrix} h_{re} \\ \boldsymbol{\alpha_{re}} = 0.1 \\ h_{im} \\ \boldsymbol{\alpha_{im}} = 0 \\ w \\ \boldsymbol{D = 0} \\ U_{\infty} \end{Bmatrix} \tag{5.20}$$

The system, consisting of 4 independent equations, is governed by the functional

$$F(x) = 0$$

as defined in Eq. 5.11:

As it is proposed by Gunes [32], using insights from the problem definition, we have 4 unknowns remaining, which we can solve using the system of 4 equations we already had to obtain a unique solution, which corresponds to the desired flutter onset point.

5.4.1 Flutter Onset Problem - Solution Scheme

The harmonic flow solver is designed to accept inputs of phase and amplitude of the complex plunge variable h, phase and amplitude of the pitch α, frequency w, and flow velocity U_∞, and produce outputs of the harmonic lift and moment acting on the airfoil.

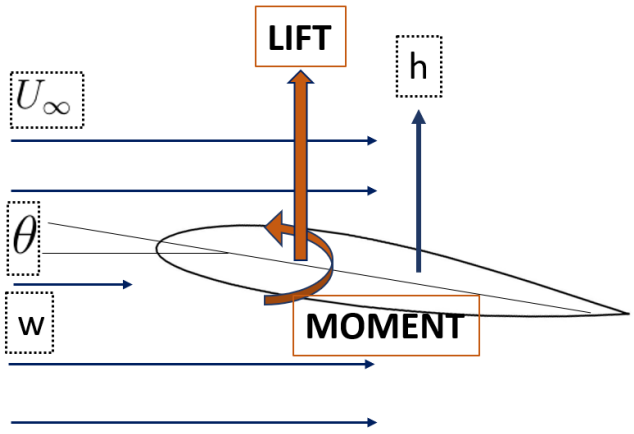

Figure 5.3: Flutter Solver Inputs and Outputs

Solving the nonlinear system defined in Eq. 5.11 involves the calculation of Jacobians for each perturbed solution variable. To obtain the Jacobians and, consequently, the solution, the harmonic CFD solver is called multiple times. The flutter onset point is found using the Gunes's scheme [32] as shown in the figure 5.4:

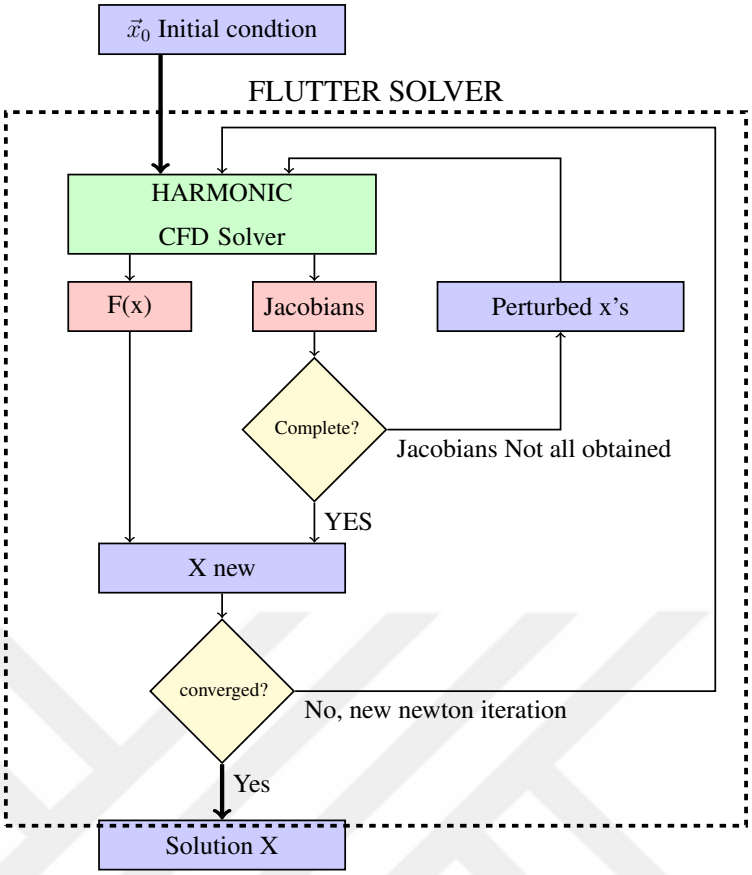

Figure 5.4: Flutter Solver Scheme Flow Chart

The solver starts with an initial guess, using the free vibration modes of the unaltered system. Upon obtaining the flow solution using these initial values, the flow state is slightly perturbed using harmonic variations to derive the system's Jacobian matrix, as shown in equation 5.17. The process involves multiple calls to the harmonic CFD solver to obtain a Jacobian. Then, the flutter solution progresses one step, deriving a new point for flutter prediction (as per equation 5.16), and this iterative process continues until convergence. Along the way, the scheme updates structural aspects like frequency, mode phases, and the flutter flow speed. Hallmark of Gunes's method [32] for finding flutter onset point is that, by treating the flow speed as a free variable, the solver identifies the nearest flutter point in the solution space, with improved convergence behavior.

CHAPTER 6

VALIDATION OF LINEARIZED HARMONIC METHOD

This chapter unfolds in a series of sections, each one spotlighting distinct aspects of the testing process. The initial segment is devoted to verification tests inspecting what will be called as the 'pseudo steady state'. The term means that the unsteady motions of the airfoil are slow enough that the entirety of the flow field is at sync with the current state of the airfoil. To understand this concept better, it must first be understood that changes in flow variables propagate in the domain at a certain finite speed. This means that any unsteadiness introduced to a fluid domain, would not be felt by the entire domain all at once. For a periodic unsteadiness introduced to a domain, this would mean that perturbations in flow variables in different places of the domain will have differences in phase.

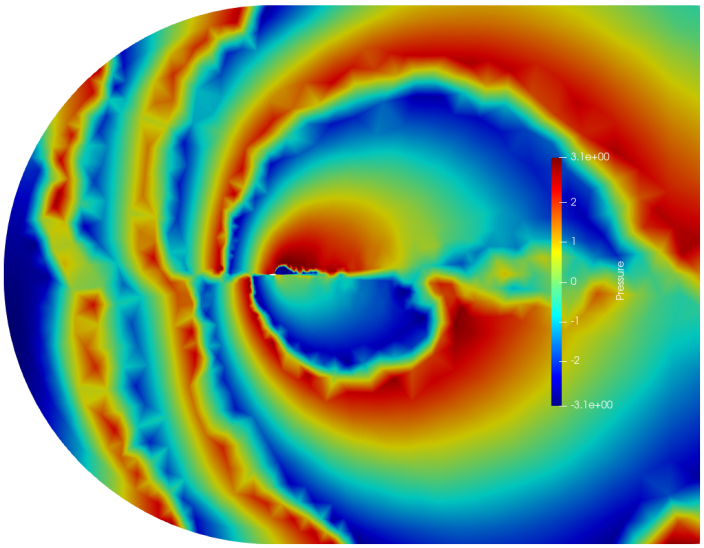

Figure 6.1: Pressure perturbation Unsteady Phase Plot

This phenomenon is shown in figure 6.1, where harmonic pitching oscillations of the airfoil create pressure perturbations in the domain and phases of those pressure perturbations with respect to the source are plotted. Having phase of zero indicates that the unsteadiness is in sync with the airfoil oscillations. Phases of pressure perturbations depend on their locations with respect to the source. It is also possible to see that unsteadiness in the domain travel at different speeds, with respect to the airfoil, which is an expected finding.

Returning back to the 'pseudo steady state' term. it was shown that the phase differences in the domain depend on the rate at which information travels in the fluid domain. Inverting this idea, it can be shown that as we get closer to oscillation frequencies of 0 Hz, changes are introduced to the domain at such a low rate that the entire flow field essentially updates to the new pitch angle of the airfoil.

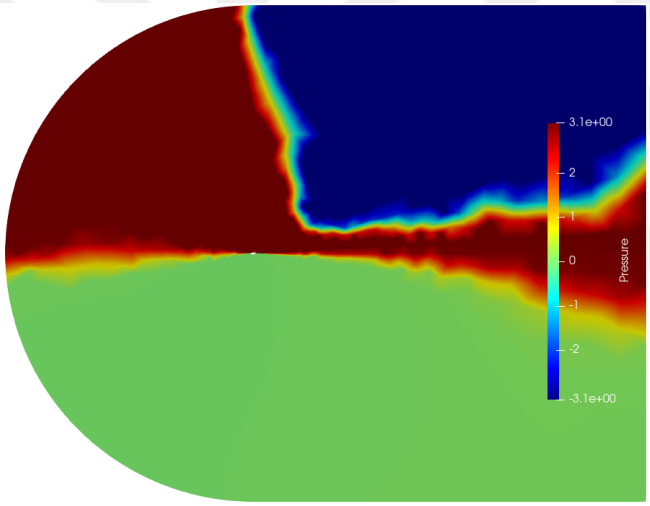

Figure 6.2: Pressure Perturbations Pseudo-steady Phase Plot

Figure 6.2 showcases one such configuration where the frequency of oscillation is 0.005 Hz. In its unsteady flow response, phase differences of the unsteady pressure in every cell in the domain are, either 0 or $\pm\pi$. In the figure 6.2, it can be that pressure perturbations in the lower side of the airfoil is perfectly in sync with the pitching oscillation of the foil. The upper side of the airfoil is also in perfect sync, with no phase delay, as indicated by the phase π and $-\pi$ except that the perturbation direction is opposite to the pitching direction. In other words, as airfoil pitches in the positive

direction increasing its angle of attack, the pressure increases in the lower portion of the domain and decreases in the upper portion, all of it being in perfect sync with the airfoil motion.

These types of flows, where the entire domain is in sync with the airfoil oscillations, are termed as 'pseudo-steady flows'. Although the problem involves unsteady oscillations of an airfoil, if the oscillation frequency is sufficiently slow, the flow field at any time of that unsteady motion will behave as if the airfoil is stationary at that instant, essentially acting like a steady state solution for that airfoil pitching angle. This idea proves to be powerful in the testing schemes, where linearized harmonic method can be used in pseudo-steady flows to make predictions on lift coefficients at different angles of attack, where under ideal circumstances, the results should align with recognized steady-state solutions for that angle of attack.

This unique verification approach allows us to generate a multitude of test cases for the harmonic method implementation, providing a robust means of establishing its validity.

The chapter subsequently unveils actual unsteady solutions, where the results undergo validation against two distinct test cases with experimental results.

In the concluding segment of the chapter, attention is drawn towards the results gleaned from the implemented flutter solver utilizing the linearized harmonic method. The results are compared against foundational analytical approximations. This multilayered approach to verification and validation warrants a meticulous and rigorous assessment of the method.

6.1 Pseudo-Steady Testing for NACA0012 at 2.89 Degrees Angle of Attack

Parameters for this test case are detailed in table 6.1. The test's objective is to obtain a harmonic solution for an oscillating pitch sinusoidal motion of 1.89 degrees, where the mean angle of attack is 1 degree. Oscillation frequency of 0.005 Hz is used. At $\frac{1}{4}$ of the period, it should be that the solution to be equivalent to a steady state solution for a 2.89 degree angle of attack. This hypothesis had been tested using steady state CFD solver. Similarly, the solution near the $\frac{3}{4}$ period should correspond to a steady state solution for a -0.89 degrees angle of attack, as indicated in figure 6.3.

Steady Parameters	**Value**
Airfoil Steady State Pitch (degree)	1
Pressure, p (Pa)	101325
Temperature, T (K)	300.0
Mach number, M	0.6
Harmonic Parameters	**Value**
Harmonic frequency, Hz	0.005
Airfoil pitch perturbations (degree)	1.89

Table 6.1: NACA0012 Pseudo-steady test case

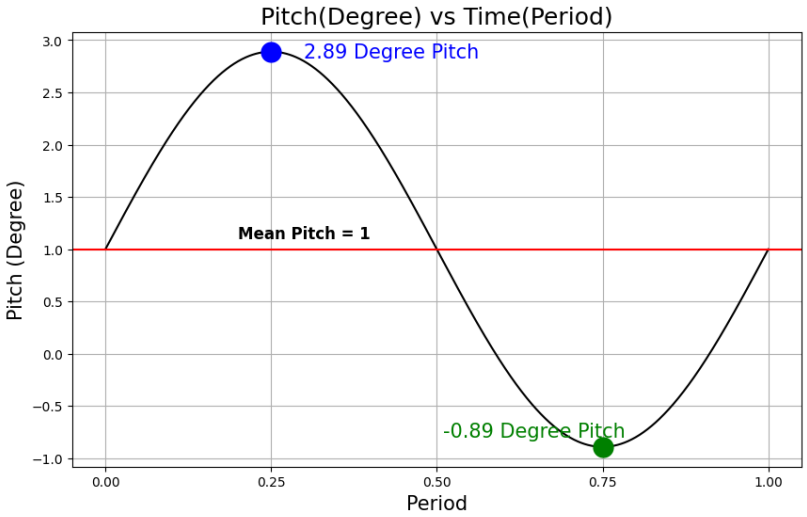

Figure 6.3: NACA0012 Airfoil Angle of Attack Profile

The resulting harmonic solution is transformed into time domain solutions that correspond to distinct periodic times. Figure 6.4 shows the results from the harmonic method and compares them with the pressure profile for a 2.89-degree pitch airfoil, obtained through steady-state CFD solver. The harmonic method's result at $\frac{1}{4}$ Period, corresponding to the pseudo-steady prediction for 2.89 degree angle of attack is provided and compared with it's corresponding steady-state CFD solver solution. As shown in figure 6.4, the harmonic method aligns well with both of the steady-state CFD solutions for 2.89-degree positive pitch and -0.89 degree negative pitch states.

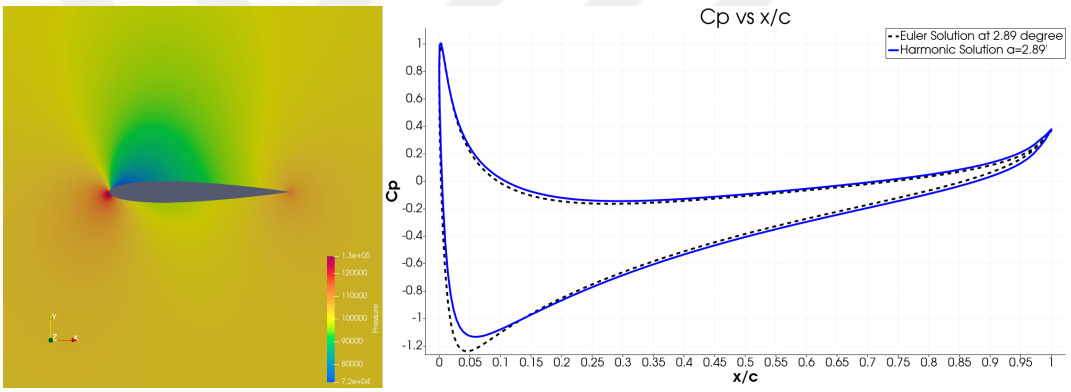

(a) Harmonic Solution at 2.89 Degree Pitch at 1/4 Period

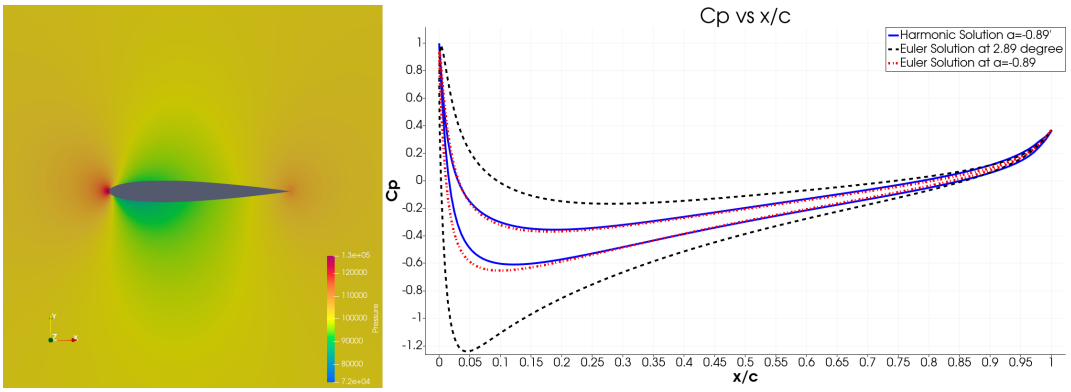

(b) Harmonic Solution at -0.89 Degree Pitch at 3/4 Period

Figure 6.4: Harmonic Method Pressure Profiles between -0.89 and 2.89 Degrees

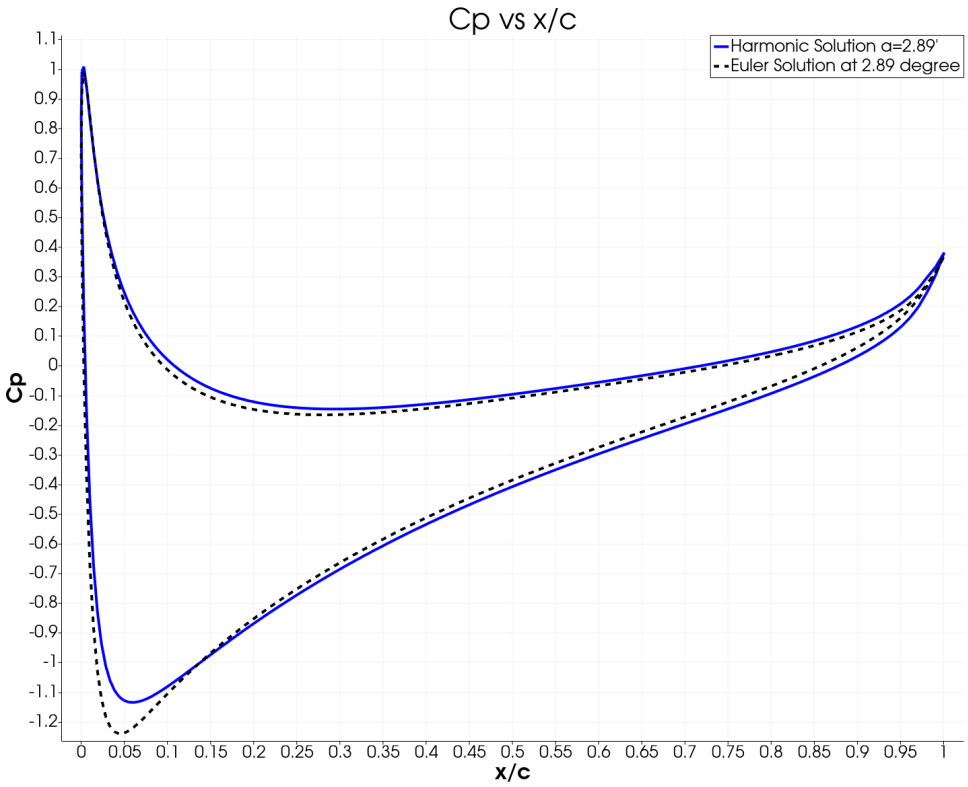

Figure 6.5: NACA0012 Harmonic Method result vs Steady state CFD result

A more detailed inspection of this verification case can be seen in figure 6.5. The linearized harmonic methods predictions succesfully matches with the expected pressure profile provided by the already verified CFD solver. Slight discrepencies are observed in the suction side of the leading edge. This is where the small perturbation assumption made in the linearization process shows its effect, the accuracy of the method suffers only in locations where large deviations in flow variables are present.

6.2 Pseudo-Steady Case for Transonic NACA64A10 at 1 Degree Angle of Attack

This section delves into the transonic test case for a NACA64A10 airfoil, aimed at examining the efficacy of Harmonic Methods in shock-involved scenarios. The unique challenge posed in this case stems from the presence of shocks on both sides of the airfoil when the angle of attack is zero, serving as the mean state of flow. The existence of these shocks is evident in figure 6.6a.

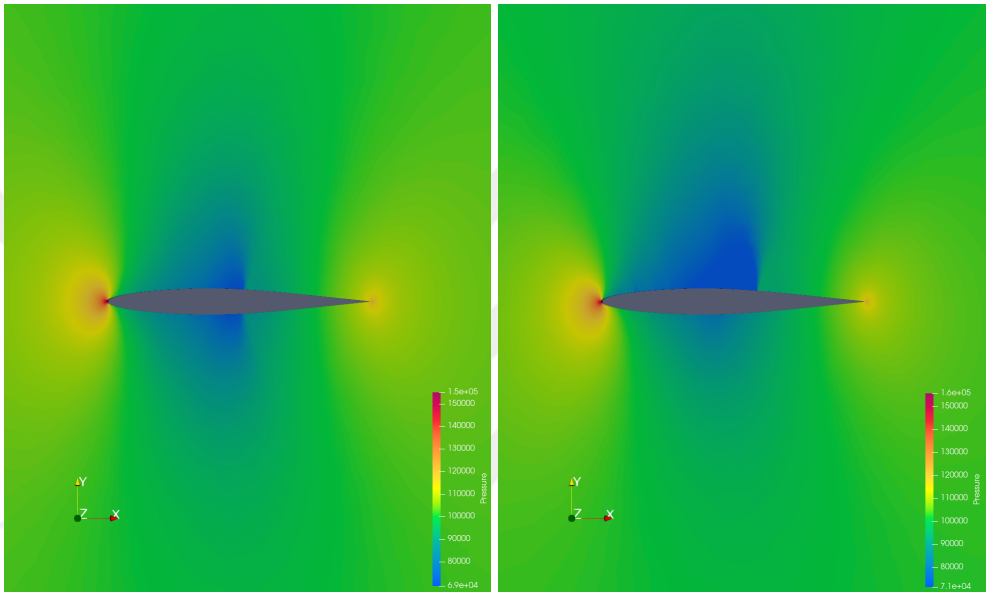

(a) 0 Degree Pitch (b) 1 Degree Pitch

Figure 6.6: Transonic NACA64A10 at 0 and 1 Degree Pitch CFD results

At a 1 degree angle of attack, the pressure side shock is absent and the suction side shock has moved significantly towards the tail of the airfoil (as seen in figure 6.6b). The displacement of the shock is the primary cause of the changes in fluid properties, with the downstream of the shock remaining unaffected and changes limited to upstream flow variables only. This case is chosen to highlight the most significant limitations of the Linearized Harmonic Method, such as the neglect of changes in mean flow due to introduced perturbations.

In the first instance, a 0-degree angle of attack solution is utilized as the mean state. A harmonic solution is calculated around this state for a 1-degree oscillating pitch, thus obtaining the solution for the airfoil in the range of 0-1 degree pitch. The parameters for the simulation, presented in a table format, can be found in table 6.2.

Steady Parameters	**Value**	**Harmonic Parameters**	**Value**
Airfoil Steady State Pitch (degree)	0	Pitch Perturbation (degree)	1.0
Pressure, p (Pa)	101325	Harmonic Frequency (Hz)	0.005
Temperature, T (K)	300.0		
Mach number, M	0.8		

Table 6.2: NACA0012 Pseudo-steady test case

The pressure profiles at 0-degree pitch and 1-degree pitch from steady CFD results are illustrated in figure 6.7, displaying clear discontinuities due to the presence of shocks. The absence of the lower shock and the considerable shift of the upper shock towards the tail of the wing at a 1-degree angle of attack can be observed again in figure 6.6b. The pressure profiles for these cases, marked by distinct discontinuities due to shocks, are also demonstrated in figure 6.7.

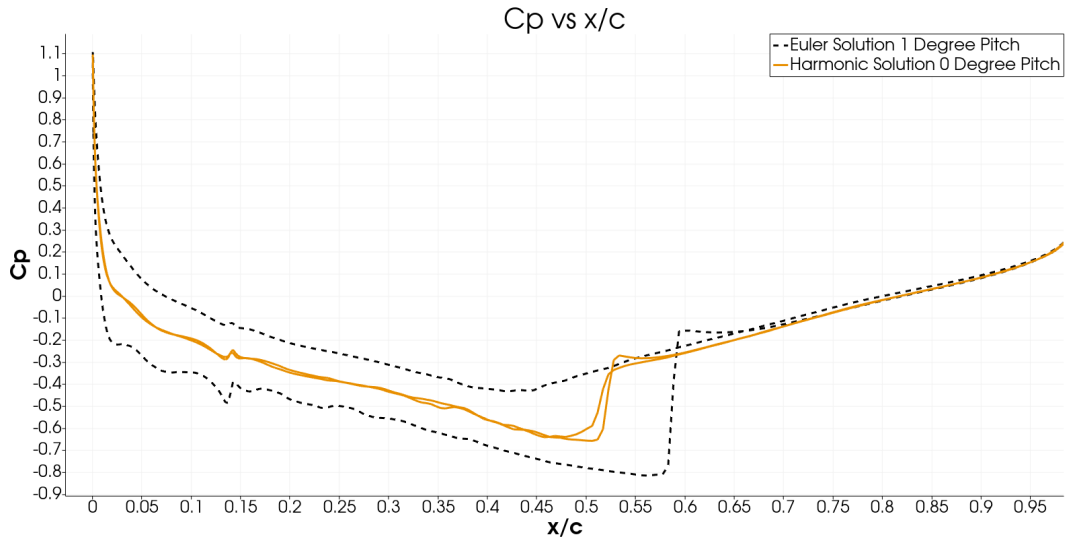

Figure 6.7: NACA64A10 Steady State 0 vs 1 Degree Pitch

The harmonic solution is transformed into time domain solutions at various periodic intervals. These results are presented in figure 6.8. The harmonic results at $\frac{1}{8}$ period and $\frac{1}{4}$ period are provided for comparison with the steady state CFD result corresponding to a 1-degree positive angle of attack.

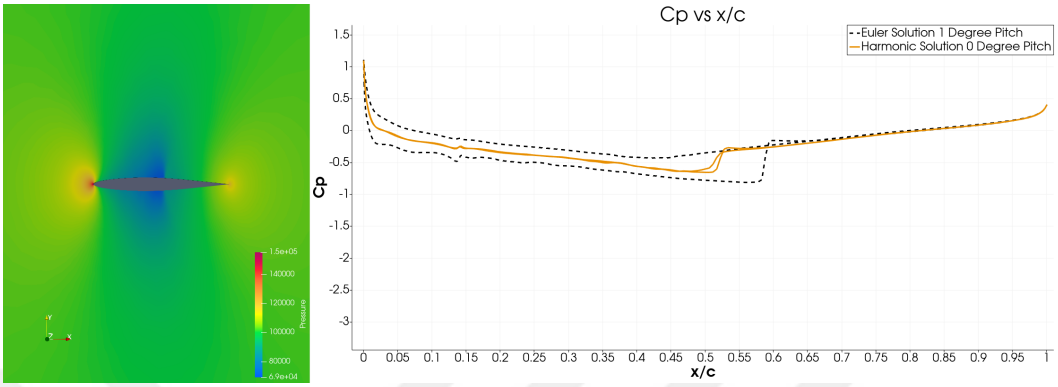

(a) Harmonic Solution at 0 Degree Pitch

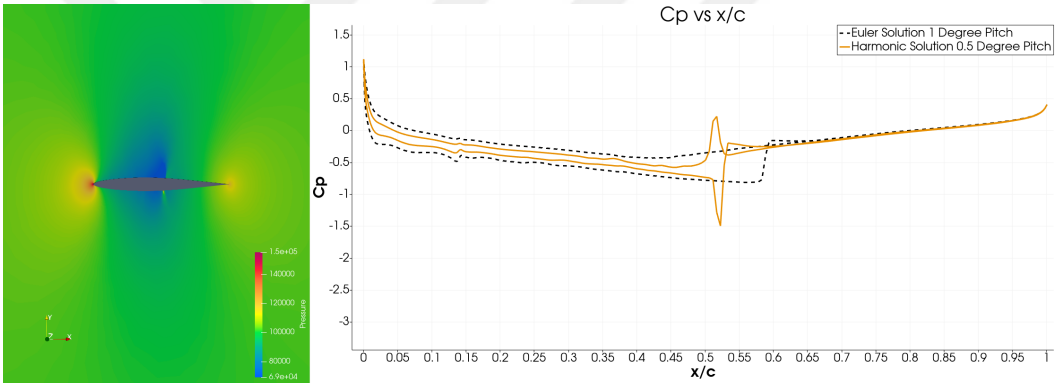

(b) Harmonic Solution at 0.5 Degree Pitch at 1/8 Period

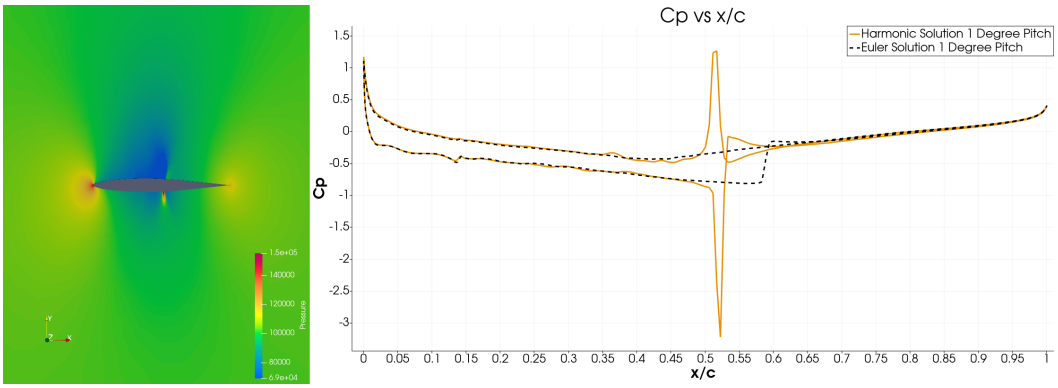

(c) Harmonic Solution at 1 Degree Pitch at 1/4 Period

Figure 6.8: NACA64A10 Pressure Profiles between 0 and 1 Degrees

Figure 6.9 exhibits the pressure profile garnered from the harmonic solver for a 1-degree pitch. The results reveal the fundamental limitation of the Linearized Harmonic Method: the absolute disregard for the effects of perturbation on mean flow during the linearization process. Normally, with the presence of a shock at the mean state used in a harmonic solution, the shock should also be displaced as perturbations are introduced. However, the Linearized Harmonic Method overlooks this by keeping the shock in the mean state at a fixed location when calculating the changes in flow values. Consequently, the governing harmonic conservation equations generate non-physical peaks at the shock locations.

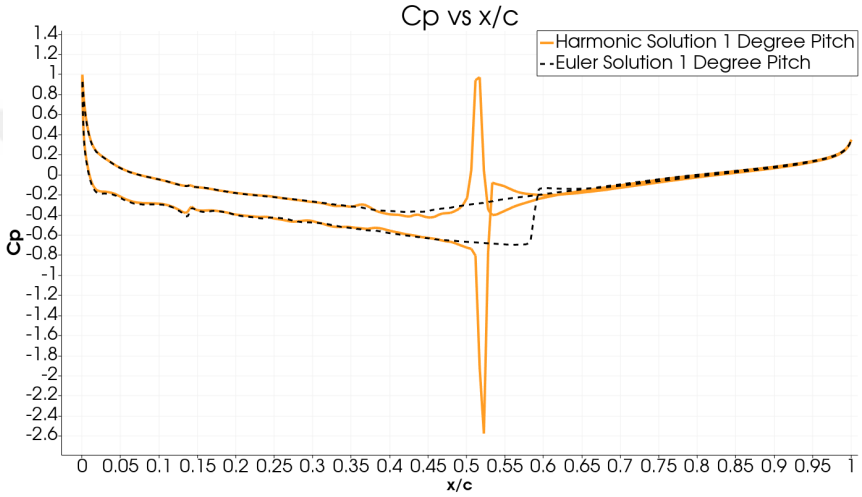

Figure 6.9: NACA64A10 Steady 1 Degree Pitch Harmonic vc Steady Euler Results

Despite this limitation, the harmonic results align impeccably with conventional CFD results in the regions upstream and downstream of the shock. Another critical observation is that despite the solution exhibiting unrealistic peaks, the lift coefficient obtained from the Linearized Harmonic method upon integrating the pressure distribution over the wing, surprisingly agrees with the expected CFD results.

Future research that concentrates exclusively on capturing the placement of the shock in the mean flow is required. Upon successful implementation of such work, Linearized Harmonic Methods would promise to deliver accurate results even in flows with shocks.

6.3 Unsteady Testing of Pitching Airfoils

The Linearized Harmonic Method has demonstrated promising results in the analysis of pseudo-state external flows. However, the primary interest lies in obtaining unsteady aerodynamic results for external flows, where the results are compared with alternative methods and with the experimental findings.

Pressure perturbation phase plot for a harmonically pitching airfoil is depicted in Figure 6.10, where the phase differences in pressure perturbations experienced by the NACA0012 airfoil at different locations is shown. Figure 6.10a shows the amplitude of the pressure perturbations due to harmonic pitching of the foil, whereas Figure 6.10b shows the phases of those pressure perturbations with respect to airfoils oscillation. It can be seen that pressure perturbations along the faces of the airfoil, continuously vary in phase. This phase difference governs the proportions of real and imaginary components of the frequency domain solution, which in turn dictates portion of the perturbation amplitude that will be ultimately be transformed back into the temporal domain at the desired time instances.

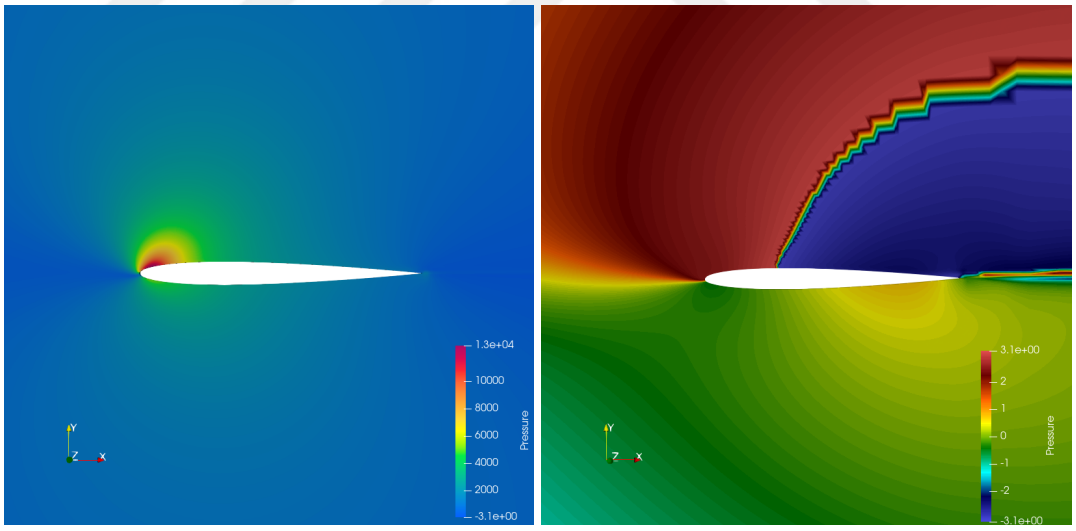

(a) Pressure Perturbation Amplitude (b) Pressure Perturbation Phase

Figure 6.10: Effect of Pitchin Frequency on Flow Perturbation Amplitude

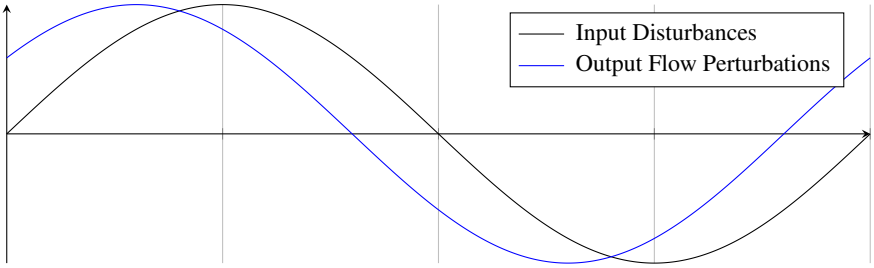

Figure 6.11: Solution Phase Difference

The variation in phase of the pressure perturbations implies that the unsteady forces experienced by the airfoil will also have phase difference relative to the actual harmonic motion the airfoil, as illustrated in Figure 6.11. This is one of the key behaviors for unsteady aerodynamics, separating it from the previously discussed 'pseudo steady' flows. When the frequency of the oscillations are sufficiently high, the fact that changes in flow properties in a fluid propagate at a finite speed and don't effect everywhere all at once, results in a phase difference between response of the flow field and the source of disturbances.

6.4 Effect of Pitching Frequency on Unsteady Lift Behavior

The overall unsteady behavior of the solution is significantly influenced by the frequency of introduced perturbations, thereby warranting a dedicated investigation into the effects of varying frequencies on harmonic perturbations with same amplitudes. This means that variations in lift experienced by an airfoil, oscilating between ± 2.89 degrees at 1 Hz, will differ in amplitude when same pitching oscillations are with a frequency of 3Hz. Test cases are setup to investigate this phenomenon. The variables for test setups are provided in 6.3. Here, both the steady-state values and the harmonic perturbation amplitudes remain constant, while only the harmonic perturbation frequencies vary between the runs, ranging from 0.1Hz to 3Hz.

Steady Parameters	**Value**	**Harmonic Parameters**	**Value**
Airfoil Steady Pitch (degree)	2.89	Pitch Perturbation (degree)	2.41
Pressure, p (Pa)	101325	Harmonic Frequency Case 1(Hz)	0.1
Temperature, T (K)	300.0	Harmonic Frequency Case 2(Hz)	1
Mach number, M	0.6	Harmonic Frequency Case 3(Hz)	3

Table 6.3: NACA0012 Pitch Oscilation Frequency Sweep Cases

The Fluid Domain, depicted in Figure 6.13, spans 110 meters in width, while the chord length of the airfoil measures 1 meter. This configuration ensures a thorough examination of the phase behavior of the wake flow, and will be used throughout all the studies.

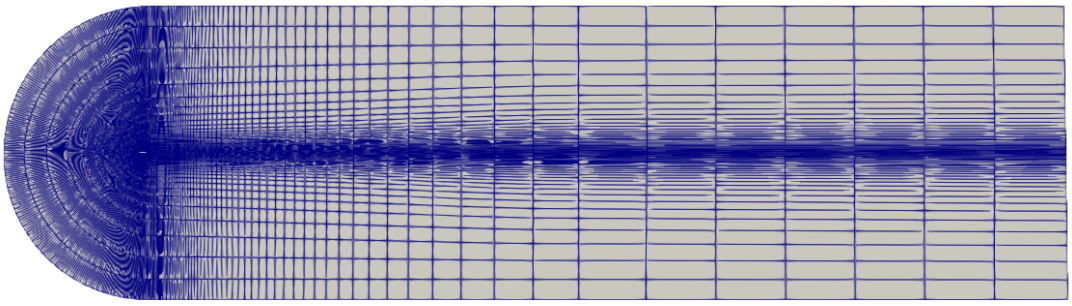

Figure 6.12: NACA0012 2.89x2.41 53 Hz

The solution for the 0.1 Hz pseudo-steady case demonstrates the anticipated behavior where the entire domain is in sync with the airfoil oscillations. During pitching oscillations, as depicted in Figure 6.14a, the pressure and suction surfaces of the airfoil undergo harmonic perturbations with a phase difference of π, suggesting that the changes instigated in the domain have opposing signs.

(a) NACA0012 Phase Plot at 0.1 Hz Oscilating Frequency

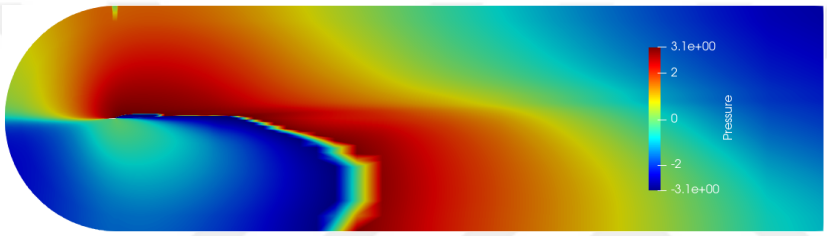

(b) NACA0012 Phase Plot at 3 Hz Oscilating Frequency

Figure 6.13: NACA0012 Unsteady Solution Phase Results

Pressure perturbation amplitudes for the test case is shown in Figure 6.14. Notably, an increase in oscillation frequency corresponds to a significant decrease in the perturbation amplitudes of the flow variables. This suggests that at higher frequencies, the fluid domain becomes less responsive to the perturbations introduced by the oscillating airfoil.

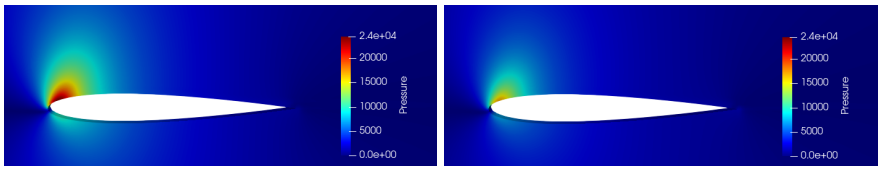

(a) 0.1 Hz Pitching Frequency (b) 3 Hz Pitching Frequency

Figure 6.14: Effect of Pitchin Frequency on Flow Perturbation Amplitude

A quantitative analysis on the oscillation frequency's impact on the unsteady Lift experienced by the airfoil is shown in Figure 6.15. Lift values with respect to the corresponding pitch of the airfoil are plotted, where each point correspond to a unique time instance as the airfoil undergoes a single cycle of its harmonic motion. The unsteady lift values for the NACA0012 airfoil, as it undergoes pitching oscillation from 0.48 to 5.3 degrees, are plotted at different pitching frequencies. The frequency as a oscilation parameter, is shown to have two key effects on the unsteady lift characteristics.

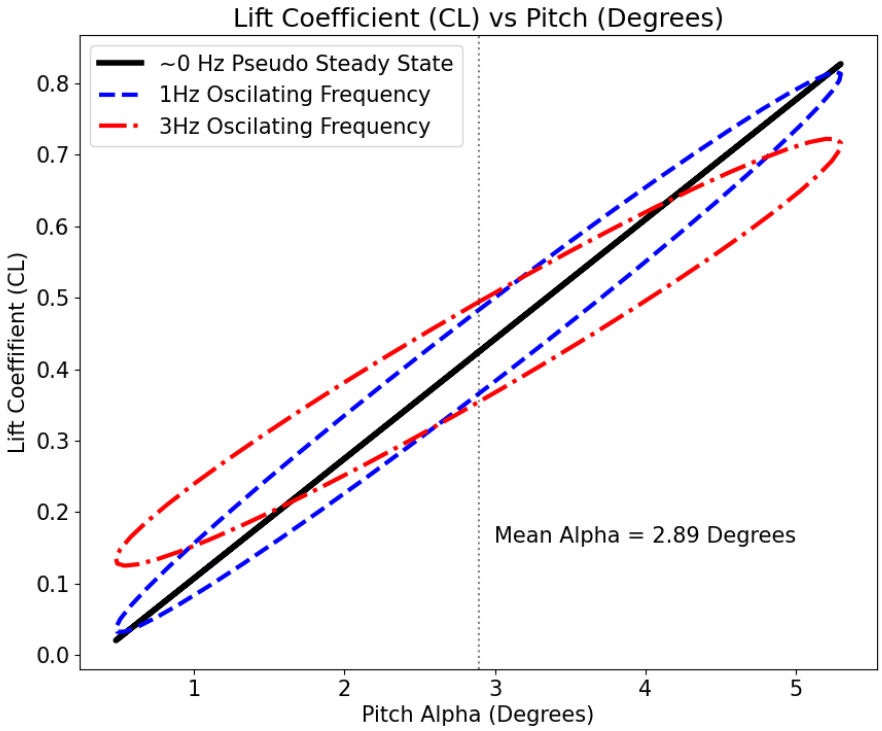

Figure 6.15: NACA0012 Pitch oscillations at 0Hz, 1Hz and 3Hz

First, as the oscillation frequency increases, the amplitude of the lift perturbations begins to decrease, indicating that the flow becomes less responsive to the airfoil's motion.

Secondly, as the frequency increases, the unsteady lift begins to exhibit hysteresis where for each angle of attack there are two different lift values depending on where the airfoil is in its periodic motion. The lift not only depends on the current angle of attack of the airfoil but also on the current direction of the pitching motion.

6.5 NACA0012 Unsteady Aerodynamics Test Case

The results obtained from the implemented Linearized Harmonic Solver are compared with the experimental findings obtained by R. H. Landon [34], the details of which are also available in the AGARD REPORT 702 [35]. The results are also compared with the Non-Linear Frequency domain methods [36], [37], [38] covering the more computationally expensive methods. The experimental setup, in non-dimensionalized properties, is presented in Table 6.4.

Airfoil	NACA0012
Mean Pitch angle (°)	2.89
Pitch angle variation (°)	2.41
Mach	0.6
Reduced Frequency k	0.08008

Table 6.4: Landon experiment parameters

The reduced frequency k is defined as:

$$k = \frac{\omega c}{2U} \tag{6.1}$$

where ω denotes the oscillation frequency in radians per second, c represents the chord length, and U corresponds to the free-stream velocity.

For this case setup, the chord of the airfoil is 1 meter in length, which results in a harmonic excitation frequency of 5.293 Hz. The complete list of parameters used in the Harmonic Solver is provided in Table 6.5.

Steady Parameters	**Value**	**Harmonic Parameters**	**Value**
Airfoil Steady Pitch (degree)	2.89	Pitch Perturbation (degree)	2.41
Pressure, p (Pa)	101325	Harmonic Frequency Case (Hz)	5.293
Temperature, T (K)	300.0		
Mach number, M	0.6		

Table 6.5: NACA0012 Pitch Oscilation Frequency Sweep Cases

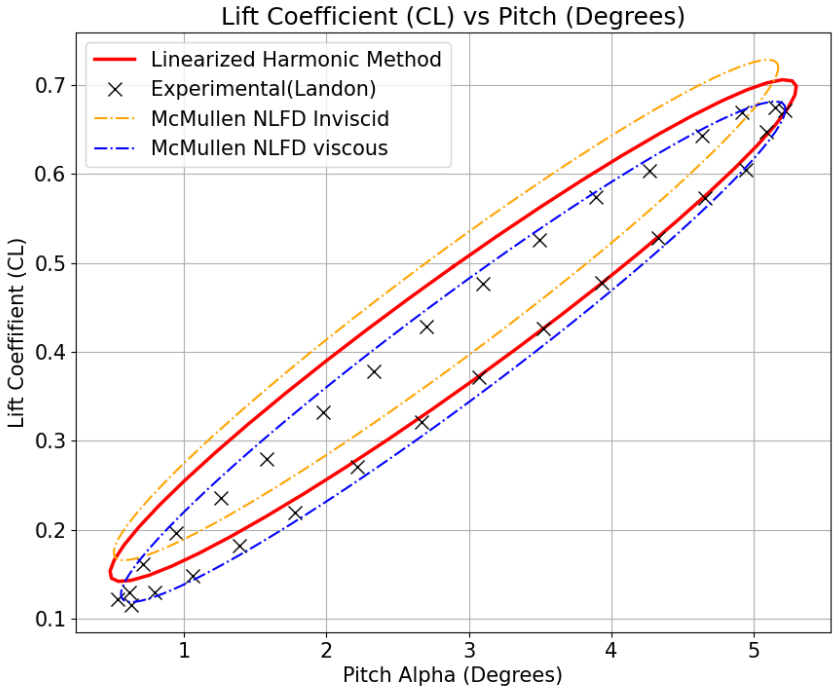

Figure 6.16: NACA0012 Linearized Harmonic vs Experimental Results

The Unsteady Lift results obtained by the Linearized Harmonic Solver for the NACA0012 case are displayed in Figure 6.16. The results are plotted alongisde the experimental findings, and McMullens Non-Linear Frequency Domain method [38] in both of its viscous and inviscid formulation.

One limitation of the Linearized Harmonic Method that becomes apparent is that it relies on inviscid Euler equations for the steady-state results, which it subsequently uses as the mean state. Consequently, the errors incurred by eliminating viscous effects from the steady results are directly transferred to the unsteady solution. This is particularly apparent upon inspecting the mean Lift coefficient, where the inviscid steady state solution overestimates the lift. Essentially, this overestimation shifts the lift estimations for the entire solution regime by a constant error. The McMullens inviscid method [38] also contains the same error, which lead him to developing a viscous formulation, eliminating the error.

This error is solely caused by the steady state solution scheme, which is not the scope of this work. Upon inspecting only the unsteady part of the solution this error can be eliminated, enabling better inspection of the scheme. The unsteady results actaully showcase near perfect prediction for the amplitude of the Unsteady lift. The results of unsteady lift variations for the same harmonically pitching airfoil is given in figure 6.17. The linearized harmonic method, successfully captures the target unsteady lift phenomena, and matches the accuracy of the more expensive Non-linear frequency domain method.

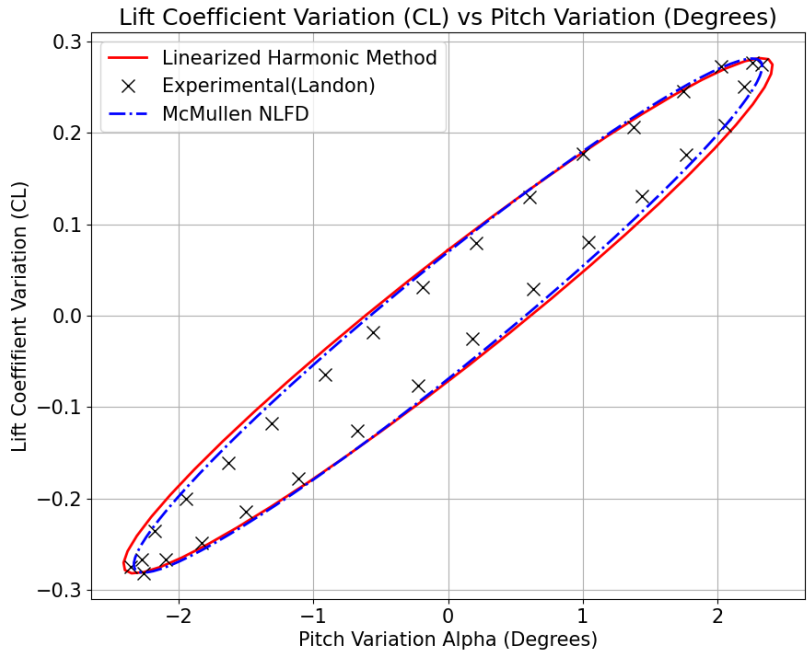

Figure 6.17: NACA012 Landon Case Unsteady Lift Variations

Inspecting oscilating airfoil at its mean pitch value at 2.89 degrees(0 degree variation), the solution exhibits hysterisis behavior as expected, where there are 2 different corresponding lift coefficient, depending on the pitching direction of the airfoil at its current state. The harmonic methods, shown to be overestimating the hysterisis, where they are more sensitive to the pitching rate, then experimental results indicate. Elimination of this error necessisates further work on frequency domain methods.

6.6 NACA64A10 Unsteady Aerodynamics Test Case

The findings from the Linearized Harmonic Solver for the NACA60A10 airfoil, are compared with experimental data obtained by S. S. Davis [39]. The findings of [38] also included, showcasing the differences between linear and non-linear frequency domain methods. The case presents a unique challenge due to being transonic, which is expected to bring out the shortcomings of the linearized harmonic method.

The non-dimensionalized properties of the experimental setup is presented in Table 6.4.

Airfoil	NACA64A10
Mean Pitch angle (°)	0
Pitch angle variation (°)	1.01
Mach	0.796
Reduced Frequency k	0.202

Table 6.6: Davis experiment parameters

For this simulation case, the chord length measures 1 meter, which results in a harmonic excitation frequency of 17.6435 Hz. The complete set of parameters utilized in the Harmonic Solver is outlined in Table 6.7.

Steady Parameters	**Value**	**Harmonic Parameters**	**Value**
Airfoil Steady Pitch (degree)	0	Pitch Perturbation (degree)	1.01
Pressure, p (Pa)	101325	Harmonic Frequency Case 1(Hz)	17.65
Temperature, T (K)	300.0		
Mach number, M	0.796		

Table 6.7: NACA64A10 Pitch Oscilation Frequency Sweep Cases

The NACA64A10 case incorporates transonic flow, where the flow around the airfoil includes shocks. Large flow gradients and shocks posing a significant challenge to Linearized Harmonic Methods, the unsteady lift predictions of the linearized harmonic method showcases poor accuracy, having 10 percent error, which is quite large, in its prediction of unsteady lift amplitude along with poor predictions on hysteresis behavior of the unsteady Lift. The Non-linear frequency domain approach [38] on the other hand, showcases good accuracy on obtaining unsteady lift amplitude along with acceptable predictions on hysteresis behavior.

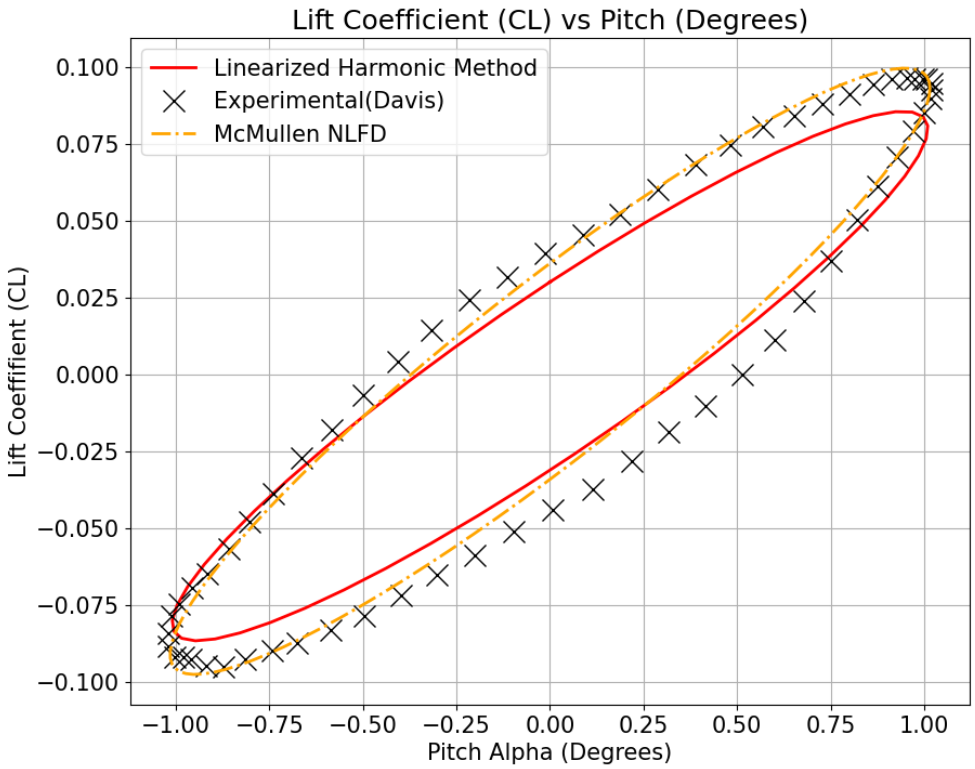

Figure 6.18: NACA64A10 Linearized Harmonic vs Experimental Results

6.7 2 DOF Airfoil Flutter Analysis

The proposed linearized harmonic method was ultimately developed as a tool to target aeroelasticity problems specifically those concerning flutter, where the need efficient flow solvers is significant. In this section, the proposed linearized harmonic method is applied to a canonical 2D oscillating airfoil scenario for which established analytical solutions exist.

Theodorsen's theory [40], which serves as the benchmark for our comparison, is a seminal work in aeroelasticity, where it's results had been validated in the literature one such being the work of Halfman [41]. Originally formulated to predict the unsteady aerodynamic loads on an oscillating think flat plates, it provides a robust foundation for analyzing the flutter phenomenon in thin airfoils. The theory is especially usefull for its treatment of airfoil motions, encompassing both pitching and plunging degrees of freedom. However, it's worth noting its inherent limitations: Theodorsen's theory primarily caters to thin airfoils under subsonic flow conditions.

Given the symmetrical and relatively thin nature of the NACA0012 airfoil, Theodorsen's theory emerges as a particularly appropriate analytical solution against which our linearized harmonic model can be juxtaposed. The symmetry of the NACA0012 airfoil simplifies the analysis by reducing the complications arising from camber effects, thereby falling more neatly within the purview of Theodorsen's assumptions. For the Simulations, the same domain is used across all simulations, where the details are already provided in earlier sections.

6.7.1 Flutter Speed Prediction

To validate the code's robustness across various simulation parameters, a test setup has been established. the detailed description of the tested scheme is provided in section 5.4. The Theodorsen method in its formulation deals with the pitch center location as a free variable. 10 different theoretical flutter test cases had been setup, by altering the location of the elastic axis with respect to the midchord. Subsequently comparing the flutter frequency and flow velocity outcomes from the linearized harmonic solver to those predicted by Theodorsen's theory.

Variable	Value
b	0.5
x_a	0.4
α	$-0.5 \ldots + 0.5$
I_{foil}	$2.402\,\text{kg}\,\text{m}^2$
k_h	$28,064\,\text{N/m}$
$k_{\alpha_{\text{center}}}$	$4680\,\text{N}\,\text{m/rad}$
m	$44.43\,\text{kg}$

(a) Structural Parameters

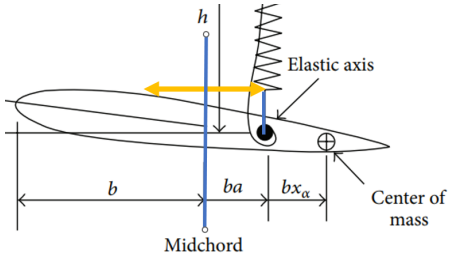

(b) Elastic axis with respect to mid chord

Figure 6.19: Testing setup

The structural parameters are depicted in figure 6.19a, emphasizing the variable α, which corresponds to the elastic axis location across the foil's chord. For this test, the flow parameters are standardized to atmospheric conditions: 300 Kelvin temperature and 101.3 kPa pressure.

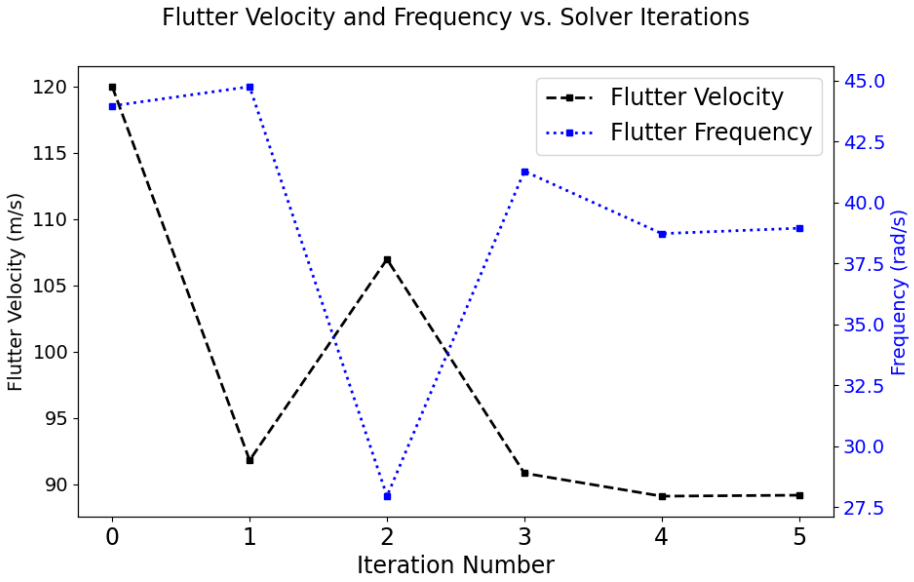

Figure 6.20: Flutter Solution Progressions for α=-0.5

Upon examining the linearized harmonic flow solver's performance, it's evident that even with initial guesses far away from the anticipated flutter point, convergence is

achieved within roughly five outer iterations (as illustrated in figure 6.20). Within these iterations, each new flutter computation necessitates four distinct CFD solution calls from the structural solver to ascertain the requisite Jacobians.

A significant advantage of the proposed method is its efficiency, each linearized harmonic solver solution is approximately ten times faster than its steady-state counterpart. With a total of 200 separate simulations needed for sweeping over ten pitch center locations, the entire process, on an 32 core consumer desktop PC with a 200,000-cell mesh, is completed in approximately 10 hours.

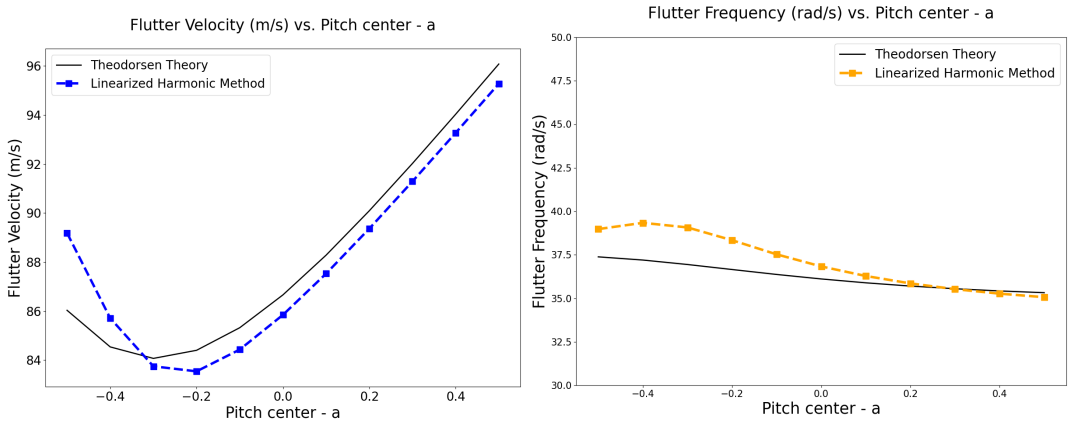

(a) Flutter Velocity

(b) Flutter Frequency

Figure 6.21: Flutter characteristics with different pitching Center Locations

The results in figure 6.21 align well with those from Theodorsen's theory. However, as a reminder to the reader, Theodorsen's theory primarily targets flat plates. Thus, the observed discrepancies can be attributed to the inherent differences between an airfoil and a flat plate—even for a slender one like NACA0012.

Overall, the linearized harmonic method succesfully captures the anticipated flutter behavior of the airfoil.

6.7.2 Modal Characteristics of NACA0012 at Near Flutter Speeds

A deeper examination into the flutter behavior of the NACA0012 airfoil is provided in figure 6.22. Here, the pitch axis is maintained at α = -0.4, while the other parameters mirror those shown in figure 6.19a. Rather than setting the damping value to zero for discerning the flutter onset speeds, this analysis opted for fixed velocities, solving instead for the corresponding damping and frequency values for each vibrational mode. The sheer number of Computational Fluid Dynamics (CFD) calls, exceeding 500 in total, showcasing the true utility of the proposed linearized harmonic method.

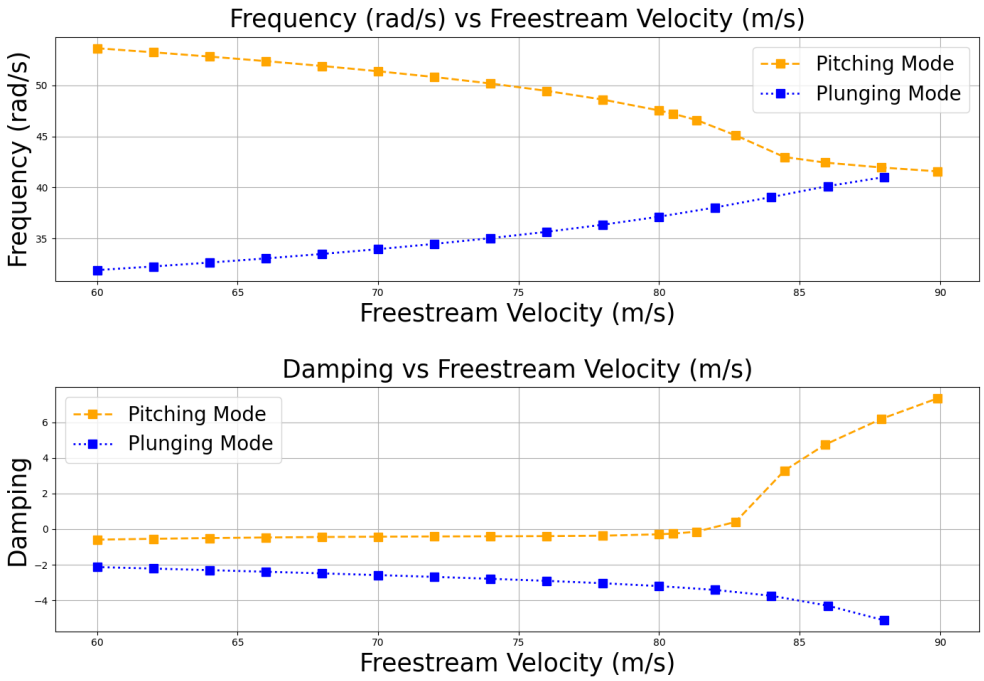

Figure 6.22: NACA0012 Flutter at a = -0.4

The results presented in figure 6.22 accentuate the system's natural vibration modes: pitching and plunging.

Unsteady airflow over the airfoil generates a force that serves a structurally dissipative role, essentially functioning as a damper. This phenomenon can be represented in governing equations as a damping term; a negative value denotes energy dissipation by the force. Intriguingly, as highlighted in figure 6.22, this damping term isn't perpetually negative.

When the damping values turn positive, it indicates that the unsteady aerodynamic forces are in fact augmenting themselves. Even an infinitesimal displacement of the airfoil at specific free-stream velocities can initiate a flow field. This flow, in turn, harmonically intensifies its unsteady displacement, culminating in an even larger unsteady aerodynamic force, thereby setting off a self-reinforcing loop.

Contrary to initial beliefs, flutter isn't triggered purely by aerodynamic forces. As evidenced, it emerges as a structural phenomenon where the fluid domain is intricately intertwined with the structure. Upon reaching the flutter onset point, the system descends into instability. At this juncture, even the slightest disturbance could catalyze deleterious outcomes.

A key observation from figure 6.22 is the system's vulnerability post reaching free-stream velocities exceeding 84 m/s. Beyond this point, the pitching mode destabilizes, marking the flutter onset. Hence, any flow rate at or surpassing this velocity threshold poses a tangible risk to the system's structural integrity.

CHAPTER 7

CONCLUSION

The present work offered an in-depth investigation into the performance of Linearized Harmonic Solver in the context of unsteady aerodynamics and flutter problems. It's accuracy had been tested in two aerodynamic cases: NACA0012 and NACA64A10, and the method proved to be accurate in subsonic problems, and shown to be promising in transonic cases where future work is needed. For the NACA0012 case, the method accurately predicted the amplitude of Unsteady lift oscillations, with deviations primarily stemming from the steady-state solution scheme rather than the harmonic analysis. In the case of NACA64A10, due the challenges posed by the transonic flow and the presence of shocks, linear harmonic methods unsteady lift predictions poorly matches with experimental data.

Nonetheless, the study revealed certain limitations inherent to the Linearized Harmonic Method. The reliance on inviscid Euler equations for steady-state solutions led to an overestimation of lift, a constant error that permeated the unsteady results. Additionally, the method exhibited shortcomings when dealing with large flow gradients and shocks. Despite that, in the domain of subsonic unsteady flow problems, the approach is shown to be accurate.

The true utility of linearized harmonic methods emerges when applied to flutter problems. Flutter problems and fluid-structure interaction problems in general, require multiple flow solutions during their operation, where a single simulation involve hundreds of flow solver calls, which leads to demand for an substantially efficient, task specific fluid solver. Given the method's inherent efficiency, it stands out as an optimal choice for aeroelastic FSI problems, flutter being a prime example. When compared against analytical models, the method is demonstrably accurate. its efficiency

renders it an exceptional tool for detailed explorations into airfoil behavior near the flutter onset, elevating the caliber of research in this domain.

7.1 Future Work

To enhance the Linearized Harmonic method, future studies should be conducted to mitigate the overestimation of lift introduced by the inviscid Euler equations. Implementing a viscous correction factor or integrating viscous effects into the steady-state solution could potentially provide more accurate base states for unsteady analysis.

The method's limitations in handling large flow gradients and shocks, present a significant area for future research. Modifications or adaptations to the method that can better accommodate these challenging conditions would constitute a major advancement.

Continued research and development of the Linearized Harmonic method holds significant promise. By addressing its current limitations and discovering new applications, this method could serve as a powerful tool for the accurate and efficient analysis of Unsteady aerodynamic problems.

REFERENCES

[1] A. Karshenass and O. Baran, *Turbomachinery Analysis in Frequency Domain*, pp. 133–147. 07 2017.

[2] A. Karshenass and O. Baran, "Cfd in axial turbomachines: A harmonic approach," 12 2019.

[3] R. Kurniawan, "Numerical study of flutter of a two-dimensional aeroelastic system," *ISRN Mechanical Engineering*, vol. 2013, pp. 1–4, 01 2013.

[4] B. A. Miller and J. J. McNamara, "Efficient fluid-thermal-structural time marching with computational fluid dynamics," *AIAA Journal*, vol. 56, no. 9, pp. 3610–3621, 2018.

[5] B. E. Mitchell, *Direct computation of the sound generated by subsonic and supersonic axisymmetric jets*. PhD thesis, Stanford University, 1995.

[6] R. H. Ni and F. Sisto, "Numerical Computation of Nonstationary Aerodynamics of Flat Plate Cascades in Compressible Flow," *Journal of Engineering for Power*, vol. 98, pp. 165–170, 04 1976.

[7] K. C. Hall, *A linearized Euler analysis of unsteady flows in turbomachinery*. PhD thesis, Massachusetts Institute of Technology, 1987.

[8] K. C. Hall and E. F. Crawley, "Calculation of unsteady flows in turbomachinery using the linearized euler equations," *AIAA Journal*, 1989.

[9] J. G. Marshall and M. B. Giles, "Some applications of a time-linearized euler method to flutter & forced response in turbomachinery," pp. 225–240, 1998.

[10] W. Ning and L. He, "Computation of Unsteady Flows Around Oscillating Blades Using Linear and Nonlinear Harmonic Euler Methods," *Journal of Turbomachinery*, vol. 120, pp. 508–514, 07 1998.

[11] M. Schnoes, A. Schmitz, G. Goinis, C. Voß, and E. Nicke, "Strategies for multi-fidelity optimization of multi-stage compressors with throughflow and 3d cfd," 09 2019.

[12] M. Hembera, A. Loos, H.-P. Kau, and E. Johann, "Comparing a 40 mio grid-points full-annulus computation with a 7 mio gridpoints nonlinear harmonic computation," 01 2009.

[13] C. Haldeman, M. Dunn, J. Barter, B. Green, and R. Bergholz, "Aerodynamic and heat-flux measurements with predictions on a modern one and 1/2 stage high pressure transonic turbine," vol. 127, 01 2004.

[14] K. Hall, W. Clark, and J. Thomas, "Computation of unsteady nonlinear flows in cascades using a harmonic balance technique," *Aiaa Journal - AIAA J*, vol. 40, pp. 879–886, 05 2002.

[15] K. C. Hall, J. P. Thomas, and W. S. Clark, "Computation of unsteady nonlinear flows in cascades using a harmonic balance technique," *AIAA Journal*, vol. 40, no. 5, pp. 879–886, 2002.

[16] *A Harmonic Balance Approach for Modeling Three-Dimensional Nonlinear Unsteady Aerodynamics and Aeroelasticity*, vol. 5th International Symposium on Fluid Structure Interaction, Aeroelasticity, and Flow Induced Vibration and Noise of *ASME International Mechanical Engineering Congress and Exposition*, 11 2002.

[17] J. Thomas, E. Dowell, K. Hall, and C. Denegri, *Further Invesitgation of Modeling Limit Cycle Oscillation Behavior of the F-16 Fighter Using a Harmonic Balance Approach*.

[18] J. Howison, J. Thomas, and K. Ekici, "Aeroelastic analysis of a wind turbine blade using the harmonic balance method," *Wind Energy*, vol. 21, 12 2017.

[19] H. Li and K. Ekici, *Aeroelastic Modeling of a Three-Dimensional Wing Using the Harmonic-Balance-Based One-shot Method*.

[20] J. Thomas and E. Dowell, *A Fixed Point Iteration Approach for Harmonic Balance Based Aeroelastic Computations*.

[21] A. Karshenass, *DEVELOPMENT OF AN UPWIND LINEARIZED HARMONIC FLOW SOLVER FOR TURBOMACHINERY FLOWS*. PhD thesis, 08 2022.

[22] J. L. Steger and R. Warming, "Flux vector splitting of the inviscid gasdynamic equations with application to finite-difference methods," *Journal of Computational Physics*, vol. 40, no. 2, pp. 263–293, 1981.

[23] P. D. Lax, "Weak solutions of nonlinear hyperbolic equations and their numerical computation," *Communications on Pure and Applied Mathematics*, vol. 7, no. 1, pp. 159–193, 1954.

[24] G. Hristov and P. J. Ansell, *Post-Stall Hysteresis and Flow Field Unsteadiness on an NACA 0012 Airfoil*.

[25] J. Blazek, *Computational Fluid Dynamics: Principles and Applications*. Butterworth-Heinemann, 3 ed., 2015.

[26] P. L. Roe, "Approximate riemann solvers, parameter vectors, and difference schemes," *Journal of Computational Physics*, vol. 135, pp. 250–258, 1997.

[27] E. F. Toro, *Riemann Solvers and Numerical Methods for Fluid Dynamics*. Springer, Berlin, Heidelberg, 1 ed., 30 March 2009.

[28] A. LAFON and H. YEE, *On the numerical treatment of nonlinear source terms in reaction-convection equations*.

[29] J. L. Thomas and R. W. Walters, "Upwind relaxation algorithms for the navier-stokes equations," *AIAA Journal*, vol. 25, no. 4, pp. 527–534, 1987.

[30] N. FRINK, P. PARIKH, and S. PIRZADEH, *A fast upwind solver for the Euler equations on three-dimensional unstructured meshes*.

[31] D. H. Hodges and G. A. Pierce, "Introduction to structural dynamics and aeroelasticity: Introduction to structural dynamics and aeroelasticity, second edition," 2011.

[32] G. Kösterit, *DETERMINATION OF FLUTTER SPEED OF NONLINEAR WINGS*. PhD thesis, 08 2023.

[33] J. P. Thomas, E. H. Dowell, and K. C. Hall, "Nonlinear inviscid aerodynamic effects on transonic divergence, flutter, and limit-cycle oscillations," *AIAA Journal*, vol. 40, pp. 638–646, 2002.

[34] R. H. Landon, "Naca 0012 oscillatory and transient pitching," 2000.

[35] "Agard 702 compendium of unsteady aerodynamic measurements," tech. rep., North Atlantic Treaty Organization. Advisory Group for Aerospace Research and Development. Structures and Materials Panel., 1982.

[36] Y. Gong and W. Zhang, "Efficient aeroelastic solution based on time-spectral fluid–structure interaction method," *AIAA Journal*, vol. 57, no. 7, pp. 3014–3025, 2019.

[37] W. Yao and S. Marques, "Prediction of transonic limit-cycle oscillations using an aeroelastic harmonic balance method," *AIAA Journal*, vol. 53, no. 7, pp. 2040–2051, 2015.

[38] S. Mcmullen and A. Jameson, "The application of non-linear frequency domain methods to the euler and navier-stokes equations," 06 2003.

[39] S. Davis and G. Malcolm, "Unsteady aerodynamics of conventional and supercritical airfoils," *Collection of Technical Papers - AIAA/ASME/ASCE/AHS/ASC Structures, Structural Dynamics and Materials Conference*, 02 1980.

[40] T. Theodorsen, "General theory of aerodynamic instability and the mechanism of flutter," 1934.

[41] R. L. Halfman, "EXPERIMENTAL AERODYNAMIC DERIVATIVES OF A SINUSOIDALLY OSCILLATING AIR- FOIL IN TWO-DIMENSIONAL FLOW,"